ELASTIC PITCH BEAM TAIL ROTOR OPERATIONAL SUITABILITY INVESTIGATION

Alfred S. Falcone, et al

Kaman Aerospace Corporation

Prepared for:

Army Air Mobility Research and Development Laboratory

July 1974

EUSTIS DIRECTORATE POSITION STATEMENT

Using the tail rotor of the UH-1 as a basis for comparison, an AMRDL feasibility study indicated that the Elastic Pitch Beam Tail Rotor would require 28 fewer parts and weigh 20-25% less. Limited fatigue tests indicated that a very high fatigue life was possible. Advanced development through flight test evaluation is presently under way. Results reported herein show the concept to be very rugged and inherently reliable. There are no industry standards to determine via laboratory tests the general operational suitability of rotor systems. Further, there are no comparable data for current-inventory helicopters. Consequently, declaration of how well or how much better the Elastic Pitch Beam Tail Rotor would "perform" in service is mere speculation. Nevertheless, there is considerable confidence that in terms of reliability, maintainability, damage resistance/tolerance, and cost effectiveness it would surpass current tail rotor systems. Both UTTAS helicopters under development have tail rotors akin to the Elastic Pitch Beam testifying to this confidence. Tail rotors of this variety should be considered as the "new standard" when comparing the relative merits of competitive antitorque systems. Field service evaluation of an Elastic Pitch Beam Tail Rotor system is recommended. Extension of the concept to main rotors, modified to allow folding and the one-to-one replacement of an irreparably damaged blade, is logical and also appears worthy of R&D support. It would appear to have all the advantages of elastomeric rotor heads while being mechanically simpler, lighter, and less costly.

This program was conducted under the technical cognizance of Joseph H. McGarvey, Military Operations Technology Division.

Unclassified

SECURITY CLASSIFICATION OF THIS PAGE *(When Data Entered)*

REPORT DOCUMENTATION PAGE		READ INSTRUCTIONS BEFORE COMPLETING FORM
1. REPORT NUMBER USAAMRDL-TR-74-60	2. GOVT ACCESSION NO.	3. RECIPIENT'S CATALOG NUMBER AD 784595
4. TITLE *(and Subtitle)* ELASTIC PITCH BEAM TAIL ROTOR OPERATIONAL SUITABILITY INVESTIGATION		5. TYPE OF REPORT & PERIOD COVERED Final 6. PERFORMING ORG. REPORT NUMBER 1207
7. AUTHOR(s) Alfred S. Falcone Frank Clark Paul Maloney		8. CONTRACT OR GRANT NUMBER(s) Contract DAAJ02-71-C-0063
9. PERFORMING ORGANIZATION NAME AND ADDRESS Kaman Aerospace Corporation Bloomfield, Conn. 06002		10. PROGRAM ELEMENT, PROJECT, TASK AREA & WORK UNIT NUMBERS Task 1F262203AH8603
11. CONTROLLING OFFICE NAME AND ADDRESS Eustis Directorate, U. S. Army Air Mobility Research and Development Laboratory, Fort Eustis, Va. 23604		12. REPORT DATE July 1974 13. NUMBER OF PAGES 129
14. MONITORING AGENCY NAME & ADDRESS *(if different from Controlling Office)*		15. SECURITY CLASS. *(of this report)* Unclassified 15a. DECLASSIFICATION/DOWNGRADING SCHEDULE

16. DISTRIBUTION STATEMENT *(of this Report)*

Approved for public release; distribution unlimited.

17. DISTRIBUTION STATEMENT *(of the abstract entered in Block 20, if different from Report)*

18. SUPPLEMENTARY NOTES

19. KEY WORDS *(Continue on reverse side if necessary and identify by block number)*

Helicopter rotors	Protective coatings	Tolerance
Composite materials	Erosion	Rain erosion
Fatigue	Protection	Sand
Leading edges	Ballistics	
Environmental tests	Damage	

20. ABSTRACT *(Continue on reverse side if necessary and identify by block number)*

The work under this contract was performed to ascertain the operational suitability of the Elastic Pitch Beam Tail Rotor being developed under Contract DAAJ02-72-C-0006 and to enhance its performance by selection of an optimized protective coating system and leading-edge erosion guard. Adiprene L-167 was selected for the protective coating based on the protection afforded to the GRP substrate in reverse-bending fatigue under cyclic environmental exposure of humidity, solar simulation, cold, and heat. Spring

DD FORM 1 JAN 73 1473 EDITION OF 1 NOV 65 IS OBSOLETE

Unclassified

SECURITY CLASSIFICATION OF THIS PAGE *(When Data Entered)*

20 - continued

rate test performed on the GRP spar assembly at various levels of CF loading from -65°F to 160°F with and without exposure to environmental cycling disclosed spring rate changes within 15 percent for the temperature extreme tested. Fatigue tests of full-scale beam assemblies following environmental exposure cycling showed no failure or degradations that could be attributed to either the exposure or the coating. It was concluded that the service life of the elastic pitch beams will not be affected substantially by adverse environmental conditions. The leading-edge erosion protection system selected was .060-inch-thick polyurethane.

SUMMARY

The work under this contract was performed to ascertain the operational suitability of the Elastic Pitch Beam Tail Rotor being developed under Contract DAAJ02-72-C-0006 and to enhance its performance by selection of an optimized protective coating system and leading-edge erosion guard. Five basic tasks were established to determine the following:

1. Protective coating for the glass reinforced plastic spar (GRP).

2. Elastic pitch beam spring rate.

3. Elastic pitch beam fatigue.

4. Erosion protection system.

5. Damage resistance and ballistic damage tolerance.

Adiprene L-167 was selected as the optimum material for the protective coating based on the protection afforded to the GRP substrate in reverse-bending fatigue under cyclic environmental exposure of humidity, solar simulation, cold and heat. The thickness of the applied coating, .010-.015 inch, possessed the added attribute of providing protection to the GRP spar against mechanical damage.

The spring rate test performed on the GRP spar assembly at various levels of CF loading from -65°F to 160°F with and without exposure to environmental cycling disclosed spring rate changes within 15 percent for the temperature extremes tested. No significant change in spring rate occurred because of environmental exposure. The degree of change in spring rate caused by temperature was not considered to have any significant effect on operation of the Elastic Pitch Beam Tail Rotor.

As a further evaluation of the influence of environmental factors on reliability and integrity of the Elastic Pitch Beam Tail Rotor, three fatigue tests of full-scale beam assemblies were conducted following exposure to the complete spectrum of humidity, solar simulation, cold and heat. Results of this test showed no failures or degradations that could be attributed to either the exposure or the coating when they were compared to the results obtained under the above-referenced contract on unexposed, unprotected specimens. It is therefore anticipated that the service life of the elastic pitch beams will not be affected substantially by adverse environmental conditions.

The selection of an optimum leading-edge erosion protection system narrowed down to .032-inch electroformed nickel and to .060-inch-thick urethane on completion of test in the Air Force Whirl Rig at the Olin Mathisen Chemical Corporation. The electroformed nickel exhibited the lowest wear rate in sand of the metallic materials and endured a combination sand and rain exposure test. The .060-inch-thick urethane erosion guard exhibited outstanding resistance to sand abrasion far in excess of that demonstrated by electroformed nickel. In the combination sand and rain tests, the polyurethane material was at best marginal in performance because of rain impingement, but the benefit of the increased thickness was demonstrated. The outstanding resistance to sand abrasion, the relative ease for repair or replacement, lower cost, and the negligible effect on structure predicated the selection of the polyurethane erosion guard for the leading-edge protection system.

The damage resistance and ballistic tolerance of the Elastic Pitch Beam Tail Rotor were demonstrated by injecting maple dowels, gravel and crushed stones into the whirling rotor, and by subsequent whirling of the rotor after inflicting multiple ballistic hits. Maple dowels up to 1/2-inch diameter caused no damage. A 5/8-inch-diameter dowel created a 1/8-inch dent on the leading edge, but the damage was not sufficient to preclude further whirl. Since seasoned maple is stronger than green wood, it is implied that live brush and tree branches somewhat larger than 5/8-inch diameter could be digested by the whirling rotor without damage. The polyurethane erosion guard sustained a continuous bombardment of gravel for a whirl run duration of 32 minutes. Crushed stones tore open the erosion guard in a 10-minute whirl run duration. The amount and size of material injected into the rotor were considered to be in excess of that normally encountered in service. Ballistic tolerance was demonstrated by inflicting six 7.62mm ball hits on the rotor - four through skin to core structure, one through trailing-edge spline, and one through the aluminum leading edge - followed by over four hours of whirl without any damage propagation. Subsequent 7.62mm AP hits to the ballast weight region, outboard spar termination station, and leading-edge skin to forward channel rendered further whirl running too risky. Damage from these last three hits would likely cause vibration sufficient to abort the mission. Direct hits on the spar structure with 12.7mm AP ammunition were sufficient to cause catastrophic damage.

TABLE OF CONTENTS

LIST OF ILLUSTRATIONS

LIST OF TABLES

INTRODUCTION

The Elastic Pitch Beam Tail Rotor provides potential gains in reliability and maintainability compared to tail rotors in service today. This is achieved through the elimination of highly loaded pitch bearings and by minimizing the number of structural joints that must transmit blade centrifugal force. In this rotor concept, illustrated in Figures 1 and 2, two airfoil panels are bonded to the outboard portion of the elastic pitch beam spar which is continuous through the hub area. Inboard of the bonded connection (Station 13) an airfoil shaped cuff surrounds the spar. This cuff contains the integral pitch horn and provides the attachment for a shear reaction or centering bearing. Control input loads applied to the pitch horn are reacted on the centering bearing, thus producing a couple or torsional moment (load x offset, e) which is transmitted tc the airfoil panel. This moment elastically twists the pitch beam segment within the cuff region, producing the necessary pitch change. The elastic pitch beam thus accommodates all the necessary pitch change motions while transmitting full airfoil panel centrifugal force and bending moments.

The elastic pitch beam spar passes through grooves in the central hub which are lined with an elastomer. The spar is bonded to the elastomer for basic positioning of the rotor; however, this flexible joint does not tend to transmit centrifugal load from the strap to the hub. Instead, this load remains in the strap and is reacted by the opposite blade. The central hub of the rotor is articulated to the shaft through a teeter axis which maintains the standard "delta-3" angle of the UH-1 tail rotor.

The spar is fabricated from unidirectional S glass straps and a tapered web of $\pm$45-degree layup S glass. Filament winding at the apex of the tapered structure reacts the splitting load resulting from centrifugal force and torsional deformations. The airfoil panels are formed of aluminum (6061) leading edge and channels, glass reinforced skins (BP-919/7581 fabric), nomex core and glass reinforced trailing-edge spline. The adhesive system employed is a midtemperature epoxy. An abrasion strip is bonded to the outboard portion of the airfoil panel's leading edge for erosion protection.

The purpose of the test program described herein was to provide a preliminary evaluation of the operational suitability of the concept. Development tests of environmental protective coatings for the spar and erosion protection systems for the leading edge were also included. The basic flightworthiness of this design is being demonstrated in a separate program.

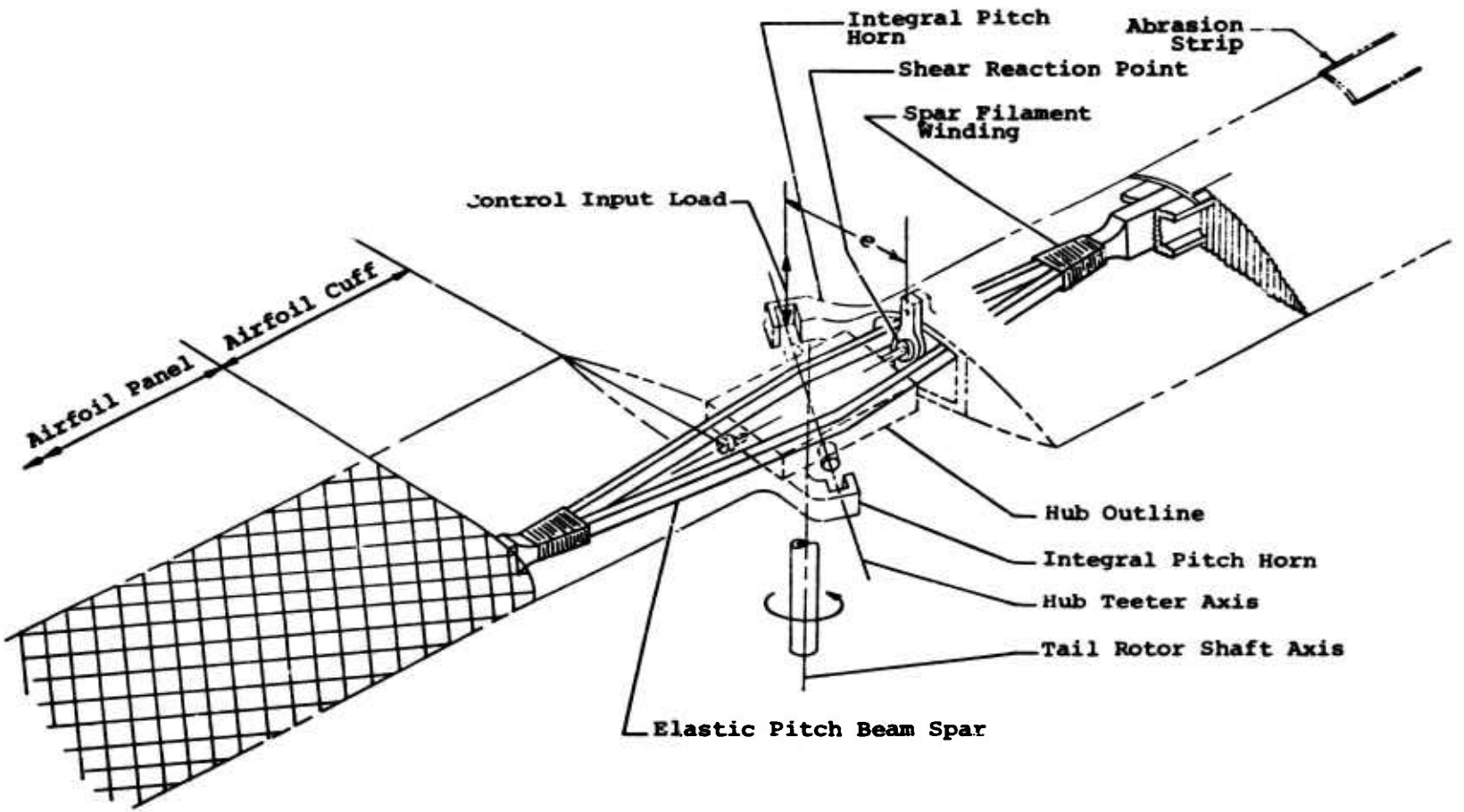

Figure 1. Elastic Pitch Beam Tail Rotor Concept.

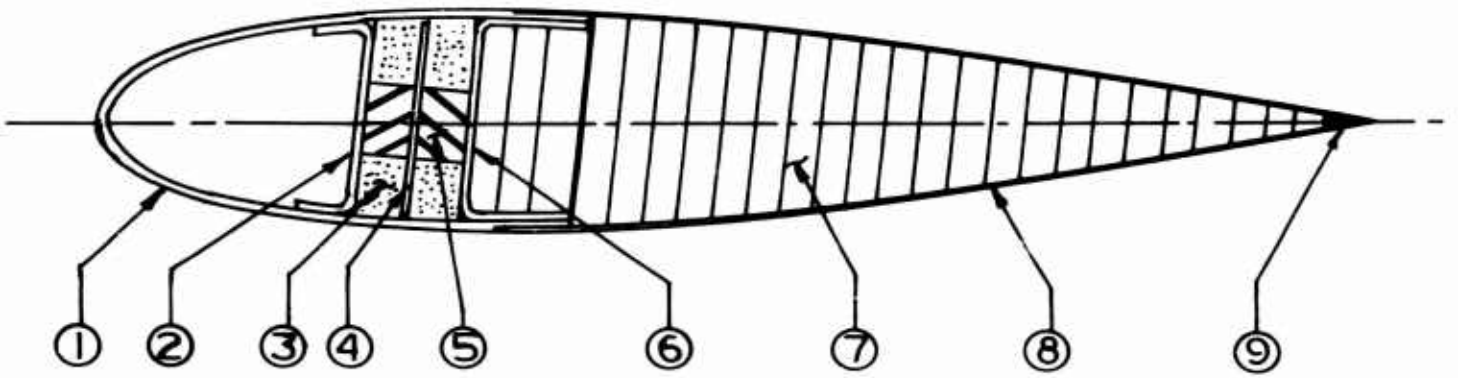

NOMENCLATURE

1. Spar, .050-In.-Thick 6061-T6 Al Alloy.
2. Forward Channels, .063-In.-Thick 6061-T6 Al Alloy.
3. Blocks, Molded Chopped Glass Fiber.
4. Web, .040-In.-Thick 301 CRES 1/4 Hard.
5. Straps, .600-In. x .380-In. 1002-1014S Glass.
6. Aft Channel, .063-In.-Thick 6061-T6 Al Alloy.
7. Core, 1/8 - 1.8 Polyamide Honeycomb.
8. Skins, .020-In.-Thick BP-919/7581 Fiberglass.
9. Spline, BP-919/7581 Fiberglass.

Figure 2. Cross Section Details at Station 13.

The object of the coating system was to obtain a protective coating for the inboard portion of spar and hub region which would endure high strain and repeated flexing and afford maximum protection to the spar against degradation from environmental factors. This task was accomplished by means of a specially designed fatigue test run at high levels.

The elastic pitch beam spring rate test evaluated the spring rate of spar assemblies at various temperatures and levels of centrifugal loading, and also the effect of environmental exposure conditions of humidity, temperature and solar simulation on the spring rate to ascertain the operational suitability of this design. Components fabricated for this test were coated with the protective system selected in the first task.

The elastic pitch beam fatigue test utilized components after completion of spring rate testing to assess the influence of environmental exposure on fatigue performance. One specimen was fatigue tested to 10^6 cycles at a high maneuver stress level, one specimen was tested to 10^7 cycles at a stress level exceeding high-speed level-flight conditions of the UH-1H, and one specimen was step-tested to 10^7 cycles in an effort to establish the endurance limit as well as to determine the onset of torsional stiffness degradation. At the start, and periodically during the fatigue test, the spring rates of the spar components were redetermined to evaluate the effect of fatigue cycling on stiffness properties.

The erosion protection task evaluated various leading-edge materials for possible utilization on the Elastic Pitch Beam Tail Rotor. Tests were conducted on a whirling arm rig at velocities approaching tail rotor tip speeds under controlled rates of sand and rainfall to simulate operational service in the Army environment. The leading-edge system employed on the UH-1H tail rotor was tested for a standard to judge relative performance of the candidate materials.

To further assess the operational suitability of the Elastic Pitch Beam Tail Rotor, the tail rotor was subjected to additional whirling to evaluate its damage resistance and ballistic tolerance. Maple dowels, gravel and crushed stones were injected into the whirling rotor and damage was recorded. Ballistic hits with 7.62mm ammunition were inflicted on the rotor in stages of increasing severity until the damage was judged too risky to warrant further whirl. On termination of the whirl program, additional 7.62mm AP shots were fired into the rotor and the damage was recorded.

A spar component and an outboard blade section were sent to the Ballistic Research Laboratories, Aberdeen Proving Ground, Maryland for 12.7mm AP firing tests, and the damage was recorded.

The Elastic Pitch Beam Tail Rotor was shown to be capable of operation in the Army environment and to provide a significant degree of damage tolerance without catastrophic failure.

PROTECTIVE COATING SYSTEM

COATING SELECTION

A review of available materials was initiated for the selection of candidate coatings. Parameters used in determining the suitability of coatings were as follows:

1. Flexibility at temperatures of -65°F.
2. Adhesion to fiberglass surfaces.
3. Tear and gouge resistance (for mechanical damage resistant coating).
4. Resistance to ageing and weathering.
5. Resistance to synthetic oils and fuels.
6. Ease of application.

Because of the inherent twist and flexing of the elastic pitch beam tail rotor, only coating classifications reporting excellent flexibility at -65°F were considered.

Relative ratings of poor, fair, good and excellent were then assigned to the remaining parameters based on handbook data.

Materials considered and assigned ratings are listed in Table I.

The alkyd, cellulose, and rubber materials were eliminated primarily because of their reported[1] poor resistance to synthetic lubricants. Polyester coatings were excluded based on their reported low adhesion to glass reinforced plastics. Coatings representing each of the remaining classifications were applied to .030-inch aluminum test panels and subjected to a bend test around a 1-inch mandrel at -65°F. Samples of the epoxy system were the only specimens to fail this test, and the coating was therefore discarded. The fluorosilicone coating tested, even though exhibiting good flexibility at -65°F, was judged to be unacceptable because it exhibited very poor tear resistance and was readily damaged by minor abuse. This property is characteristic of fluorosilicone materials, so they were eliminated from further consideration.

TABLE I. CLASSIFICATION OF COATING PROPERTIES

Selection Parameters	Alkyd	Acrylic	Cellulose	Epoxy	Polyester	Rubber	Urethane	Fluoro-silicone
Flexibility at -65°F	E	E	E	G	G	E	E	E
Adhesion to GRP	E	G	G	E	F-P	G	E	F-G
Abrasion Resistance Taber No.*	G 3500	F 2500	F 2500	E >5000	G 3500	E 5000	E >7500	P
Impact Resistance	VG	E	E	E	F	E	E	F
Weather Durability	E	E	E	E	E	E	E	E
Resist. to Oils & Fuel	G	G	G	E	G	F	F	F
Resist. to Synthetic Lub	P	G	P	E	G	P	E	E
Ease of Application	E	G	G	E	F	G	E	E

*Cycles to wear through
CODE: E - Excellent; VG - Very Good; G - Good; F - Fair; P - Poor.

The three remaining coating systems retained for further consideration were as follows:

1. Acrylic Nitro-Cellulose System

MIL-C-8514	Wash Primer (.0004-.0007)
MIL-C-7962	Primer (.0003-.0006)
MIL-L-19538	Acrylic Lacquer (.0005-.0008)

2. Urethane System

MIL-P-23377	Epoxy Primer (.0006-.0009)
MIL-C-81773	Aliphatic Urethane (.001-.0015)

3. Urethane

MIL-C-23377	Primer (.0006-.0009)
Adiprene L-167	Moca (.010-.015)

SPECIMEN DESIGN AND FABRICATION

The design of the fatigue specimen for this phase of the program is shown in Figure 3. The precured phenolic insert was incorporated in the buildup to achieve increased thickness at the retaining clamp location so as to reduce the bending stress and preclude premature fretting failures. The design also provided for the peak bending stress to occur at the apex of the phenolic wedge and for a gradual decrease in bending stress along the tape since the section property effect was more predominant than the increased bending moment.

Initial specimens were laminated in a 10-1/2-inch square cavity mold with the base matching the taped side of the specimens. Six plies of unidirectional S glass were laid in the mold, followed by the positioning of the precured and machined phenolic wedge. The one short ply of S glass was laid along the neutral axis up to the apex of the wedge, followed by six additional full plies. Specimens were bagged and cured under fluid pressure of 60 psi at 340° ± 10°F for 90 minutes at temperature. The cured laminate was cut and machined to a 1-inch width.

Specimens fabricated in this manner exhibited nonuniform thickness, but they were used only for preliminary testing. These specimens, when installed in Krause plate reverse-bending fatigue machines at 25,000 psi steady stress and ± 45,000 psi vibratory stress, delaminated along phenolic insert to glass interface after within 10,000 to 100,000 cycles. Additional specimens were fabricated in the same manner except that

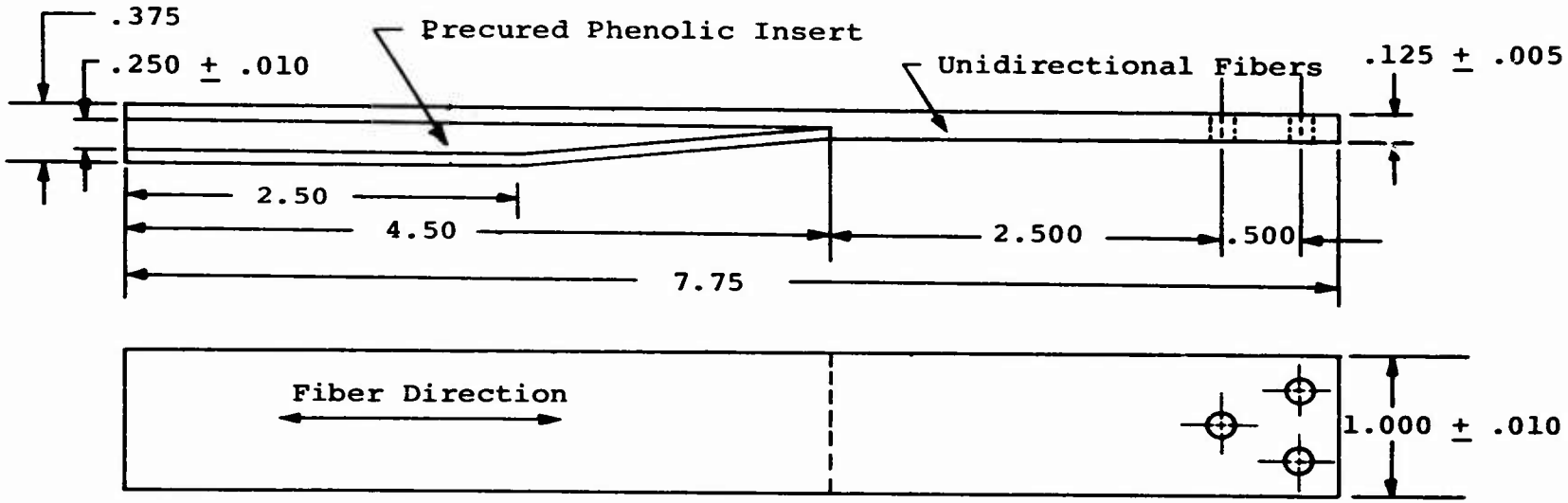

Materials: Phenolic Insert - Machined from Laminate of Style 128 Fabric and Palmer No. 1000 Resin
Unidirectional Fibers - 1014S Glass in Epoxy Matrix (3M-1002 System)

Dimensions Are in Inches.

Figure 3. Fatigue Specimen Design.

polyamide adhesive film was applied along the faying surfaces of the phenolic wedge to glass prepreg. This second group of specimens was run in the Krause fatigue tester at the same stress condition. It was immediately observed that specimens of this design were running hot compared to the previous group, and early delamination occurred at the adhesive film interface.

Again, additional specimens were fabricated in the same manner except the polyamide film was now replaced by an epoxy resin consisting of EPON 820, DTA and Versamid in a ratio of 100-10-6 parts by weight, respectively. These specimens did not heat up nor did they appear to be susceptible to premature delamination.

In an attempt to overcome thickness variation, three molds were fabricated for individual 1-inch-wide specimens. Again the bottom surface of the mold matched the taped side of the specimen. The layup was similar except that glass plies and phenolic wedge were 1 inch wide. After layup, a 1-inch-wide by .020-inch-thick caul plate was placed over the specimen followed by a pressure diaphragm. End plates and a cover plate were screwed into place. A pressure line was attached to an end plate fitting to pressurize the diaphragm, and a gage was attached to the fitting at the other end plate to monitor pressure. Specimens and tool assemblies were placed in a platten press, which acted only as a heat source. Specimens were cured under fluid pressure of 60 psi at $340^{\circ} \pm 10^{\circ}F$ for 90 minutes. Temperature was monitored by a thermocouple within each tool.

After cure, the adhesive flash was removed from the specimen by light hand sanding along the edges, and the specimens were cut to length at each end at the specified distance from the apex of the phenolic wedge.

Specimens fabricated in this manner were consistently flat with parallel faces, but thickness varied from specimen to specimen, typically within $\pm$ .010-inch tolerance. This variation presented concern since multiple specimens were to be tested simultaneously at a given deflection. To evaluate the effect of thickness variation, several specimens were installed in the Krause tester, equally loaded, and the deflection measured. Even though thickness varied, the same deflections were measured for a given stress condition.

The experiment was then repeated with strain gages mounted on two additional specimens, and a plot was made of deflection versus strain data as shown in Figure 4. From this experiment it was concluded that thickness variation between specimens

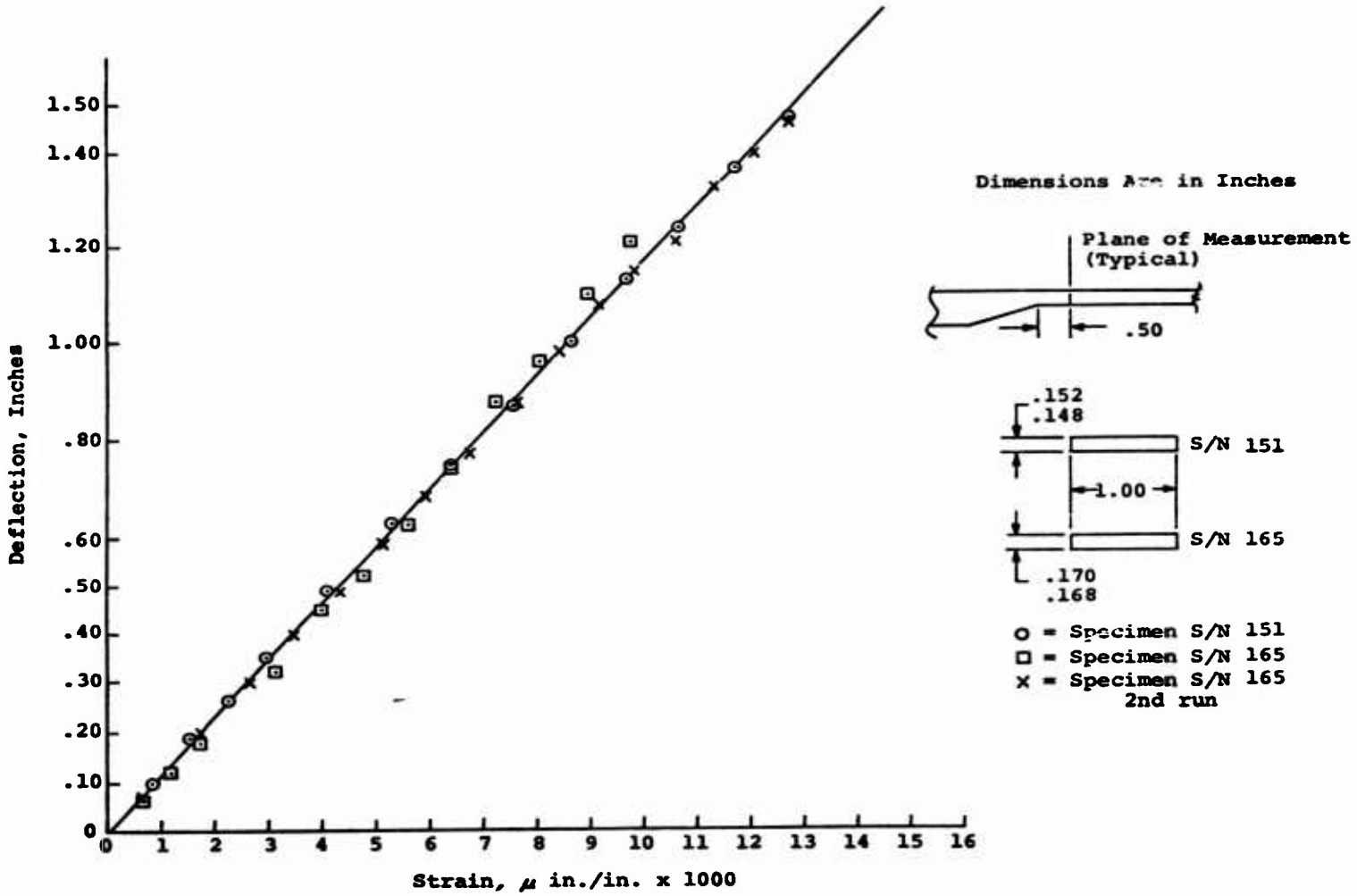

Figure 4. Load Deflection Curve for Fatigue Specimens of Two Thicknesses.

fabricated with the same number of plies had no significant effect on the load-deflection relationship.

Part of the thickness variation could be attributed to the adhesive squeeze-out and to multiple tooling. However, adhesive squeeze-out appeared minimal and rather uniform from specimen to specimen, and thickness of specimens from each tool appeared to be random with no correlation that one tool yielded thicker or thinner specimens than the other two tools.

TEST PROCEDURE

A special flexure rig was designed and built to fit inside an American Research Corporation Environmental Chamber Model No. SH027 capable of temperature cycling, humidity control and solar simulation. See Figure 5. The rig tested up to five specimens at a time to the same theoretical steady and vibratory strain levels. This was accomplished by adjusting the offset on a cam driven by a variable-speed drive motor. The frequency of all coupon testing was maintained at 200 rpm.

The initial plan was to seek a stress level which would generate specimen failures between 2.5 to 3.5 x 10^6 cycles or within 10 to 12 days of testing to provide ample time for environmental effects to show on subsequent testing.

After successive trial tests at increasing stress levels, a load condition of 25,000 psi steady and 71,000 psi vibratory was selected for a base-line condition even though valid specimen failures were not obtained within the target 3.5 x 10^6 cycles. Results of tests on specimens not exposed to environmental change are shown in Table II.

All subsequent tests were run under environmental cycling conditions with the chamber programmed for the following 3-day cycle:

48 hours at 95 percent relative humidity at 120°F
8 hours under solar simulation at approximately 105°F
8 hours at -65°F
8 hours at 130°F

MIL-STD-810A was the controlling specification for environmental parameters. The chamber, however, contained a General Electric VA11B tungsten filament lamp for ultraviolet exposure but no provision for infrared capability for the complete sunshine spectrum as specified by MIL-STD-810A. The lamp was therefore supplemented with six General Electric 250 R40 infrared reflector heat lamps to form a light cluster which would cover the required light wave spectrum. The light

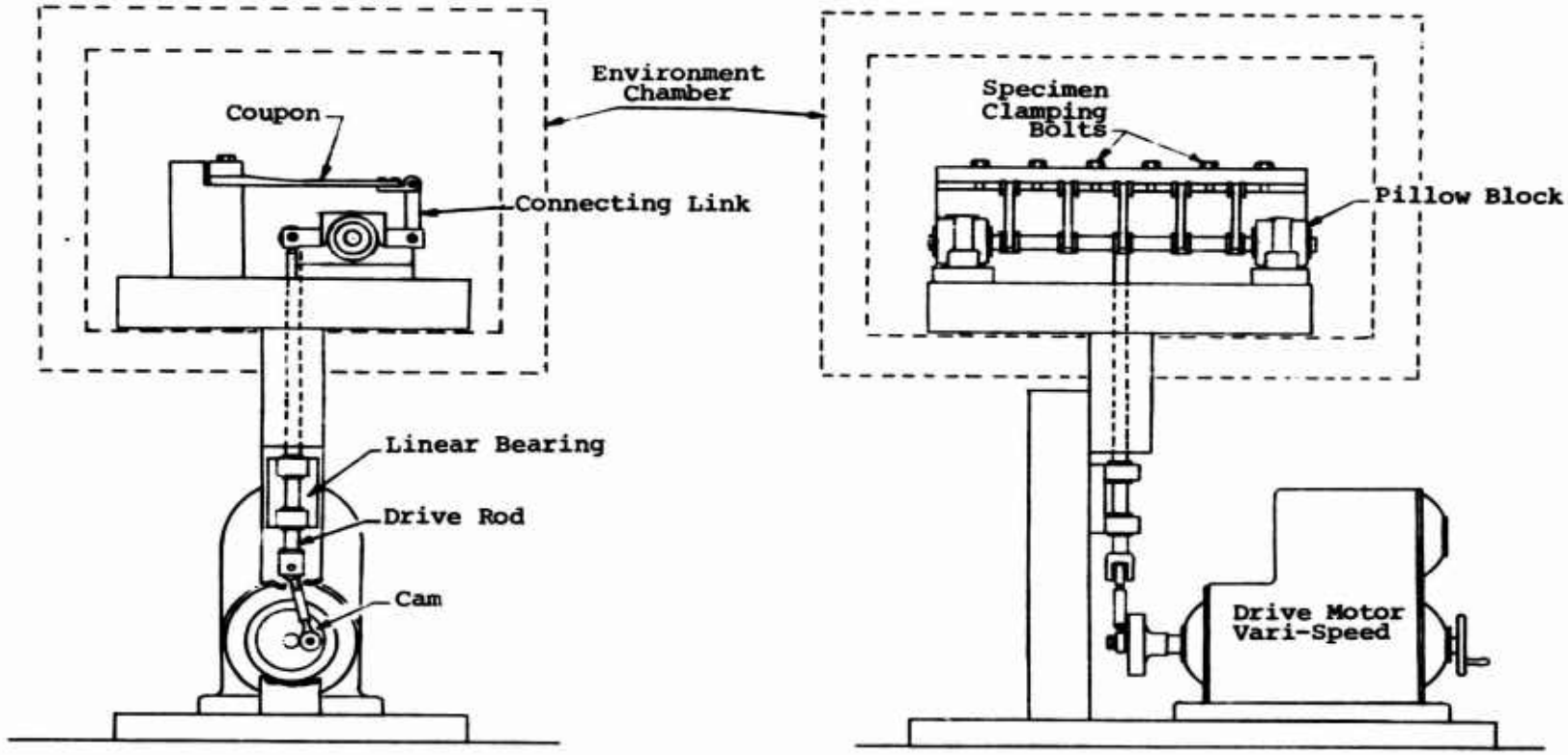

Figure 5. Test Setup.

TABLE II. CONSTANT-DEFLECTION REVERSE-BENDING FATIGUE TEST DATA

Specimen No.	Coating	Specimen Thickness (in.)	Defl (in.)	Maximum Stress (psi) (approx)	Cycles x 10^6	Comments
124	Bare	.148	1.36	81,200	4.0	Runout - Matl XP 114-1014S
126	Bare	.148	1.36	81,200	10.0	Runout - Matl XP 114-1014S (Speed 1720 RPM)
127	Bare	.148	1.36	81,200	3.6	Runout - Matl XP 114-1014S
134	Bare	.150	1.44	86,700	2.1	Runout
134	Bare	.150	1.50	90,200	1.1	Runout
150	Bare	.144	1.60	96,000	4.1	Runout
152	Bare	.147	1.60	96,000	4.0	Runout
154	Bare	.149	1.60	96,000	3.5	Premature Failure - Delaminated
161	Bare	.146	1.60	96,000	4.5	Runout
162	Bare	.146	1.60	96,000	3.2	Premature Failure - Delaminated

Material - Unidirectional S Glass Type 1002-1014S (200 EC) except where noted.

Loading - 25,000 psi steady $\pm$ vibratory to equal maximum stress.

Speed - 200 cpm except where noted.

Test Conditions - Room temperature, humidity not controlled.

cluster was set up to facilitate vertical adjustment to yield the specified intensity on the upper surface (the maximum stress side) of the exposed specimens.

Temperature and humidity conditions within the chamber were program controlled and continuously recorded. Specimens were installed for test both unprotected or protected with one of the three candidate coatings. During the installation, MIL-S-8802 polysulfide sealant was employed at rig attachment points and allowed to cure 24 hours to facilitate complete sealing of coated specimens.

Tests were run continuously on a 24-hour basis except weekends, with frequent monitoring for specimen condition from 8:00 a.m. to 12 midnight. Specimens exhibiting failures at the first daily viewing were assumed to have failed at the mid-point time from previous viewing. A maximum error of $\pm$ 50,000 cycles in failure point could result from this inspection procedure. Such an error, however, would not be significant to influence the outcome of this task.

Results of tests under environmental conditions are shown in Table III and graphically represented in Figure 6. Typical conditions of specimen groups after testing are shown in Figures 7 through 10.

DISCUSSION OF RESULTS

The influence of 95 percent relative humidity at 120°F on flexure testing was most dramatic, with all groups showing severe degradation prior to completing the first 3-day cycle. Bare and MIL-L-19537 acrylic coated specimens were characterized as the earliest failures, with the bare specimens exhibiting the most gross damage and the acrylic coating affording essentially no protection. MIL-C-81773 urethane and Adiprene L-167 coated specimens delayed onset of failure compared to bare and acrylic groups. All specimens tested at the 85,000 psi stress level exhibited detrimental effects from environment, but to a significantly lower degree compared to the higher stressed specimens. This marked improvement in performance at the lower stress level suggests that significant improvement in the environmental resistance of both material and coatings can be expected at the still lower operating stress levels of the Elastic Pitch Beam Tail Rotor as reported in the pitch beam fatigue test section.

The MIL-L-19537 acrylic and MIL-C-81773 urethane protected specimens disclosed surface checks in the coating as a result of repeated flexing. Checking of the acrylic coating was observed to be more severe and extended over a greater area of the specimens compared to that evident on the urethane

TABLE III. RESULTS OF CONSTANT-DEFLECTION REVERSE-BENDING FATIGUE TEST UNDER ENVIRONMENTAL CONDITIONS

Specimen No.	Coating	Specimen Thickness (in.)	Defl (in.)	Maximum Stress (psi) (approx)	Cycles x 10^6	Time (hr)	Comments
170	Bare	.145	1.6	96,000	.33	26	-
172		.145	1.6	96,000	.33	26	-
174		.148	1.6	96,000	.52	44	-
175		.153	1.6	96,000	.14	11	-
176		.140	1.6	96,000	.33	26	-
201		.137	1.42	85,000	1.81	144	No failure.
171	Acrylic	.137	1.6	96,000	.57	48	-
180	MIL-L-19537	.164	1.6	96,000	.12	10	-
181		.135	1.6	96,000	.12	10	-
198		.150	1.42	85,000	.94	72	No failure - finish severely checked.
199		.136	1.42	85,000	.94	72	No failure - finish severely checked.
182	Urethane	.137	1.6	96,000	.87	72	No failure.
183	MIL-C-81773	.139	1.6	96,000	.53	44	-
184		.136	1.6	96,000	.30	20	-
185		.138	1.6	96,000	.60	48	-
186		.137	1.6	96,000	.60	48	-
193		.138	1.42	85,000	1.14	96	Premature failure from clamp fretting - coating exhibits checking.
202		.140	1.42	85,000	1.76*	144	Coating checked.
204		.138	1.42	85,000	1.76*	144	Coating checked.
207		.143	1.42	85,000	4.19	360	Coating checked at 1.6 x 10^6.
208		.138	1.42	85,000	4.19	360	Coating checked at 1.6 x 10^6.

TABLE III - Continued

Specimen No.	Coating	Specimen Thickness (in.)	Defl (in.)	Maximum Stress (psi) (approx)	Cycles x 10^6	Time (hr)	Comment
188	Adiprene L167 .009/.010 Thk	.147	1.6	96,000	.87	72	Premature failure - fretting from loose clamp.
190		.146	1.6	96,000	.60	48	-
191		.147	1.6	96,000	.60	48	Premature failure - delaminated.
195		.154	1.42	85,000	2.71	216	Start of spanwise breaks in coating - 1.93 x 10^6.
203		.138	1.42	85,000	1.76*	144	Start of spanwise breaks in coating - 1.46 x 10^6.
205		.143	1.42	85,000	1.76*	144	Start of spanwise breaks in coating - 1.76 x 10^6.
206		.141	1.42	85,000	3.61	312	Start of spanwise breaks in coating - 2.08 x 10^6.
209		.138	1.42	85,000	4.19	360	Start of spanwise breaks in coating - 3.13 x 10^6.
210		.141	1.42	85,000	4.19	360	Start of spanwise breaks in coating - 3.13 x 10^6.

Material - Unidirectional S Glass Type 1002-1014S (200 EC).

Loading - 25,000 psi steady $\pm$ vibratory to equal maximum stress.

Speed - 200 CPM.

Environmental - First 48 hours @ 95% R.H. @ 120°F followed by 8 hours Sun + 8 hours @ -65°F + 8 hours @ +130°F. After 72 hours, cycle repeats.

*Clamp areas not sealed.

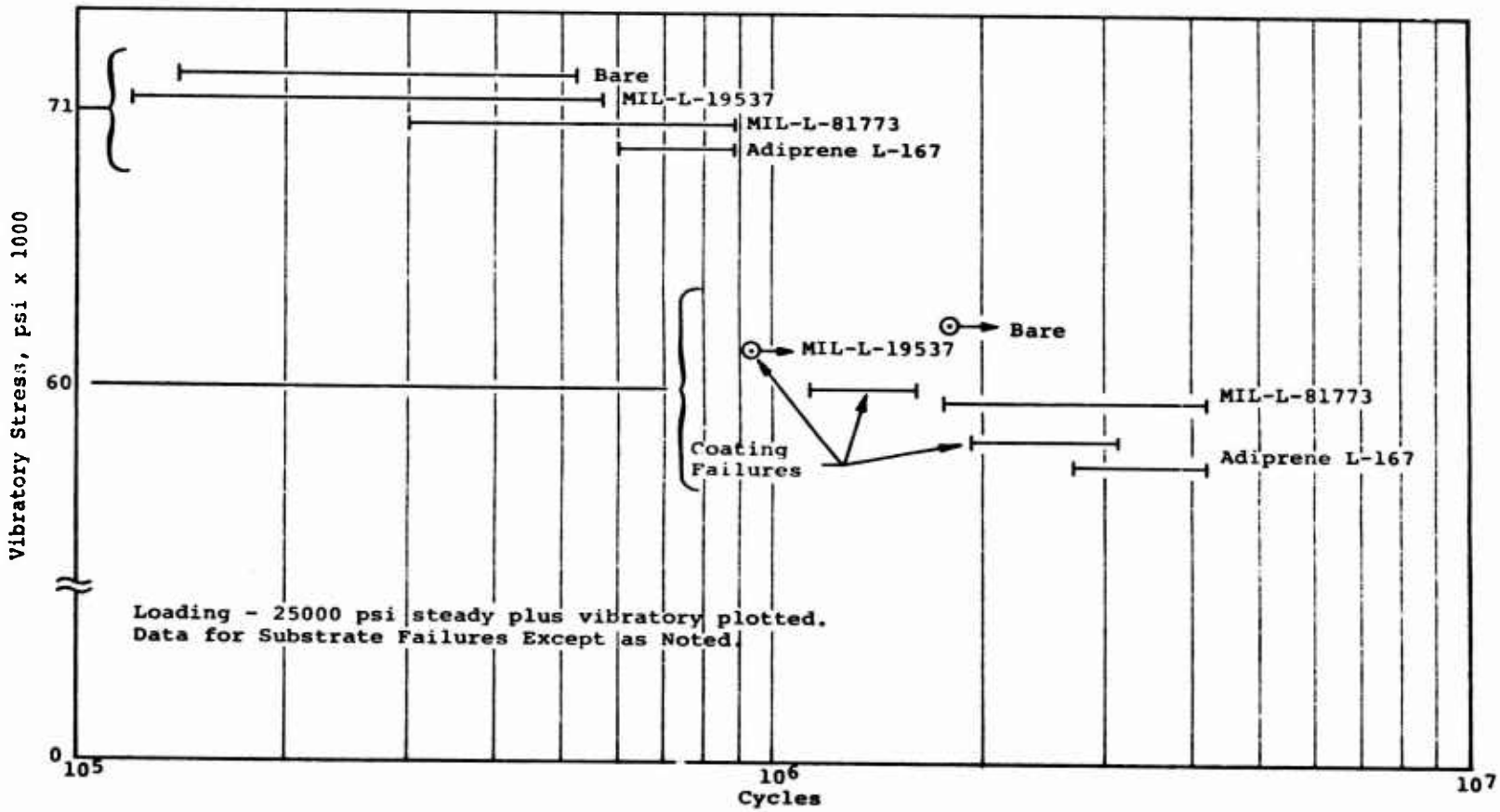

Figure 6. Fatigue Performance of Coatings Under Environmental Exposure.

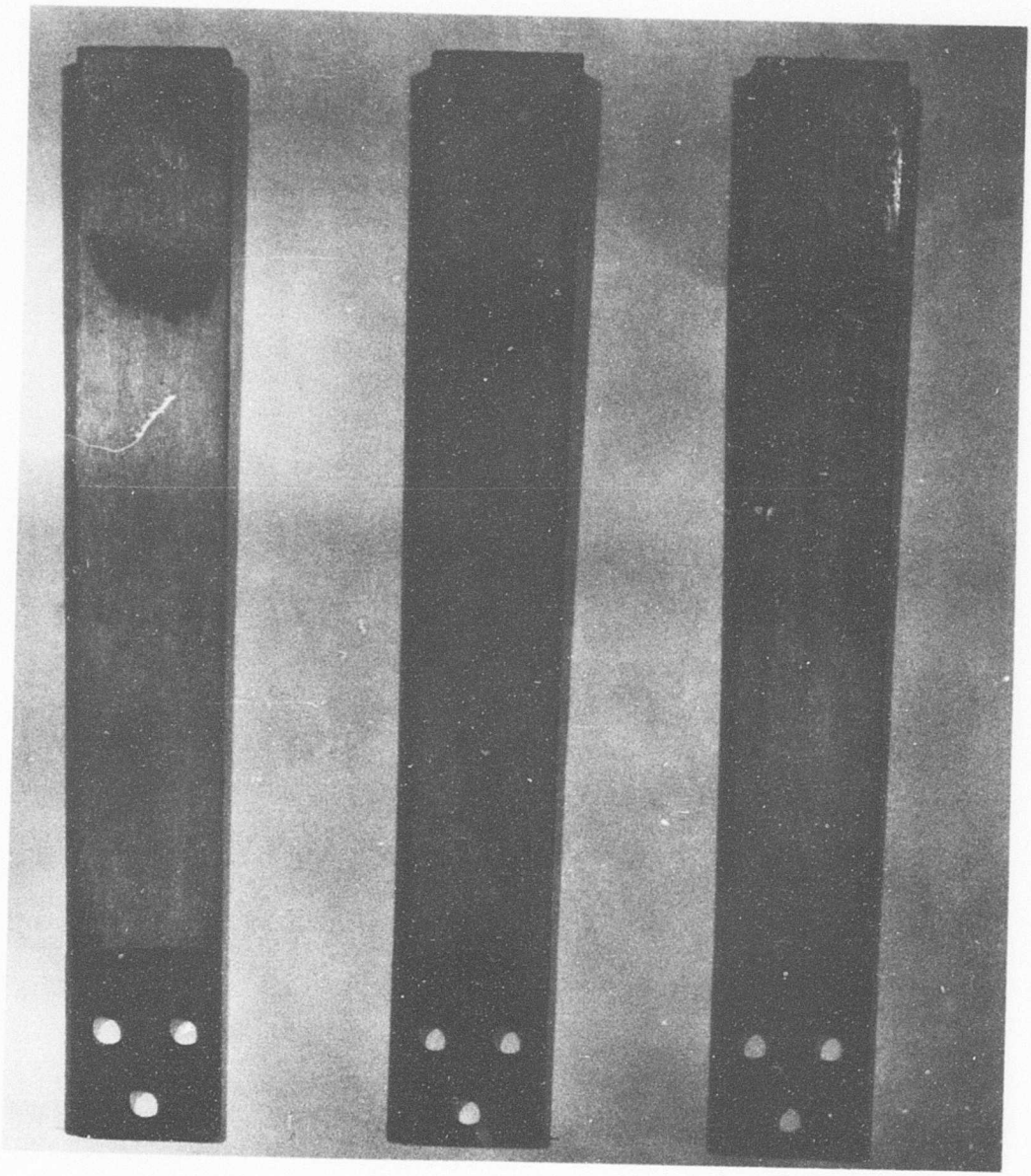

S/N 150 S/N 152 S/N 161

Figure 7. Constant-Deflection Reverse-Bending Fatigue Specimens of Unidirectional S Glass, Type 1002-1014S, Tested at 96,000 psi Maximum Fiber Stress at 200 cpm, No Environment.

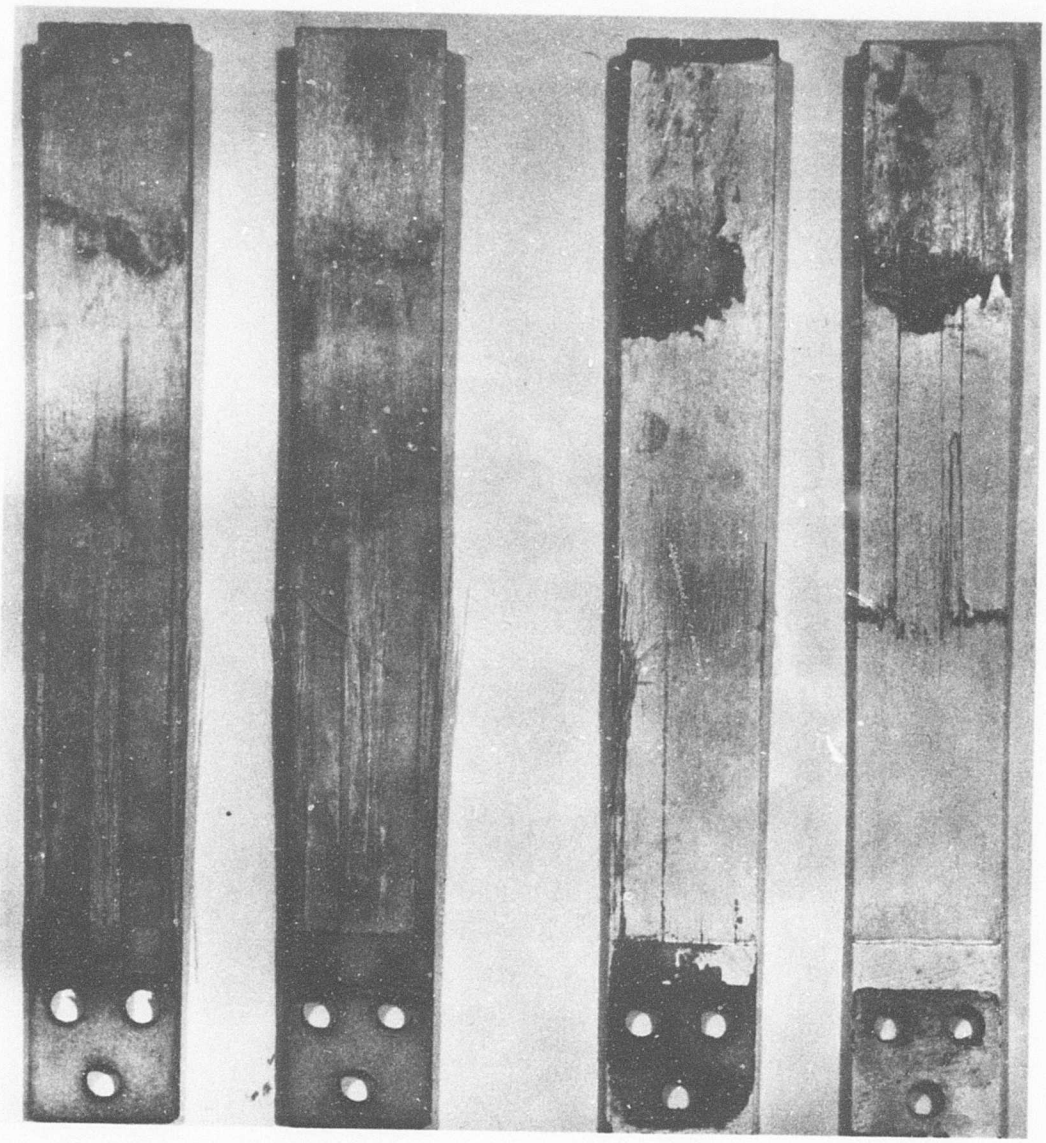

S/N 170 S/N 175 S/N 171 S/N 181

BARE SPECIMENS

COATING: MIL-L-19537
ACRYLIC

Figure 8. Constant-Deflection Reverse-Bending Fatigue Specimens of Unidirectional S Glass, Type 1002-1014S, Tested at 96,000 psi Maximum Fiber Stress at 200 cpm, Bare and Acrylic Coated Specimens Under Environmental Conditions.

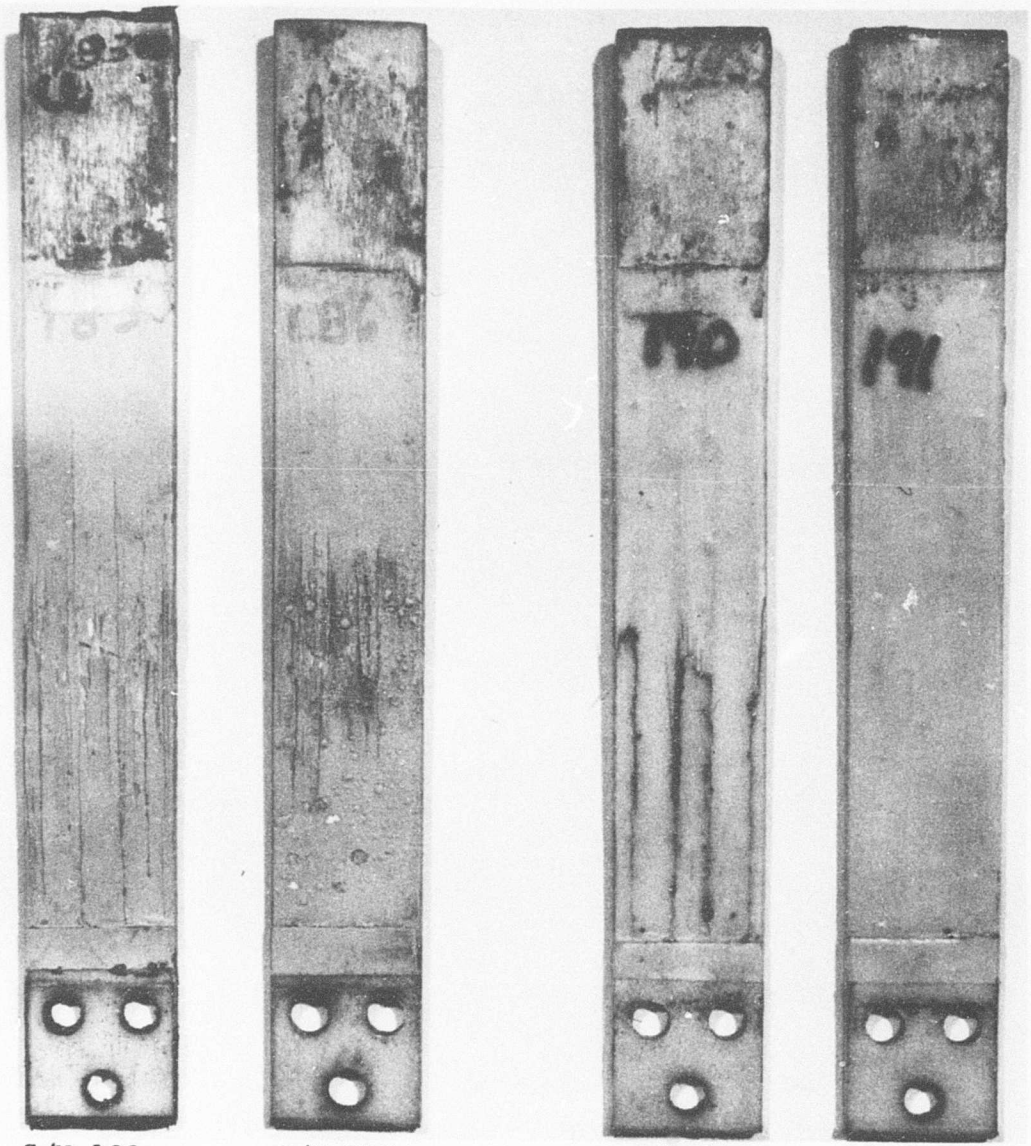

Figure 9. Constant-Deflection Reverse-Bending Fatigue Specimens of Unidirectional S Glass, Type 1002-1014S, Tested at 96,000 psi Maximum Fiber Stress at 200 cpm, Urethane and Adiprene Coated Specimens Under Environmental Conditions.

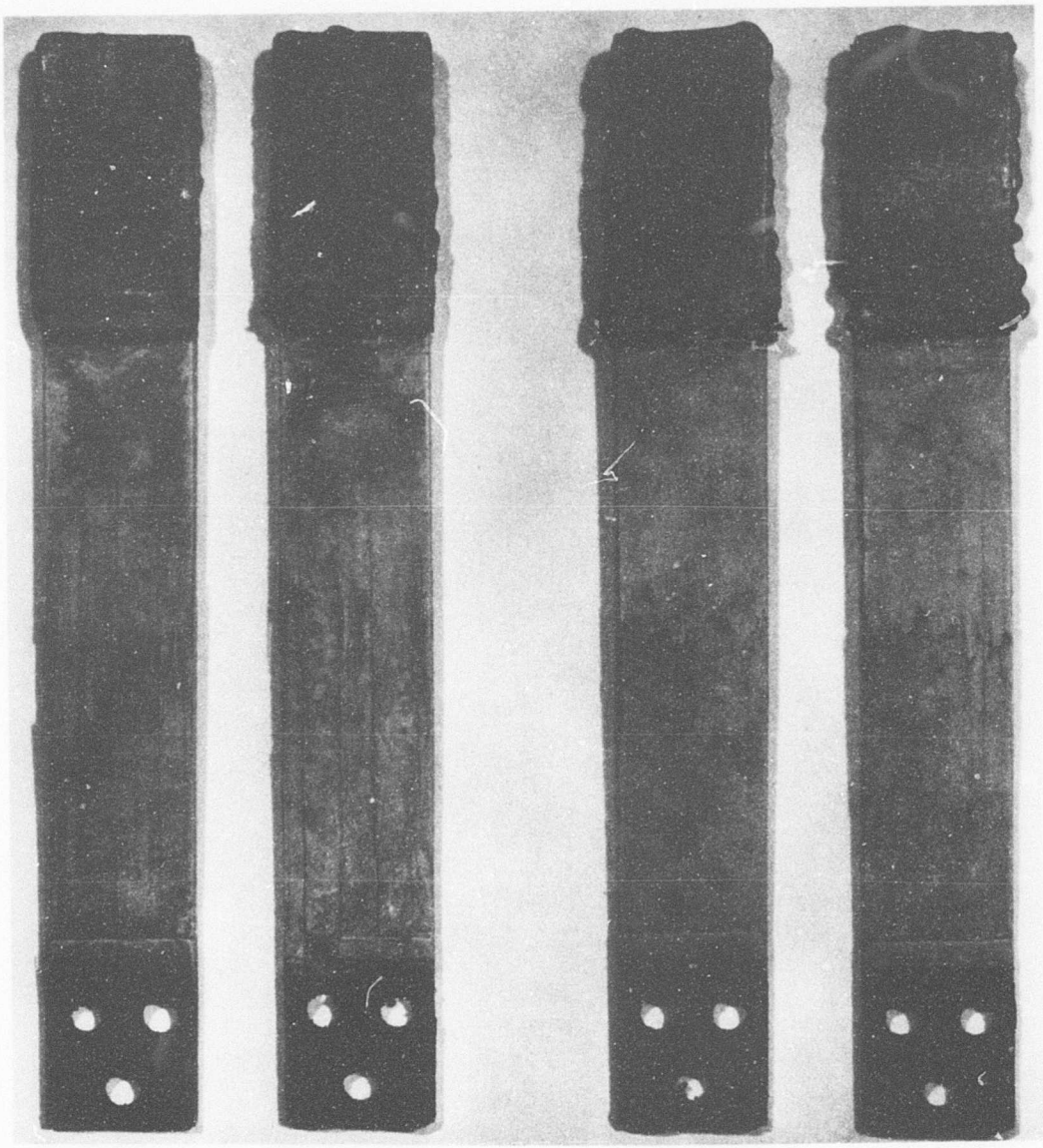

S/N 207 S/N 208 S/N 209 S/N 210

COATING: MIL-C-81773 URETHANE

COATING: ADIPRENE L167 .009/.010 INCH THICK

Figure 10. Constant-Deflection Reverse-Bending Fatigue Specimens of Unidirectional S Glass, Type 1002-1014S, Tested at 85,000 psi Maximum Fiber Stress at 200 cpm, Urethane and Adiprene Coated Specimens Under Environmental Conditions.

specimens. This mode of breakdown renders the protective system ineffective as a moisture barrier and would contribute to early failure of the substrate. The Adiprene coated specimens disclosed no evidence of checking.

The first indication of breakdown in the Adiprene coated specimens appeared as spanwise breaks which emanated from spanwise cracks in the substrate. The useful life of the coatings, therefore, appeared to be limited to the fatigue properties of the substrate at the 85,000-psi stress level.

Specimens 202 and 204 were installed without MIL-S-8802 polysulfide sealant at the clamping points, permitting a faster moisture absorption rate and early failures compared to other specimens of the group. Because of this factor, the time for coating failure was considered premature and not graphically presented in Figure 6.

No adverse effects were directly correlated to -65°F testing or to 130°F testing. The modulus change with temperature would result in a higher stress level at the low temperature and a reduced stress at the high temperature end. Low-temperature testing conceivably could promote checking of the surface finish, though this was not correlated by test.

Solar simulation caused noticeable discoloration of the white acrylic finish and Adiprene L-167 finish. No detectable discoloration was evident on the gray MIL-C-81773 urethane.

CONCLUSIONS

1. The fatigue property of unidirectional S Glass Type 1002-1014S under flexure is severely degraded by humidity when tested at 96,000 psi maximum stress. Coatings provide no significant protection at this stress level.

2. Fatigue properties of unidirectional S Glass Type 1002-1014S are adversely affected by environmental cycling at the 85,000 psi stress level. The marked improvement in performance compared to the 96,000 psi stress level indicates that greater resistance to environmental factors could be expected at lower stress levels typical of normal design usage.

3. Of the candidate materials, Adiprene L-167 affords the greatest protection and is least influenced by flexing.

4. The acrylic coating per MIL-L-19537 and urethane coating per MIL-C-81773 generate surface checks at the stress levels employed, facilitating early moisture entry and early failure compared to Adiprene L-167.

SPRING RATE TEST

SPECIMEN FABRICATION

Specimens were fabricated from full-size elastic pitch beam assemblies including channels and leading-edge attachment. The spar member, however, was terminated at Station 26.5 instead of Station 27.875, and the channel members were shortened forward of the inboard attachment point to the spar since these changes facilitated spring rate testing without compromising the results.

During the bonding operation, aluminum doublers were bonded at the outboard extremities of the specimens to strengthen the section through which the loading was to be applied. Next the beam assembly was attached to the hub utilizing urethane strips and adhesive, except that a mold release agent was applied to the hub to facilitate removal, whereas in the actual installation the hub is bonded to the assembly. As the final step, the exposed glass reinforced plastic sections were coated with MIL-C-23371 epoxy primer and Adiprene L-167 mechanical-damage-resistant coating of .010 inch minimum thickness followed by the application of a fillet of MIL-S-8802 polysulfide sealant at the beam-to-channel and beam-to-hub interface. Figure 11 shows two of the three fabricated specimens.

TEST PROCEDURE

Testing was accomplished in a 60,000-lb-capacity Tinius Olsen Tensile Tester with a Conrad/Missimer Temperature Cabinet positioned between the loading heads. The cabinet was set to the desired test temperature with the spar temperature being monitored at the hub and each extremity of the flexible spar element. After the elastic pitch beam component was stabilized at the required test temperature for a minimum of 10 minutes, the load was applied. Tests were performed at three load levels of 6,000, 12,500 and 15,000 pounds, respectively. The 12,500-lb load represents the normal operating CF load of the UH-1 tail rotor blade.

Load was transmitted to the specimen through 3/4-inch-diameter holes at each end. Wedge-shaped aluminum grips were fabricated with a matching taper to the tensile tester load heads and fastened to the specimen with a 3/4-inch-diameter pin. As the load head extended, the wedge-shaped grips nested into position and rigidly locked the specimen.

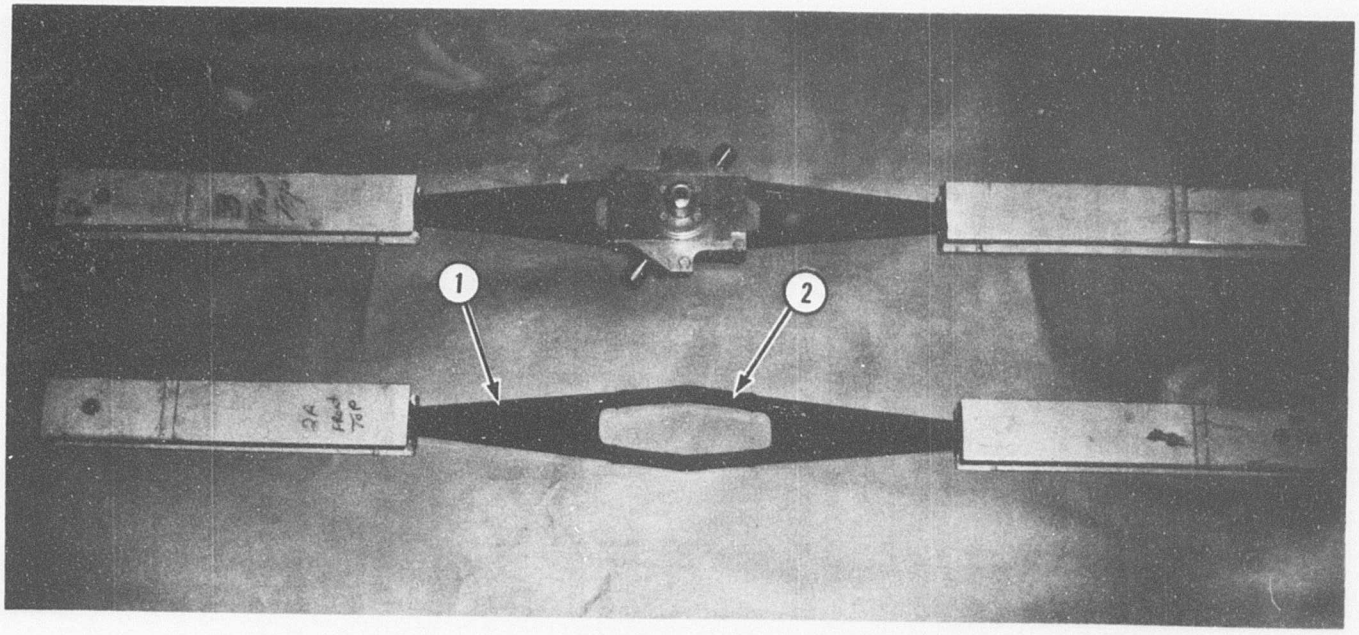

(1) Adiprene L-167 Coating - Elastic Pitch Beam Region.

(2) Urethane Filler Hub to Spar Attachment Area.

Figure 11. Elastic Pitch Beam Test Specimens With and Without Hub Installation.

Torsion loading was applied to the specimen through a torque tube suspended from a 1/2-inch-diameter pin through the center of the hub. The base of this torque tube consisted of a 10.187-inch-diameter flange with a .125-inch-deep circumferential groove into which two 1/8-inch-diameter cables were attached 180 degrees apart to support weights which exerted the torsional load. A retaining plate was mounted to the underside of the chamber and above the torque tube flange containing three bearing rollers 120 degrees apart for positioning and to facilitate torsion movement. Angular displacement was measured with the aid of a scale mounted along the flange circumference and a hairline indicator applied to each pan. The displacement was measured to the nearest 1/32 inch. This 1/32-inch displacement along the circumference of the 10.187-inch-diameter circle was equivalent to 0.36 degree of twist. Torque load was calculated based on the total weight in both pans times the torque radius of 5.031 inches divided by 2. Division by 2 is required to obtain torque necessary to twist one elastic pitch beam arm, since in the test setup both arms were twisted simultaneously. Torque load divided by angular displacement provided the spring rate. The test setup is illustrated in Figures 12 and 13.

TEST RESULTS

Table IV tabulates twist angle at the maximum applied torque for the test temperatures and load levels following the various exposure conditions. The number reported in each block represents that obtained from the second run or in some cases a third run in order to duplicate the data points or to obtain good correlation between consecutive runs. It was observed at the start of this task that the initial run could result in an error of approximately 1 degree maximum since on loading and unloading, the scale did not necessarily return to the initial zero position. However, on second and third runs, the zero position would repeat within 1/32 inch or 0.36 degree.

Table V converts data from Table IV into spring rate for the same test temperature, load levels, and exposure conditions.

Specimens were stabilized at the designated test temperature, and the required CF load was applied. The zero reading on the scale was recorded to the nearest 1/32 inch, and weights were added to each pan. For each of 10 load increments, the scale reading was recorded to the nearest 1/32 inch and torque versus degree of twist was calculated. Plots of the data of torque versus twist yielded a straight-line function from zero to the final data point. Consequently, the raw data for torque versus degrees of twist are not being reported, since the plots can be readily duplicated from the data reported.

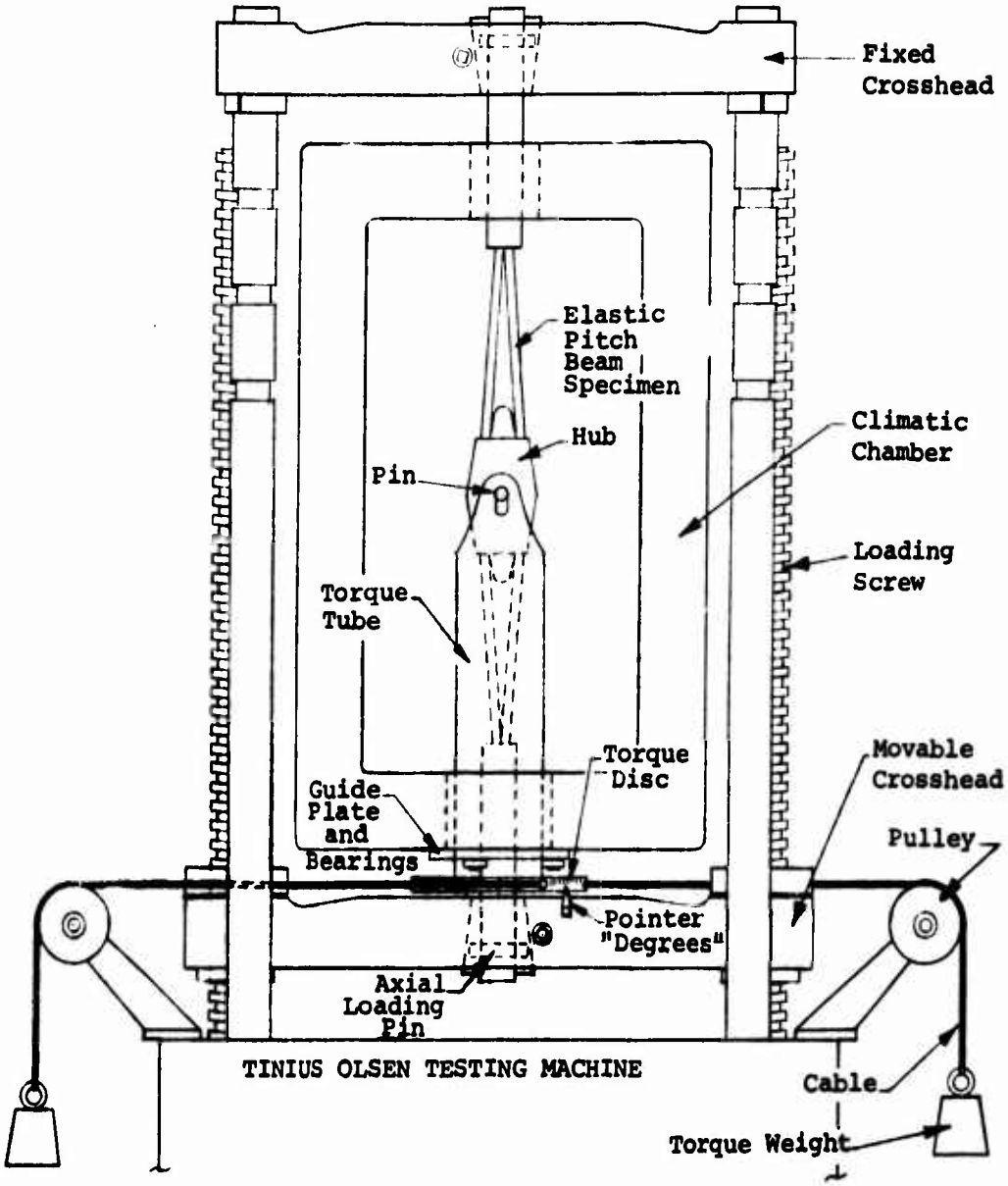

Figure 12. Spring Rate Test Setup.

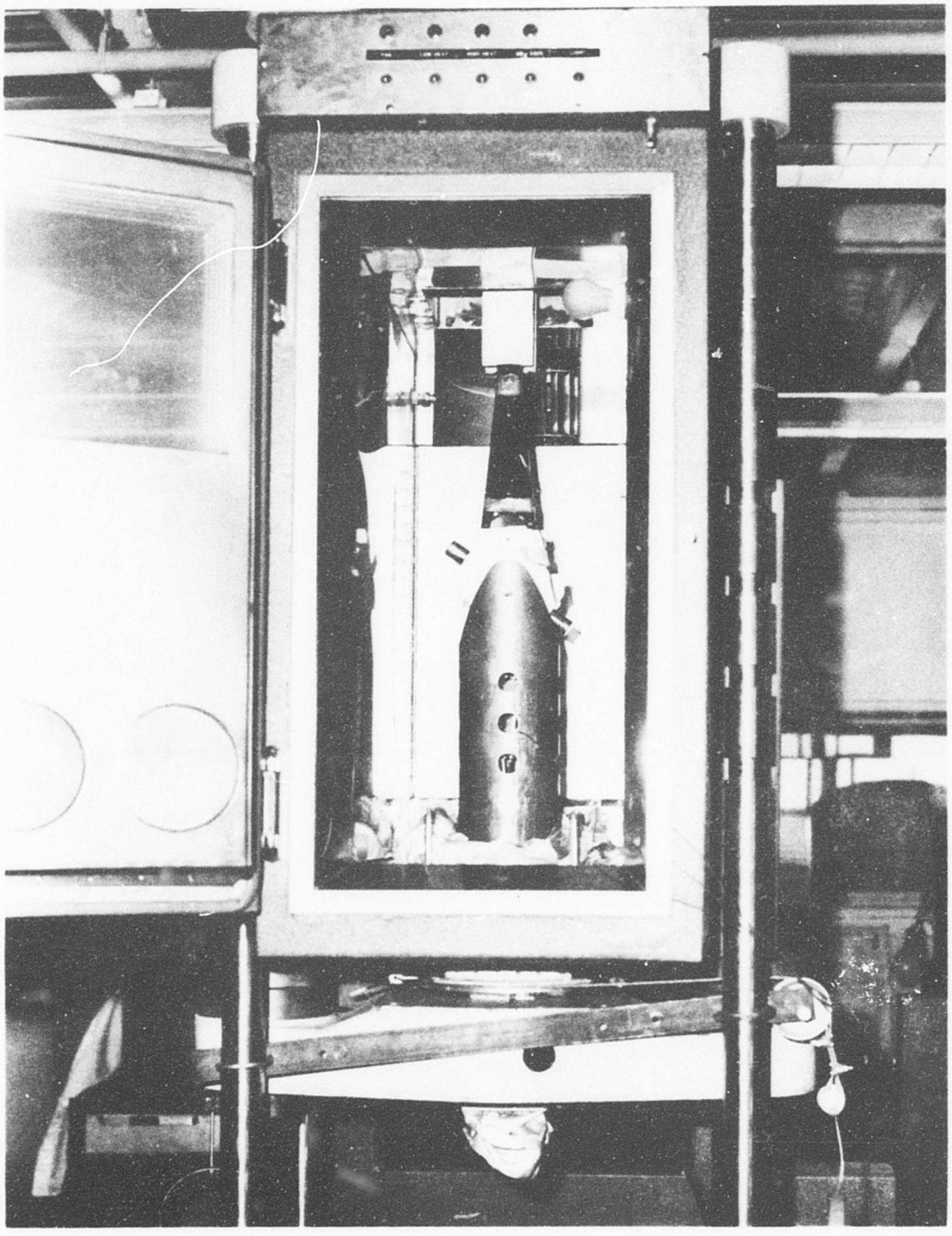

Figure 13. Installation of Flexural Spar in Tinius Olsen Tensile Tester.

TABLE IV. DEGREES OF TWIST AT 955 IN.-LB TORQUE AT VARIOUS TEMPERATURE AND LOAD LEVELS FOLLOWING ENVIRONMENTAL EXPOSURE

Test Temperature		-65°F			Room Temp			130°F			140°F			150°F			160°F		
C.F. Load (lb)		6,000	12,500	15,000	6,000	12,500	15,000	6,000	12,500	15,000	6,000	12,500	15,000	6,000	12,500	15,000	6,000	12,500	15,000
Spar No.	Environmental Exposure																		
2A	-	13.4	11.3	-	14.8	12.7	-	15.5	13.4	-	-	-	-	-	-	-	-	-	-
2B	-	12.7	12.0	-	15.5	14.1	-	14.8	13.4	-	-	-	-	-	-	-	-	-	-
3	-	12.7	11.3	-	14.8	13.4	-	15.5	13.4	-	-	-	-	-	-	-	-	-	-
2A	48 Hr @ -65°F	12.7	11.3	-	15.5	14.0	-	15.9	14.1	-	-	-	-	-	-	-	-	-	-
3	48 Hr @ -65°F	13.4	12.0	-	15.5	13.8	-	16.2	14.8	-	-	-	-	-	-	-	-	-	-
2A	48 Hr @ 130°F	13.1	11.7	-	14.8	13.1	-	15.5	13.8	-	-	-	-	-	-	-	-	-	-
3	48 Hr @ 130°F	13.1	11.7	-	14.8	13.1	-	15.5	13.4	-	-	-	-	-	-	-	-	-	-
2A	48 Hr @ 120°F and 95% R.H.	14.1	12.7	-	17.0	15.2	-	17.7	15.5	-	-	-	-	-	-	-	-	-	-
3	48 Hr @ 120°F and 95% R.H.	12.5	10.6	-	15.2	13.4	-	16.2	14.1	-	-	-	-	-	-	-	-	-	-
2A	18-Day Humidity-Sun-Heat Cycling	13.4	12.0	12.0	15.5	13.4	12.7	16.2	14.1	13.4	17.0	14.8	14.1	17.0	14.8	14.1	17.7	15.5	14.8
3	18-Day Humidity-Sun-Heat Cycling	12.7	11.7	11.3	15.9	13.4	13.1	15.2	14.1	13.4	15.5	13.8	13.4	15.9	14.1	13.4	16.6	14.8	14.1
2B	Control No Exposure	12.7	11.3	10.9	15.5	13.4	13.1	15.5	14.1	13.4	16.6	14.1	13.8	16.2	14.8	14.1	16.4	15.2	14.8

TABLE V. TORSIONAL SPRING RATE, IN.-LB/DEGREE, AT VARIOUS TEMPERATURE AND LOAD LEVELS FOLLOWING ENVIRONMENTAL EXPOSURE

Test Temperature		-65°F			Room Temp			130°F			140°F			150°F			160°F		
C.F. Load (lb)		6,000	12,500	15,000	6,000	12,500	15,000	6,000	12,500	15,000	6,000	12,500	15,000	6,000	12,500	15,000	6,000	12,500	15,000
Spar No.	Environmental Exposure																		
2A	-	35.7	42.2	-	32.2	37.6	-	30.8	35.7	-	-	-	-	-	-	-	-	-	-
2B	-	37.6	39.9	-	30.2	33.0	-	32.2	35.7	-	-	-	-	-	-	-	-	-	-
3	-	37.6	42.2	-	32.2	35.7	-	30.8	35.7	-	-	-	-	-	-	-	-	-	-
2A	48 Hr @ -65°F	37.6	42.2	-	30.8	34.1	-	30.4	33.9	-	-	-	-	-	-	-	-	-	-
3	48 Hr @ -65°F	35.7	39.9	-	30.8	34.6	-	29.5	32.2	-	-	-	-	-	-	-	-	-	-
2A	48 Hr @ 130°F	36.5	40.8	-	32.2	35.4	-	30.8	34.6	-	-	-	-	-	-	-	-	-	-
3	48 Hr @ 130°F	36.5	40.8	-	32.2	35.4	-	30.8	35.7	-	-	-	-	-	-	-	-	-	-
2A	48 Hr @ 120°F and 95% R.H.	33.9	37.6	-	28.1	31.4	-	27.0	30.8	-	-	-	-	-	-	-	-	-	-
3	48 Hr @ 120°F and 95% R.H.	38.1	45.0	-	31.4	35.7	-	29.5	33.0	-	-	-	-	-	-	-	-	-	-
2A	18-Day Humidity-Sun-Heat Cycling	35.7	39.9	39.9	30.8	35.7	37.6	29.5	33.0	35.7	28.1	32.2	33.9	28.1	32.2	33.9	27.0	30.8	32.2
3	18-Day Humidity-Sun-Heat Cycling	37.6	40.8	42.2	30.4	35.7	35.4	31.4	33.0	35.7	30.8	34.6	35.7	30.4	33.0	35.7	28.8	32.2	33.0
2B	Control No Exposure	37.6	42.2	43.8	30.2	35.7	35.4	30.8	33.0	35.7	29.8	33.9	34.6	29.5	32.2	33.9	29.1	31.4	32.2

The spring rate on Specimen 3 after 48 hours humidity exposure exhibited a slight increase in stiffness at the -65°F test condition compared to the other components. This test article, on removal from the humidity chamber in a wet condition, was quickly tested at -65°F, resulting in a coating of frost and ice particles. Other specimens, on removal from the environmental chamber, were tested at room temperature, at elevated temperature, and finally at -65°F.

CONCLUSIONS

1. The three full-scale elastic pitch beam spar and hub assemblies exhibit equivalent spring rates for a given exposure and test condition.

2. The spring rate at 130°F is essentially the same as that determined at room temperature; whereas at -65°F, a 10 to 15 percent increase in stiffness is evident.

3. At 160°F, the spring rate is approximately 10 to 15 percent softer than at room temperature.

4. The various exposure conditions have no significant effect on spring rate.

PITCH BEAM FATIGUE TEST

BACKGROUND

The three pitch beams which had undergone spring rate testing were subsequently fatigue tested. Prior to fatigue test, specimen 2B was exposed to the same environmental cycles already endured by specimens 2A and 3.

TEST SETUP

A customized test fixture was designed and fabricated to conduct the fatigue portion of the test program. See Figure 14. This fixture was capable of applying the steady-state loading upon which were superimposed the cyclic in-plane and out-of-plane bending moments.

STEADY-STATE LOADING

The centrifugal loading was applied by hydraulic cylinders, and its magnitude (12,500 lb) was monitored by a calibrated strain-gaged load link. Steady shaft torque (1,700 in.-lb) was applied at the hub using deadweights attached to a torque arm. Fixed blade pitch (+10 degrees) was introduced by the blade pitch links attached to an adjustable cross beam and measured by a bubble protractor. A steady thrust load (600 lb) was applied at the hub via a bungee and cable system; this loading was also monitored by a calibrated strain-gaged load link.

CYCLIC LOADING

The in-plane and out-of-plane bending was applied simultaneously to the beam at the hub centerlines by pushrods attached to cams driven by an electric motor at a frequency of 565 rpm. Phasing was adjusted by indexing the timing belts such that both moments peaked together.

Both pushrods were instrumented with a full axial bridge, and a full bending bridge was installed at Blade Station 13. All bridges were calibrated prior to the test.

The output of these strain-gage bridges was fed to a computer via a PCM incoder. Test data was then tabulated every 30 minutes on a teletype; wave form and phasing were observed on oscillograms. Additionally, specimen elongation and torsional spring rate were obtained daily for detecting possible incipient failure.

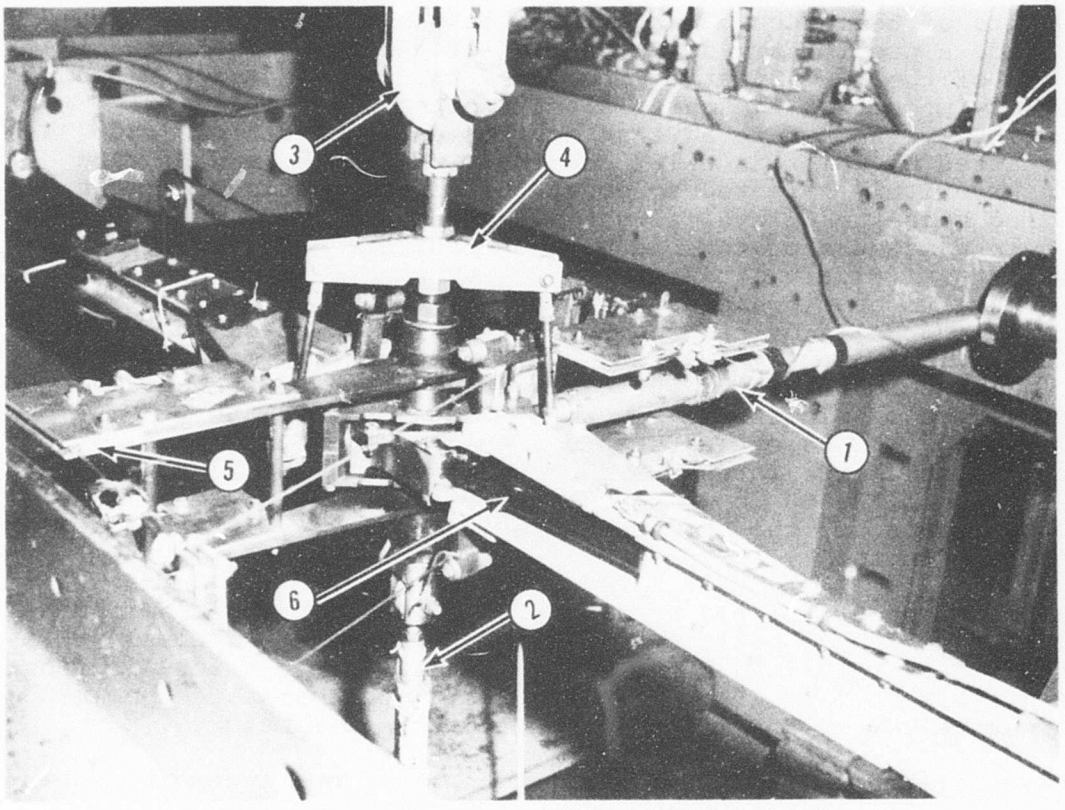

(1) In-Plane Bending Input Rod.

(2) Out-of-Plane Bending Input Rod.

(3) Steady Blade Thrust Load.

(4) Fixed Pitch Adjustment.

(5) Steady Shaft Torque Input Lever.

(6) Test Specimen.

Figure 14. Close-Up of Hub Area.

SIGNIFICANCE OF RESULTS

Results of the pitch beam fatigue tests shown in Figure 15 provide a preliminary demonstration of the structural capabilities of the UH-1 Elastic Pitch Beam tail rotor design. Load levels imposed on the three elastic pitch beam specimens previously exposed to adverse environmental conditions and protected by Adiprene L-167 coating (S/N 2A, 2B, and 3) were conservatively selected to cover the flight loadings anticipated during high-speed level flight and the majority of maneuvers to obtain a measure of the pitch beam's fatigue performance. The ordinate of Figure 15 is the vibratory stress in the composite spar due to bending loads imposed while the abscissa is the number of cycles of bending stress endured, plotted to a log scale. The steady mean stress due to centrifugal force applied to all specimens was 27,400 psi. In addition to the bending stress cycles plotted in Figure 15, specimens 2B and 3 were subjected to 2000 cycles each of repeated application of centrifugal force (ground-air-ground cycle). The load range was zero to 12,500 lb (0 to 27,400 psi) simulating repeated rotor runups for the purpose of including low cycle fatigue damage effects.

Superimposed at the top of Figure 15 is the torsional spring rate specimen 2A, plotted versus number of stress cycles. Preliminary results had shown some decrease in torsional spring rate for specimens 2B and 3 after test; consequently, specimen 2A was tested to specifically monitor this parameter.

Loads applied to the elastic pitch beam fatigue specimens shown in Figure 16 were converted to stresses at Station 3 so that direct comparisons may be made with two unexposed and unprotected UH-1 elastic pitch beam tail rotor assemblies fatigue tested under Contract DAAJ02-72-C-0006. As shown in Figure 15, elastic pitch beam specimen S/N 2B and blade assembly S/N 4 were tested to 10^6 cycles at a vibratory stress level of $\pm$39,100 psi to simulate a maneuver condition, while elastic pitch beam specimen S/N 3 and blade assemblies S/N 3 and 7 were tested to 10^7 cycles at a vibratory stress level of $\pm$28,000 psi to simulate a level somewhat higher than the high-speed level-flight condition. Elastic pitch beam specimen S/N 2A was step-tested in 2×10^6 cycle increments to 10^7 cycles at a maximum vibratory stress level of $\pm$15,900 psi in an effort to establish the endurance limit and to determine the onset of torsional spring rate decay.

Observations made during the test program and examinations of the specimens following completion of these tests indicated the following:

1. All specimens continued to transmit full centrifugal force when testing was terminated.

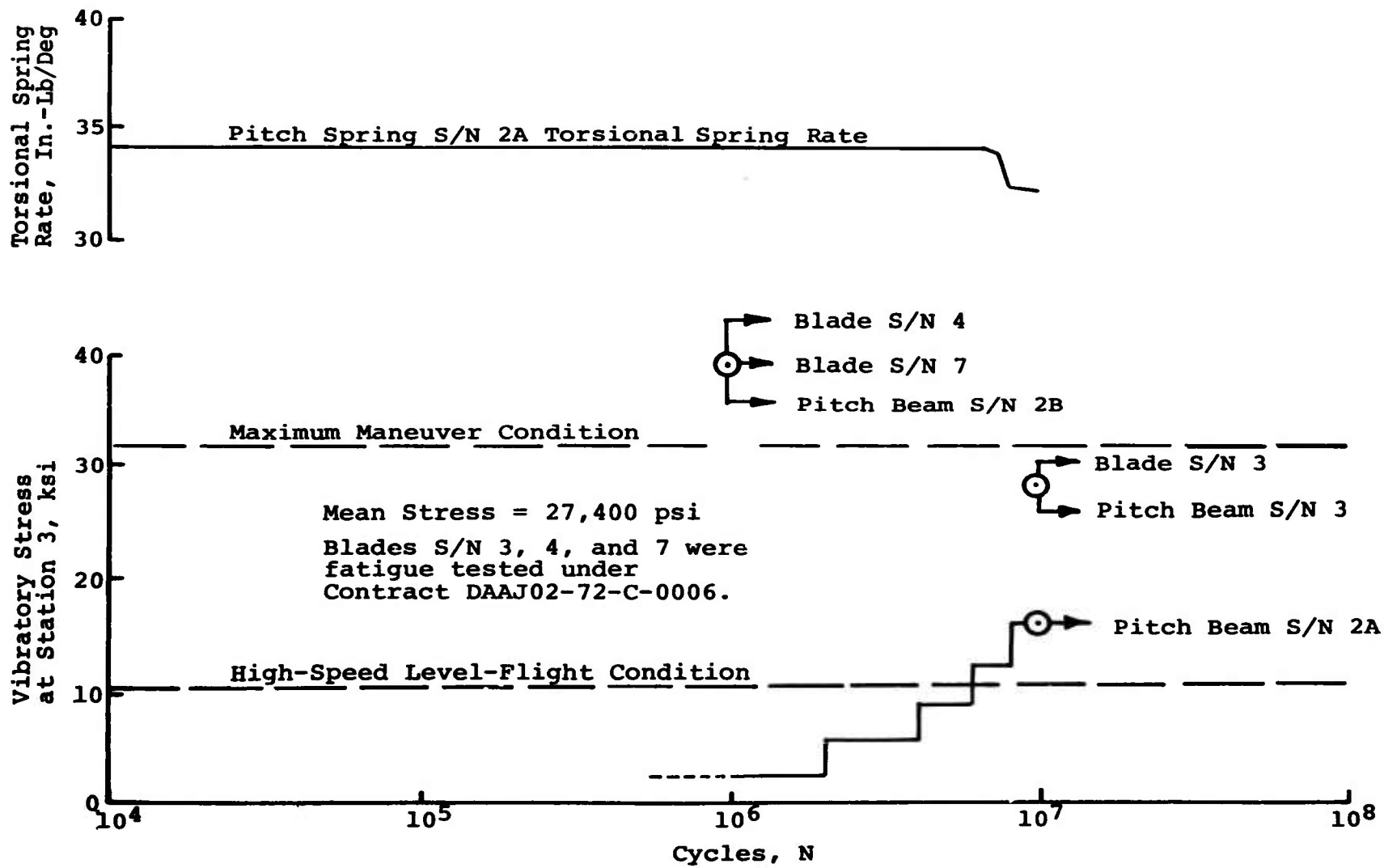

Figure 15. Fatigue Test Results of UH-1 Elastic Pitch Beam Specimens.

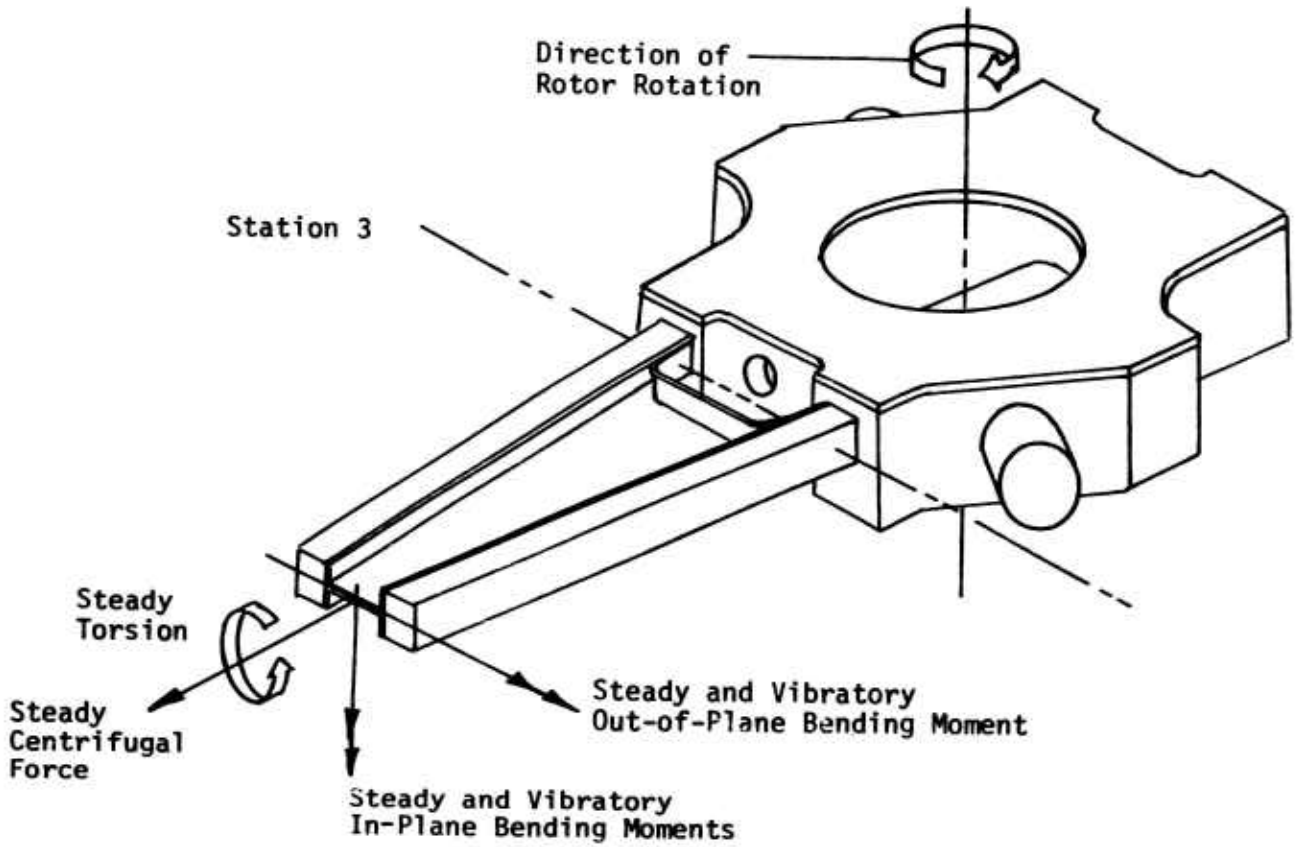

Figure 16. Fatigue Loading Applied to Station 13.

2. No elastic pitch beam strap failures were noted.

3. Delamination of the bond between the elastic pitch beam straps and the flanges of the interconnecting web was evidenced on all three specimens. These separations were the result of high shear stresses caused principally by both edgewise and flatwise bending moments, in part by tensile stresses in the bond in the vicinity of the strap apex as a result of centrifugal force induced splitting forces, and in part by shear stresses in the bond caused by twisting of the elastic pitch beam strap to attain a +10-degree pitch angle.

4. Failure of the filament winding at the outboard juncture of the two elastic pitch beam straps was noted on all three fatigue specimens. These failures were primarily due to excessive tensile stresses imposed on the filaments by the splitting loads associated with the applied centrifugal force as shown in Figure 17. Secondary stresses associated with the delamination of the interconnecting web to elastic pitch beam strap, deformations caused by twisting the straps to obtain the desired pitch angle, as well as the failure of the aluminum channels to properly contain the geometry of the straps at their interfaces may have also contributed to failure of the filament winding.

5. Fatigue cracks occurred in the aluminum channels at their inboard bonded juncture with the elastic pitch beam straps. These cracks are associated with flexing of the channel webs by the elastic pitch beam straps as a result of the loss of filament winding continuity.

6. As shown in Figure 15, the onset of torsional stiffness degradation of elastic pitch beam specimen 2A occurred at approximately 7×10^6 cycles and a vibratory stress level of 4800 psi. At 10^7 cycles and vibratory stress level of approximately 6200 psi, a 5 percent reduction in torsional stiffness had occurred. It is conjectured that this loss of torsional stiffness is related to the separation of the interconnecting web and the elastic pitch beam straps.

The critical areas of the unidirectional 1002-1014S glass elastic pitch beam straps that were closely monitored for signs of wear or filament fracture are as illustrated in Figure 17. These critical points are the point of strap emergence from the hub, the interface between the straps and the interconnecting web, the area of the straps directly under the filament winding, and the interface between the straps and the

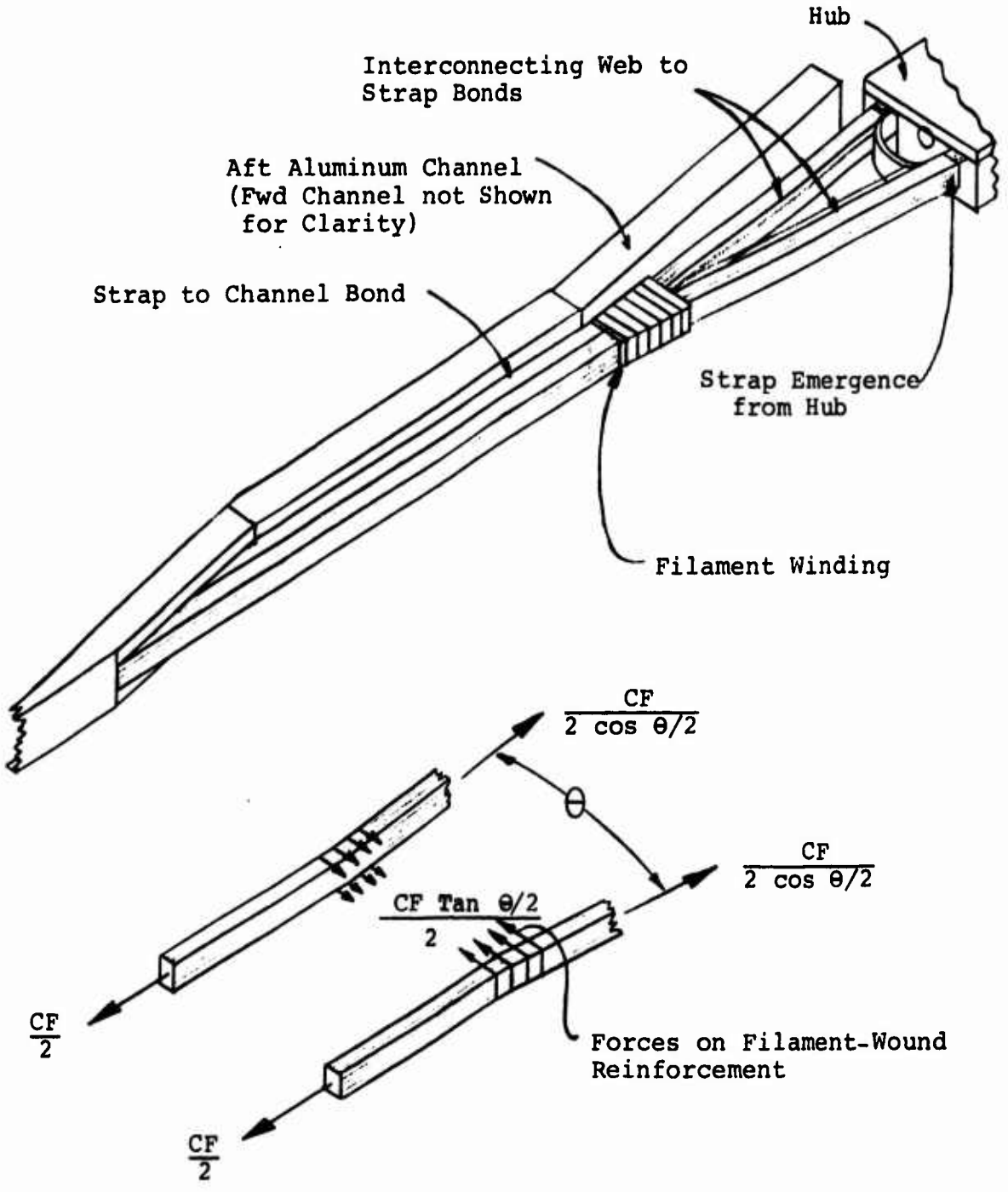

Figure 17. Elastic Pitch Beam Critical Areas.

aluminum channels. The point of strap emergence from the hub is considered to be a prime suspect area for strap failure due to the presence of high vibratory flatwise and edgewise bending stresses, axial stresses due to centrifugal force, torsional shear stresses due to twisting of the straps through the required pitch angles, as well as transverse shear stresses caused by rotor torque and thrust--all of which are conducive to producing high filament stresses, fretting damage at the hub-strap interface, interlaminar shear stresses in the straps, and bond shear stresses between the straps and the elastomer-lined hub interfaces. The straps, along their interfaces with the interconnecting web, are considered to be critical because they are subjected to high shear stresses as well as secondary lateral tensile forces required to maintain the structural continuity between the straps and the web through their bonded juncture, creating interlaminar shear stresses in the outer plies of the strap structure. The area of the straps lying directly beneath the filament winding is also critical because it is subjected to localized lateral shear and bearing forces, tending to cut or fret the filaments of the straps which are in contact with the filament winding. The filament windings are critical themselves because they are subjected to centrifugal induced splitting forces within the laminate caused by a change in strap planform configuration in this localized area. The bonded juncture of the elastic pitch beam strap with the two aluminum channels is also considered to be an area where strap damage might occur. Examination of these critical areas revealed no indication of filament breakage, interlaminar shear failure, or fretting damage associated with the strap design. The conclusion that can be drawn from this evidence is that the strength of the strap and the adequacy of its attachment to the hub and aluminum channels have been clearly demonstrated.

The separation of the interconnecting webs from the elastic pitch beam strap resulted in a degradation of the elastic pitch beam's torsional stiffness of approximately 5 percent at the load levels tested, as noted in Figure 15 for elastic pitch beam specimen S/N 2A. Similar loss of torsional stiffness for specimens 2B and 3 was evidenced; however, precise measurements were not available. Modest redesign of the strap-web connection could substantially improve the fatigue performance of this joint. An improved elastic pitch beam strap-web connection would also be instrumental in eliminating filament winding failures and fatigue cracking of the aluminum channels by redistributing the stresses in these localized areas.

The fatigue test results for the elastic pitch beam specimens previously exposed to adverse environmental conditions and protected by a coating of Adiprene L-167 show no failures or degradations that could be attributed to either the exposure

or the coating when they were compared to the results obtained from fatigue tests performed under Contract DAAJ02-72-C-0006 on unexposed, unprotected specimens (Figure 15). Coating failures were noted only in those areas where a separation between the elastic pitch beam and the interconnecting web occurred. It is therefore anticipated that the service life of the elastic pitch beams will not be affected substantially by adverse environmental conditions experienced and that the protective Adiprene L-167 coating will perform its function satisfactorily provided there is no degradation of the underlying elastic pitch beam structure.

EROSION PROTECTION SYSTEM

TEST PLAN

To accomplish the object of the erosion test program, specimens representing the UH-1 tail rotor configuration were to be subjected to sand testing on the U.S. Air Force's Whirling Arm Apparatus located at the Olin Mathisen Chemical Corporation in New Haven, Connecticut. Sand tests were to be conducted by positioning the test specimens at the outboard tip of the rotor whirling at 530 mph (777 fps) tip velocity and at a sand fall rate to obtain a failure within a 1-hour running time. After establishing the sand fall rate, additional specimens of this design were to be subjected to the same test conditions and the weight loss was to be determined at various increments of the failure time. Then specimens of each candidate configuration were to be subjected to the same sand fall to determine the wear rate and failure time or to achieve an arbitrary runout condition set at 2 hours.

Based on the above test results, the three configurations exhibiting the longest life and lowest wear rate, plus .060-inch polyurethane, and the UH-1 base-line configuration were to be subjected to sand testing for one-half of their established failure life, followed by testing at 500 mph(733 fps) in a nominal 1-inch-per-hour rainfall to failure or for a maximum 2 hours running time.

Based on published data[2-5], it was conjectured that the .030-inch polyurethane material would be one of the better sand-erosion-resistant coatings but that its life in a rain environment would be quite limited. One explanation for the limited life of elastomers in rain is that the relatively high mass of a water droplet exerts stresses within the coating on impact sufficient to cause bond delamination between the coating and substrate[6]. Therefore, the reason for testing the .060-inch-thick urethane in the combination sand and rain test was to ascertain whether the droplet energy could be sufficiently dissipated within the coating to preclude bond-line delamination or to enhance the rain resistance of the coating by some factor greater than that caused by the thickness increase.

TEST FACILITY

The facility selected for erosion testing was the Air Force Whirling Arm Rig at the Olin Mathisen Chemical Corporation, New Haven, Connecticut. The rig has the facilities for both

sand and rain erosion testing. This rig has been in operation for several years and has generated data primarily on elastomeric coatings[4]. The whirl rig and its operation are described in the appendix.

The sand utilized in this program was No. 4 Silica, with the following assay:

Mesh Size	Particle Size	Parts by Weight
100	.0041-.0059	27.0
140	.0041-.0029	72.5
200	.0029	0.5

MATERIAL SELECTION

Review of published literature reveals that two materials, electroformed nickel and polyurethane, have gained recognition as superior erosion-protection coatings for helicopter blade leading edges. Electroformed nickel provides excellent protection in a rain environment[2, 7], but it is susceptible to erosion wear in sand which limits the duration of its usefulness. Testing has been performed on coating thicknesses in the range of .004 to .015 inch over fiberglass and metal substrates. For this evaluation, two electroformed nickel configurations were selected: .016-inch electroformed nickel bonded to .032-inch aluminum bonded to fiberglass; and .032-inch electroformed nickel bonded directly to fiberglass. It was conjectured that a .016-inch-thick electroformed nickel coating would be sufficient to show improved performance compared to the base-line configuration. The reason for the thicker electroformed coating was to facilitate direct comparison with other candidate materials of each thickness over the same substrate.

Polyurethane materials, which are reported to provide excellent resistance to a sand environment, do not endure severe rain conditions. A prime mechanism of failure in elastomers is reported to be an adhesive failure between the coating and the substrate material due to the inability of the material to completely dissipate the impact energy of the droplet within the coating. This energy acts on the bond line as a shear force causing delamination. A delamination is manifested by a localized bubble or blister which is literally torn away by the action of subsequent droplets. It was postulated that a thicker coating would dissipate the impact energy to a greater degree and conceivably preclude premature coating failure. To evaluate this premise, .030-inch- and .060-inch-thick materials were selected for test. Estane tapered boots, manufactured by B.F. Goodrich, and urethane sheet, P0655, manufactured by Armstrong Cork Co., were obtained in both thicknesses.

Other materials selected for test were .031-inch Stellite, Alloy 6B, since the material is utilized on the UH-1 main rotor blade, and .032-inch titanium alloy (6Al-4V), because of its density advantage. A densified manganese chrome oxide ceramic, fused and chemically bonded to a 17-7 stainless steel substrate, was selected for evaluation. This coating, supplied by Kaman, is purported to have a stronger bond to the substrate than that normally obtained by flame-deposited coatings. Although flame-deposited ceramic coatings are extremely hard and afford excellent wear properties, they have exhibited poor performance because of spalling under the impact of sand and rain. Should the bond strength prove to be adequate, the hard ceramic should provide good wear resistance. The next selection was .032-inch stainless steel bonded directly to fiberglass reinforced plastic to evaluate the material in the same thickness as other configurations. The final configuration was .025-inch stainless bonded directly onto .032-inch aluminum, which is the base-line configuration presently utilized on the UH-1 tail rotor.

Specimen configurations and materials selected for erosion testing are as follows:

Specimen Config	Description
1	.025 S.S. Type 302 over .032 Aluminum over GRP
2	.032 S.S. Type 302 over GRP
3	.031 Stellite (6B) over GRP
4	.032 Titanium (6Al-4V) over GRP
5	.016 Electroformed Ni over .032 Aluminum over GRP
6	.032 Electroformed Ni over GRP
7	Manganese-Chrome Oxide over S.S. Type 17-4 over GRP
8	.030 Polyurethane (PO 655) over GRP
9	.030 Polyurethane (Estane) over GRP
10	.060 Polyurethane (PO 655) over GRP
11	.060 Polyurethane (Estane) over GRP

SPECIMEN FABRICATION

The test specimen configuration adaptable to the Olin rig is defined in Figure 18. This specimen is basically an 0025 airfoil, .125 inch thick, 4-3/8 inches long, and terminated at the 1.2-inch chord dimension from the leading edge.

To obtain this airfoil, a male mandrel approximating the 0025 airfoil less the thickness of the erosion specimens was used to form the metal leading edges. Additional tooling consisted of an aluminum base fixture 8 inches x 4 inches x 5 inches with a 5-1/2-inch x 1-1/2-inch x 4-inch cavity, forming rubber 12 inches x 5 inches x 3/4 inch thick and a 1/2-inch-thick phenolic plate with a 6-inch x 1-1/8-inch slot. The forming operation involved attachment of the male mandrel to the compression head of a 60,000-lb-capacity Tinius Olsen tensile tester over the aluminum base fixture. The metal test sample, sheared to 8 inches x 4-3/8 inches with grain parallel to the long dimension, was then sandwiched between the phenolic plate and forming rubber and placed into position between the mandrel and base fixture. The mandrel was then driven through the slot in the phenolic plate, forcing the test sample and forming rubber into the fixture cavity to yield a shape conforming to the 0025 airfoil. All sheet material except titanium was formed in this manner and cut and sanded to the 1.2-inch chord dimension. After forming, the 17-7 PH stainless specimens were austenite conditioned at 1400° ± 25°F for 90 minutes and aged to the TH 1050 condition by heating at 1050° ± 10°F for 90 minutes. The titanium specimens, 6Al-4V annealed conditioned, were formed in the same manner except that the phenolic plate was replaced by a 1/4-inch steel plate with the same size slot. However, in the restrained position within the 1/4-inch steel retaining plate, the airfoil was exactly that required. Each titanium sample as formed was cleaned and coated with Turco 5455 scale-inhibiting compound and then redriven through and restrained by the 1/4-inch steel retaining plate to the desired airfoil. The specimen and retaining plate were placed in a furnace at 1200°F for 30 minutes to relieve the clamping stress in the titanium and to yield the exact 0025 airfoil. Tooling for the forming operation is shown in Figure 19.

The electroformed nickel samples were prepared by Electro-Optical Systems, Inc., Pomona, California, on 2024-T3 alclad aluminum airfoil specimens supplied by Kaman. After plating to the specified coating thickness, the specimens were cut to size and the aluminum substrate was chemically dissolved.

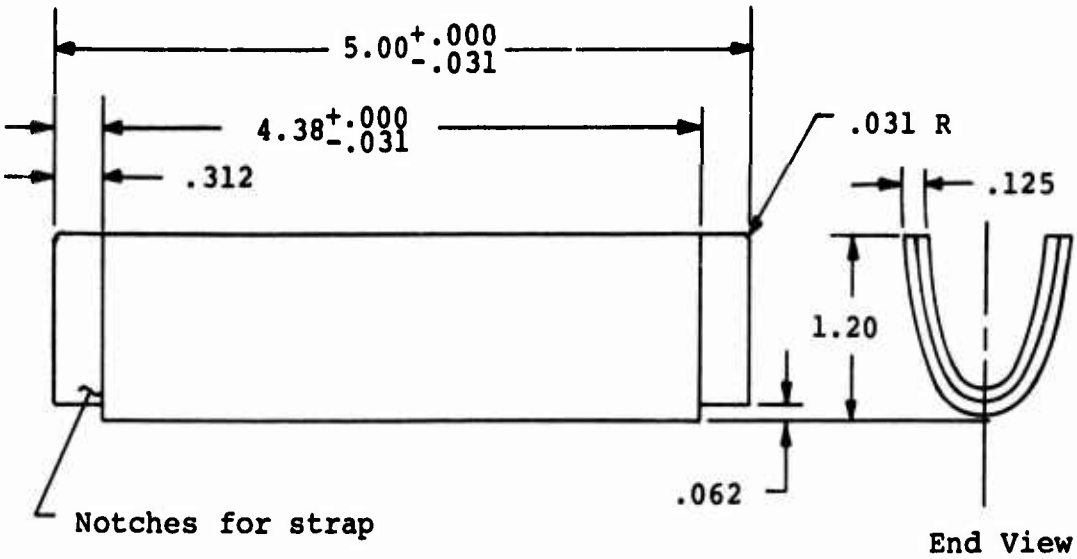

0025 Airfoil Section Coordinates

% Chord	Abscissa	Ordinate
.00	.00	.000
1.25	.05	.158
2.50	.10	.218
5.00	.20	.296
7.50	.30	.350
10.00	.40	.390
15.00	.60	.446
20.00	.80	.478
25.00	1.00	.485
30.00	1.20	.500

Dimensions Are in Inches.

Figure 18. Rain Erosion Test Specimens.

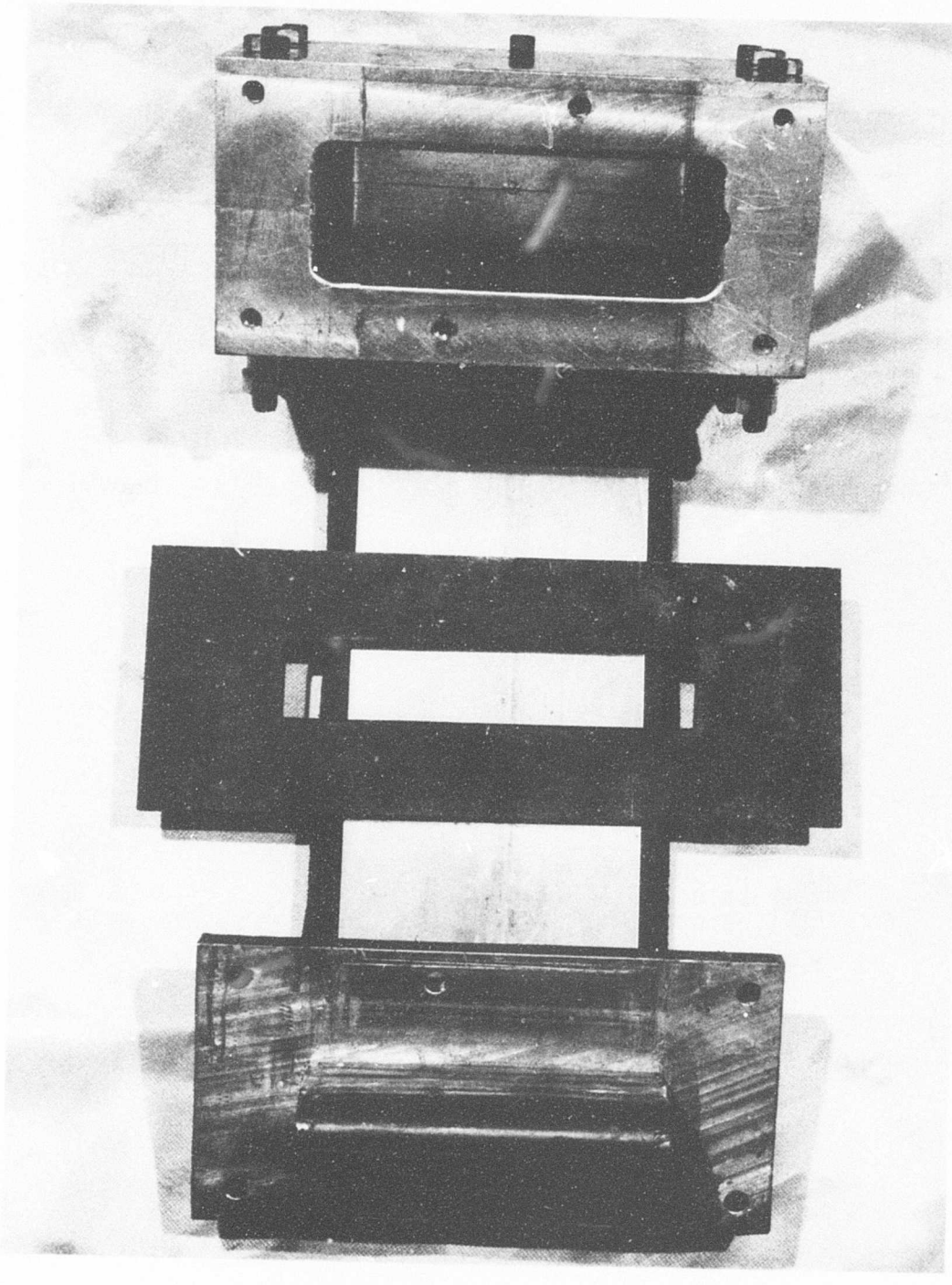

Figure 19. Tooling for Forming Operation.

The next step in the fabrication sequence was to adhere the metal details to the fiberglass reinforced plastic backing. This was accomplished by fabricating a female mold containing a 0025 airfoil cavity. The leading-edge specimen was positioned in the mold, followed by a layer of FM 1000 film adhesive and several layers of BP 919 prepreg. A male mandrel was then inserted into the cavity and the assembly positioned in a platen press. At 220°-250°F the mandrel was compressed to stops to ensure the desired 1/8-inch thickness. The temperature was increased and the layup cured at 340° ± 10°F for 60 to 90 minutes. Tooling for the molding and bonding is shown in Figure 20.

Specimens containing two metal layers were fabricated in the same manner, with a film of adhesive behind each metal layer. The number of plies of prepreg was reduced to compensate for the extra metal layer.

For the elastomeric coated specimens, shim stock equivalent to the coating thickness was inserted into the female mold, followed by a layer of peel ply fabric and the required layers of prepreg, and cured in the same manner as previous specimens. After cure, the outer shim and peel ply were removed, and elastomeric material was bonded directly to the cured laminate. The adhesive for the polyurethane samples was EPON 820 with DTA curing agent. Bonding was accomplished at 120°F to 140°F under 20 inches of vacuum for 90 minutes minimum.

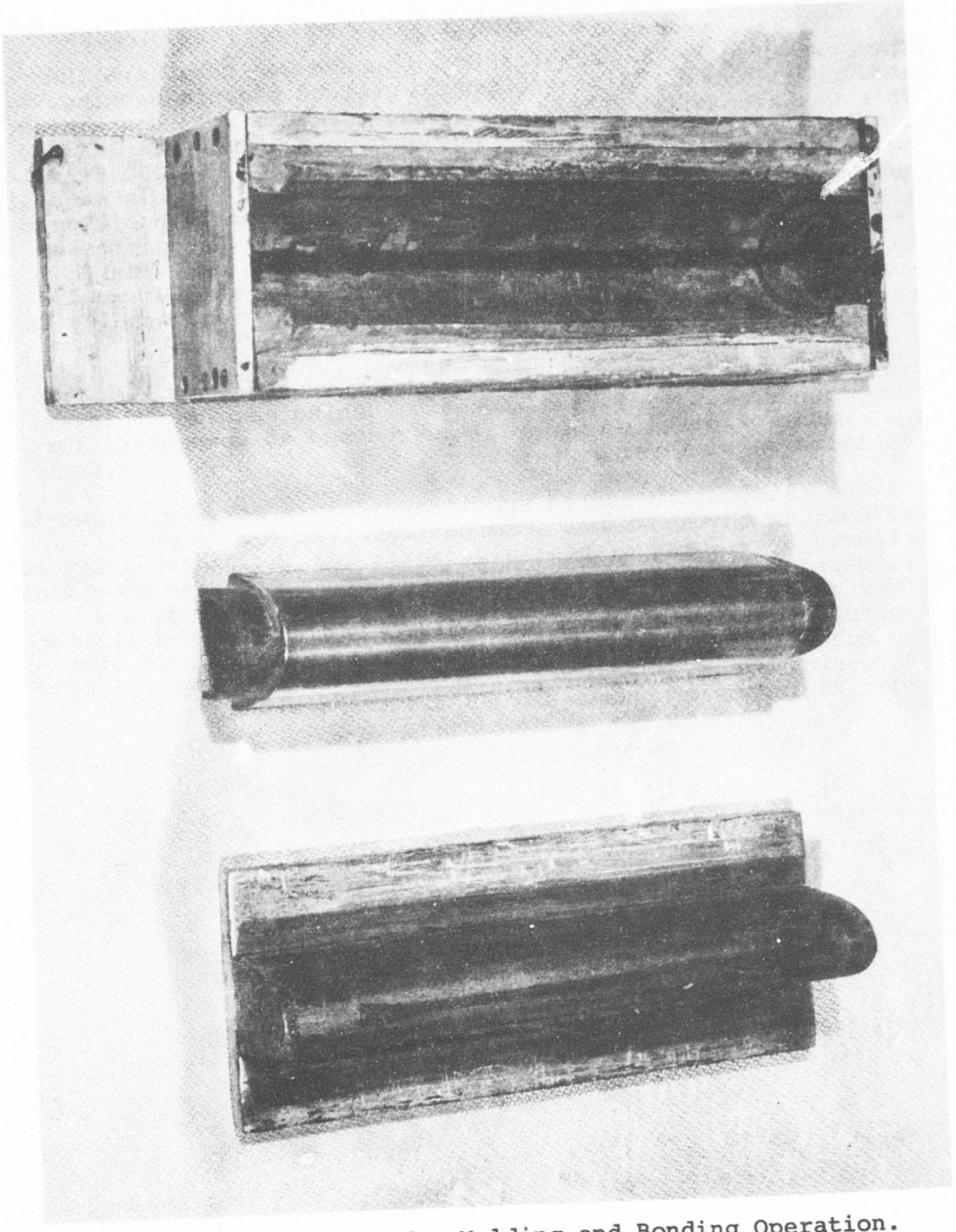

Figure 20. Tooling for Molding and Bonding Operation.

SAND TESTING

A sand rate of 144 grams per minute produced failure on the standard No. 1 configuration in 35 minutes at 530 mph (777 fps) running speed. These conditions were then maintained for all remaining sand tests. The sand test data appears in Table VI and is also plotted in Figures 21 through 28. Figure 28 is a composite plot for all configurations. Failure time in all cases was determined based on the first evidence of rippling or complete wear-through of the coating to the substrate. Figures 29 through 33 show condition of the specimens after completion of test. Note that the .025-inch and .032-inch stainless, .031-inch stellite, and .032-inch titanium exhibited rippling at the extreme leading-edge element. The .016-inch and .032-inch electroformed nickel specimens eroded through to the substrate on the upper surface as tested just aft of the extreme leading-edge element, suggesting that electroformed nickel was more resistant to direct sand impact than to sand abrasion. The manganese chrome oxide coating began to flake off from the substrate interface within seconds after the start of the test, the coating left adhering to the substrate being too scant to evaluate its erosion characteristics. The .030-inch polyurethane specimens failed by erosion on the upper surface as tested aft of the leading-edge nose. The difference in failure time between the two urethane materials was attributed to the decreased thickness of the tapered boot at the point of breakdown compared to the uniform thickness of the sheet. After sand erosion testing, the .030-inch estane material appeared to be quite smooth on the leading edge, whereas the upper and lower surfaces exhibited a roughened or washboard appearance. Inspection of the specimens at 10X magnification revealed an orange peel texture which was an outline of a massive network of superficial cuts. These cuts could be detected by dragging the thumbnail along the surface. The .030-inch PO 655 Armstrong material examined in the same manner exhibited similar cuts and superficial pitting on the leading edge and a somewhat fuzzy appearance on the upper and lower surfaces due to partially cut adhering fragments. The .060-inch polyurethane specimens did not fail on test, but they did exhibit the same wear characteristics as were evident on the .030-inch specimens.

TABLE VI. WHIRLING ARM SAND EROSION TEST DATA, 530 MPH (777 FPS) AT 144 GRAMS/MIN SAND FALL

Specimen No.	Material	Initial Wt (gr)	Test Time (min)	Weight Loss (gr)	Total Time (min)	Total Wt Loss (gr)	Erosion Rate (gr/min)
1-3	.025 Stainless	80.7414	—	—	35 (F)	5.8747	.167
1-4	.025 Stainless	81.0793	—	—	35 (F)	6.1413	.175
1-7	.025 Stainless	80.3888	10	1.9636	—	—	—
			10	1.7872	—	—	—
			10	1.6190	—	—	—
			3	.6540	33 (F)	6.0238	.183
1-8	.025 Stainless	81.1848	10	1.9361	—	—	—
			10	2.0769	—	—	—
			10	1.9651	—	—	—
			3	.7297	33 (F)	6.7078	.203
1-5	.025 Stainless	80.8634	—	—	17 (H)	3.5457	.208
1-6	.025 Stainless	80.2181	—	—	17 (H)	3.5560	.208
2-1	.032 Stainless	76.3188	—	—	32 (F)	6.2900	.197
2-6	.032 Stainless	81.6250	—	—	32 (F)	6.0951	.189
2-2	.032 Stainless	82.1484	15	2.6819	—	—	—
			15	2.4706	—	—	—
			9	1.4099	39 (F)	6.5624	.169
2-4	.032 Stainless	80.6503	15	2.6533	—	—	—
			15	2.3677	—	—	—
			9	1.3283	39 (F)	6.3493	.163
2-7	.032 Stainless	74.4005	—	—	16 (H)	3.1933	.200
2-8	.032 Stainless	73.1423	—	—	16 (H)	3.5402	.221
3-3	.031 Stellite	83.3038	—	—	27 (F)	7.3170	.272
3-4	.031 Stellite	82.9258	—	—	27 (F)	7.8573	.290
3-2	.031 Stellite	82.8790	15	3.4857	—	—	—
			14	3.1783	29 (F)	6.6640	.226
3-6	.031 Stellite	81.9114	15	3.4669	—	—	—
			14	3.1665	29 (F)	6.6334	.225
3-7	.031 Stellite	83.1303	—	—	13.5 (H)	3.8181	.283
3-8	.031 Stellite	82.7075	—	—	13.5 (H)	4.2974	.319
4-6	.032 Titanium	57.7161	—	—	36 (F)	4.6268	.129
4-7	.032 Titanium	58.4919	—	—	36 (F)	4.6282	.129
4-1	.032 Titanium	59.0262	15	1.9274	—	—	—
			15	1.9670	30 (F)	3.8944	.130
4-3	.032 Titanium	55.3730	15	2.0133	—	—	—
			15	2.0355	30 (F)	4.0488	.135
4-2	.032 Titanium	57.4884	—	—	18 (H)	2.9236	.162
4-8	.032 Titanium	61.2216	—	—	18 (H)	3.1658	.175

TABLE VI - Continued

Specimen No.	Material	Initial Wt (gr)	Test Time (min)	Weight Loss (gr)	Total Time (min)	Total Wt Loss (gr)	Erosion Rate (gr/min)
5-6	.016 Electroformed Ni	74.9410	—	—	26	3.3838	.130
5-8	.016 Electroformed Ni	68.1535	—	—	26 (F)	4.0991	.154
5-3	.016 Electroformed Ni	70.9670	15	1.8466	—	—	—
			15	1.8882	30 (F)	3.7348	.125
5-4	.016 Electroformed Ni	67.7104	15	1.8896	—	—	—
			15	1.9608	30 (F)	3.8504	.128
5-1	.016 Electroformed Ni	71.1232	—	—	13 (H)	1.6909	.130
5-2	.016 Electroformed Ni	75.2184	—	—	13 (H)	1.6528	.127
6-2	.032 Electroformed Ni	75.7595	—	—	59	9.2750	.157
6-4	.032 Electroformed Ni	72.3870	—	—	59 (F)	8.8118	.150
6-1	.032 Electroformed Ni	75.1696	15	2.1411	—	—	—
			18	2.6578	—	—	—
			12	1.7818	—	—	—
			15	2.3884	60 (F)	8.9691	.150
6-3	.032 Electroformed Ni	78.9879	15	1.9854	—	—	—
			18	2.5302	—	—	—
			12	1.6568	—	—	—
			15	2.2945	60 (F)	8.4669	.142
6-5	.032 Electroformed Ni	71.5009	—	—	29	3.7506	.129
6-7	.032 Electroformed Ni	76.0291	—	—	29	4.1044	.142
7-1	Mn Chrome Oxide	80.9024	—	—	25 Sec	1.2178	—
7-2	Mn Chrome Oxide	81.0037	—	—	25 Sec	1.2626	—
8-1	.030 Polyurethane Sheet	45.5270	15	.2570	—	—	—
			15	.1861	—	—	—
			15	.2582	—	—	—
			15	.2547	—	—	—
			15	.2785	—	—	—
			40	.5401	115 (F)	1.7746	.011
9-1	.030 Polyurethane Boot	37.3069	15	.3565	—	—	—
			15	.2799	—	—	—
			15	.3641	45	—	.022
			—	—	52 (F)	—	—
			15	.5091	60	1.7978	—
10-2	.060 Polyurethane Sheet	41.6788	30	.3436	—	—	—
			20	.2759	—	—	—
			70	1.2669	120	1.8864	.016
11-2	.060 Polyurethane Boot	45.8058	15	.2674	—	—	—
			45	.7964	—	—	—
			60	1.0875	120	2.1513	.018

(F) - Failure Time
(H) - Half-Life

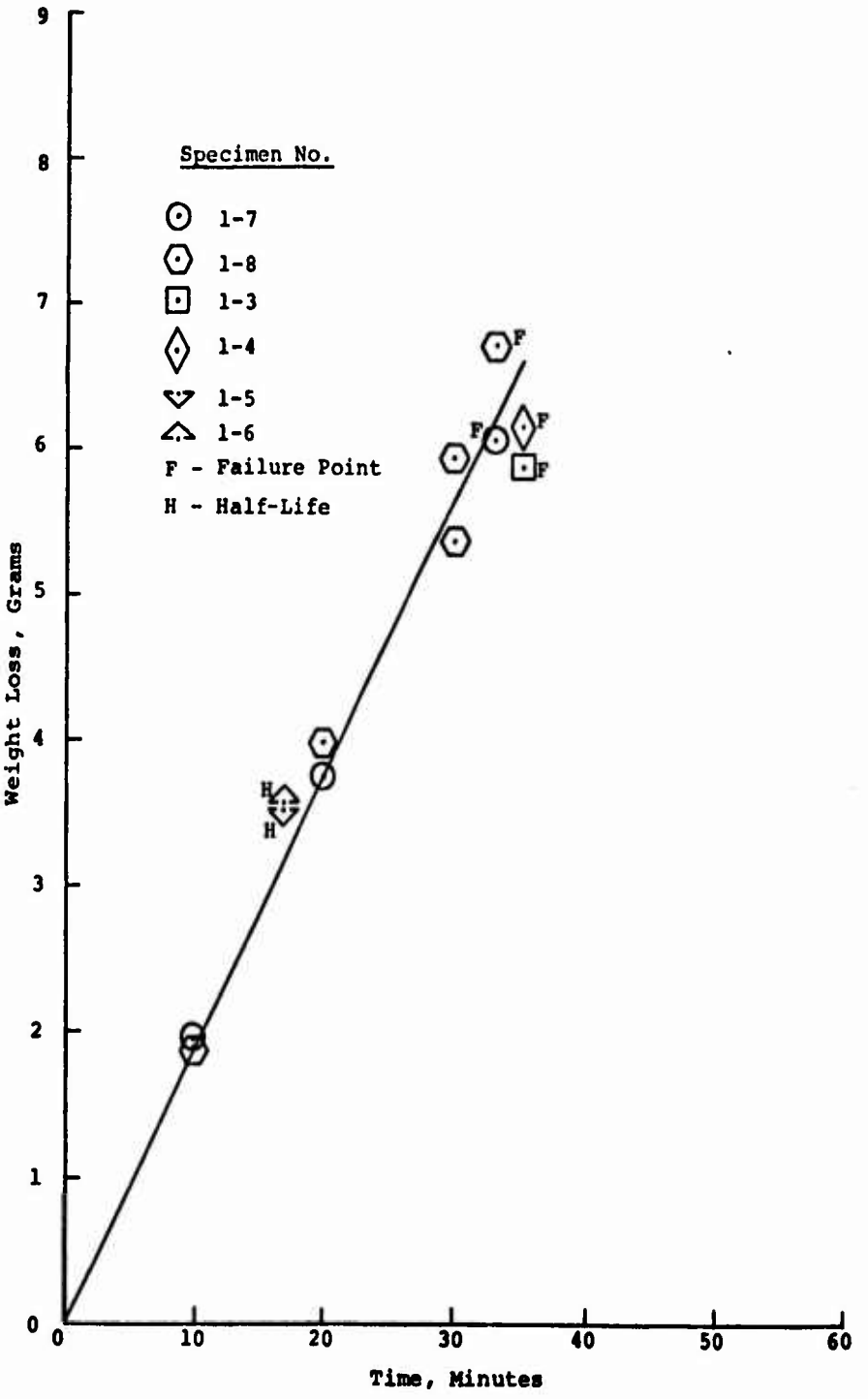

Figure 21. Sand Erosion Wear Rate, .025 Stainless Type 301-1/4 Hard, Configuration 1.

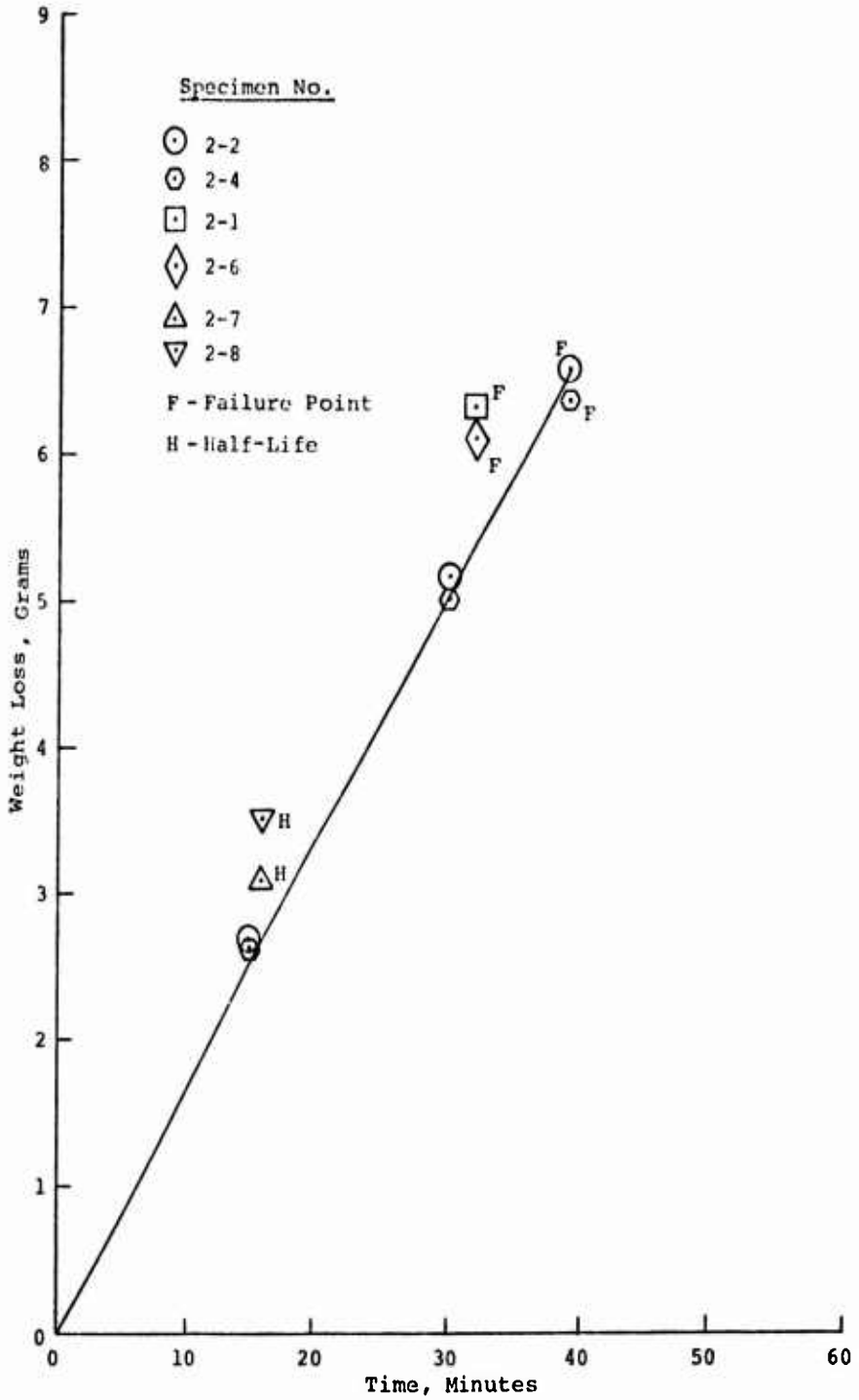

Figure 22. Sand Erosion Wear Rate, .032 Stainless, Type 301-1/4 Hard, Configuration 2.

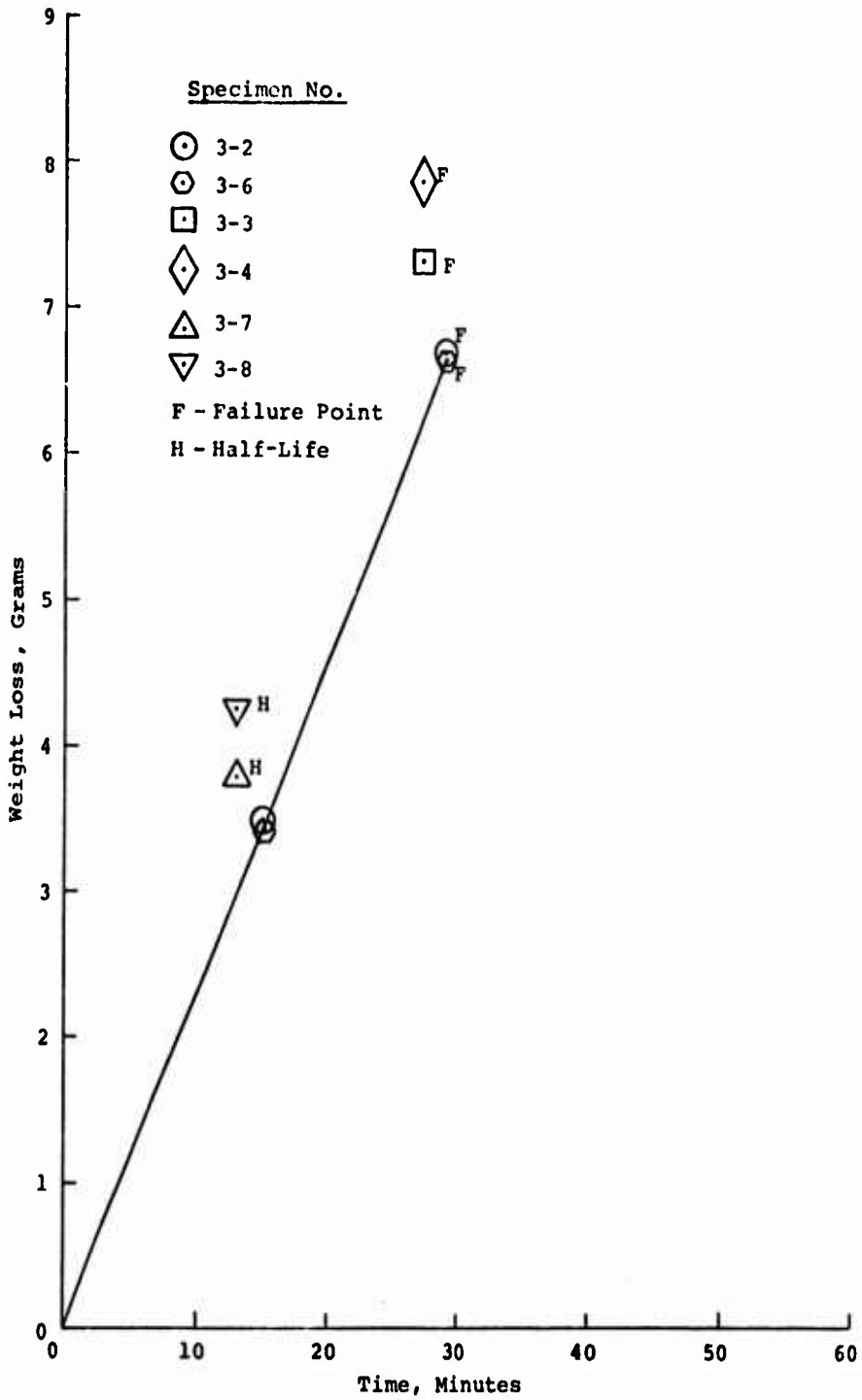

Figure 23. Sand Erosion Wear Rate, .031 Stellite Alloy 6B, Configuration 3.

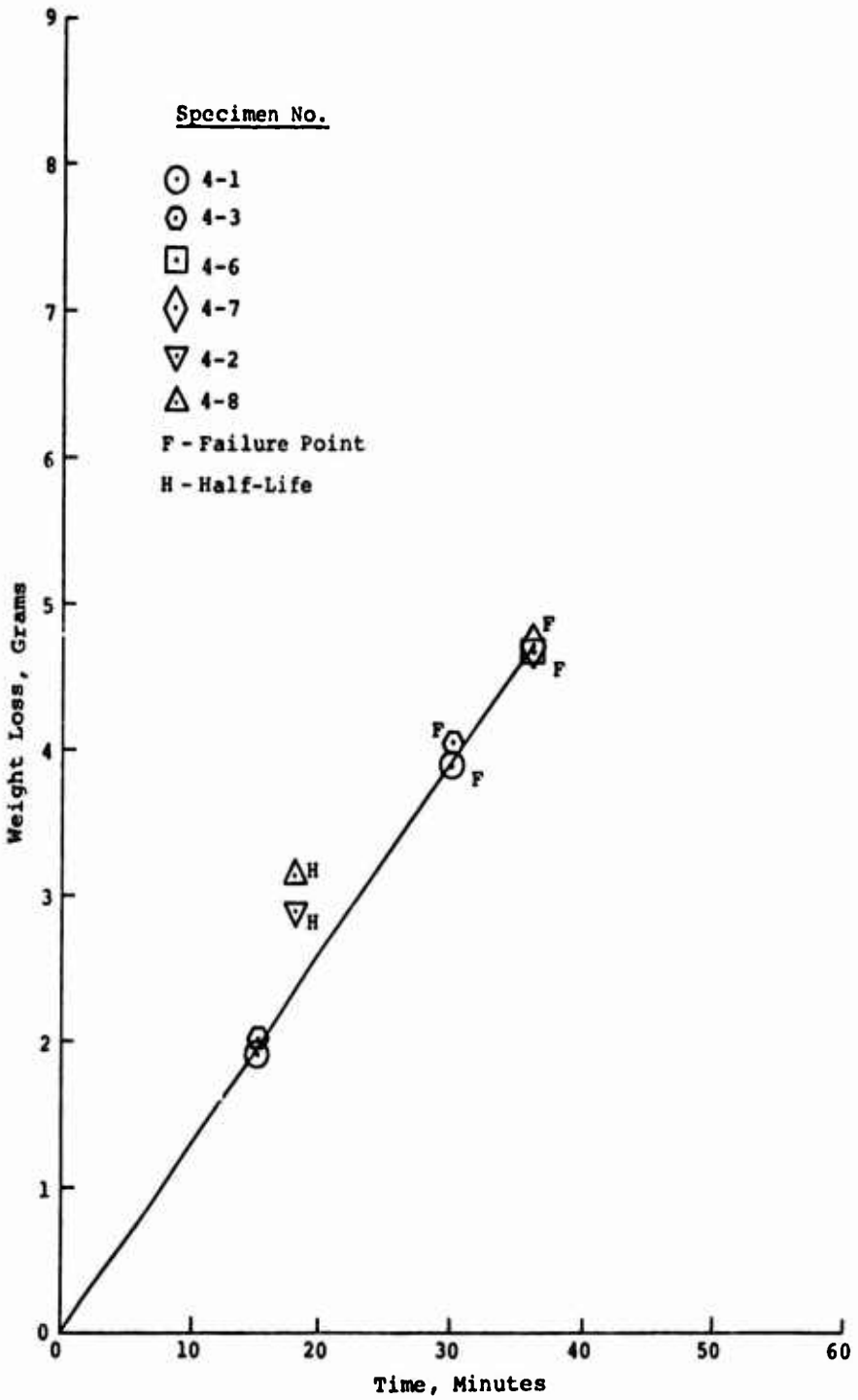

Figure 24. Sand Erosion Wear Rate, .032 Titanium Alloy 6Al-4V, Configuration 4.

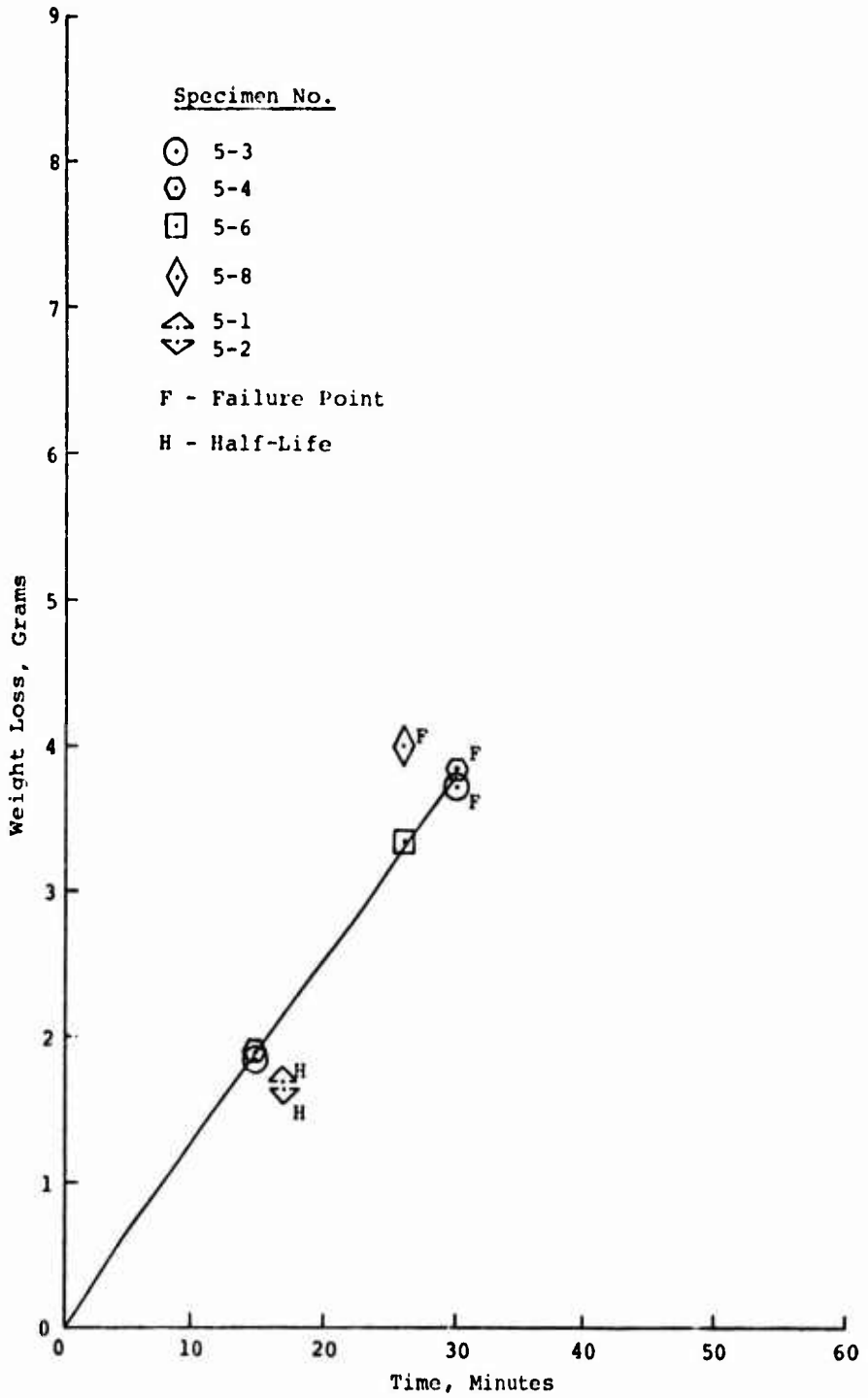

Figure 25. Sand Erosion Wear Rate, .016 Electroformed Nickel, Configuration 5.

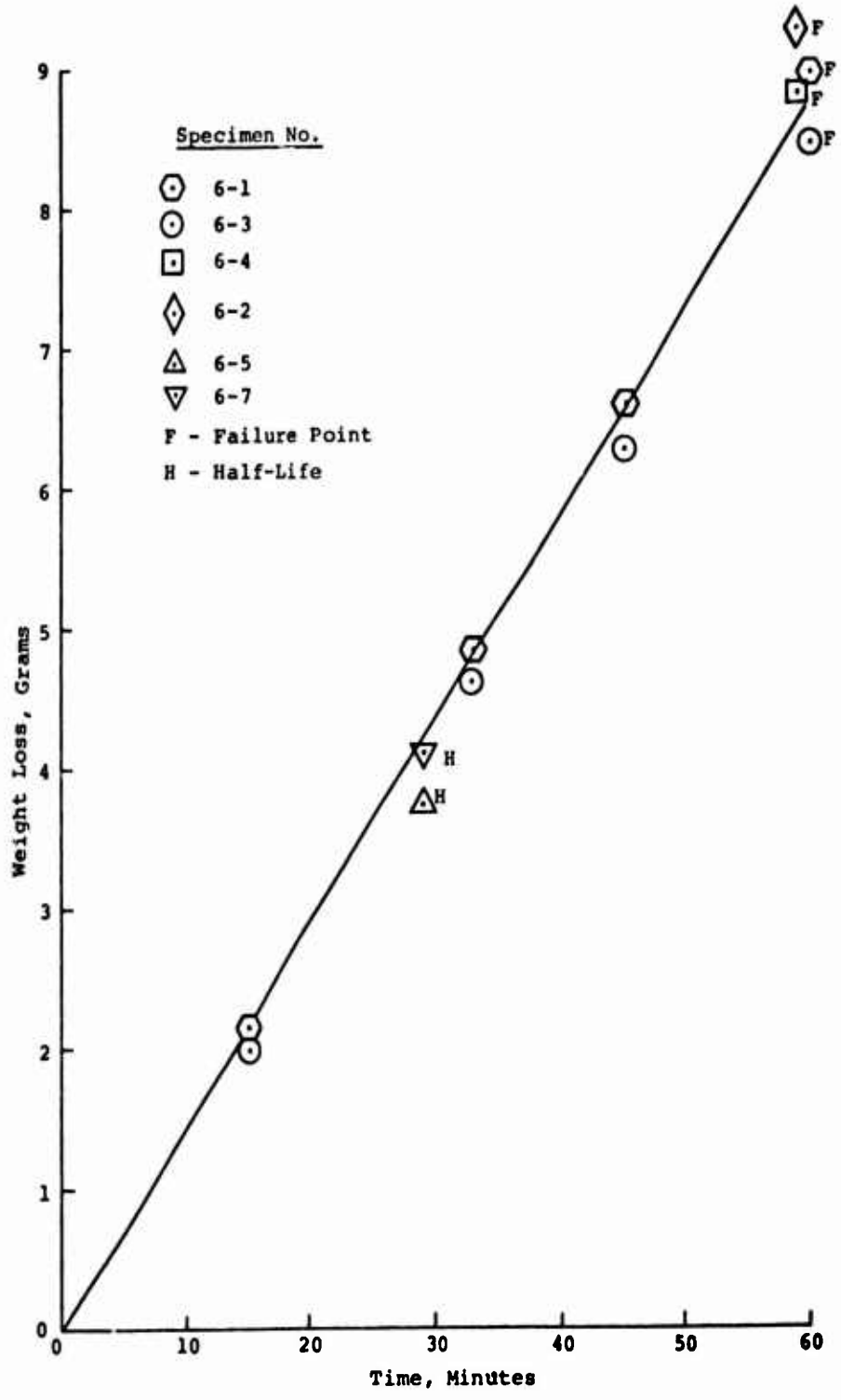

Figure 26. Sand Erosion Wear Rate, .032 Electroformed Nickel, Configuration 6.

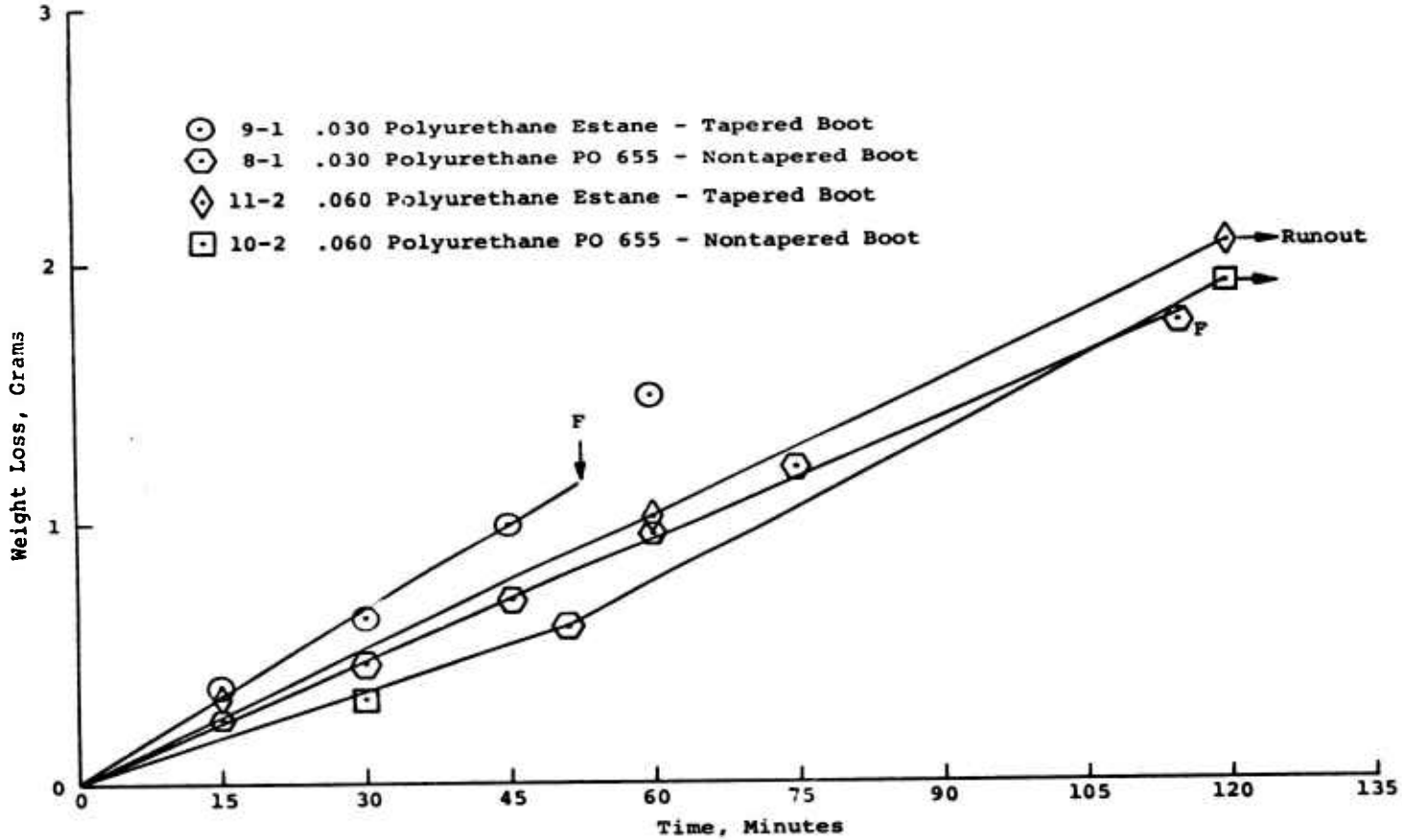

Figure 27. Sand Erosion Wear Rate, Polyurethane.

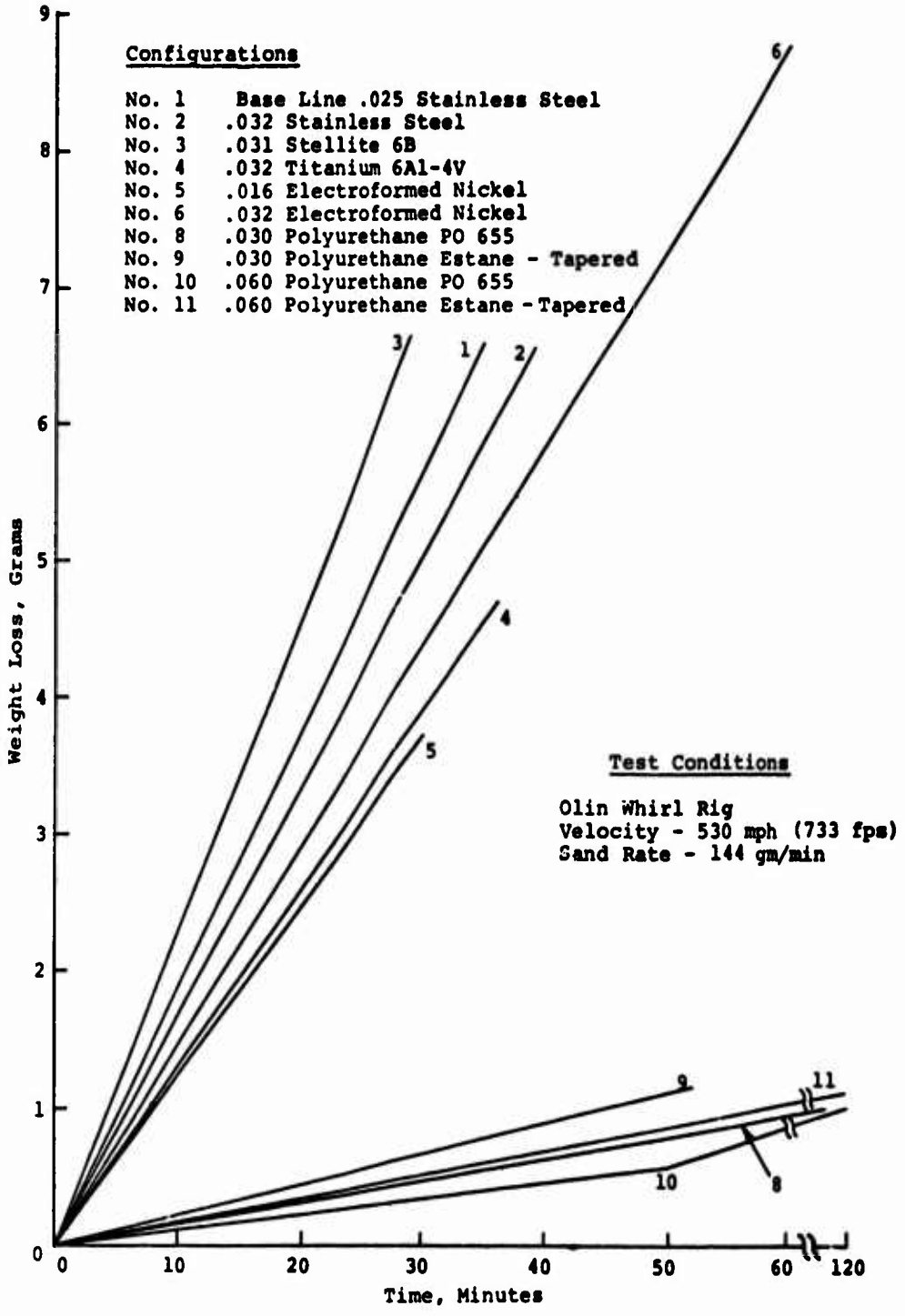

Figure 28. Sand Erosion Wear Rate, Comparative Summary.

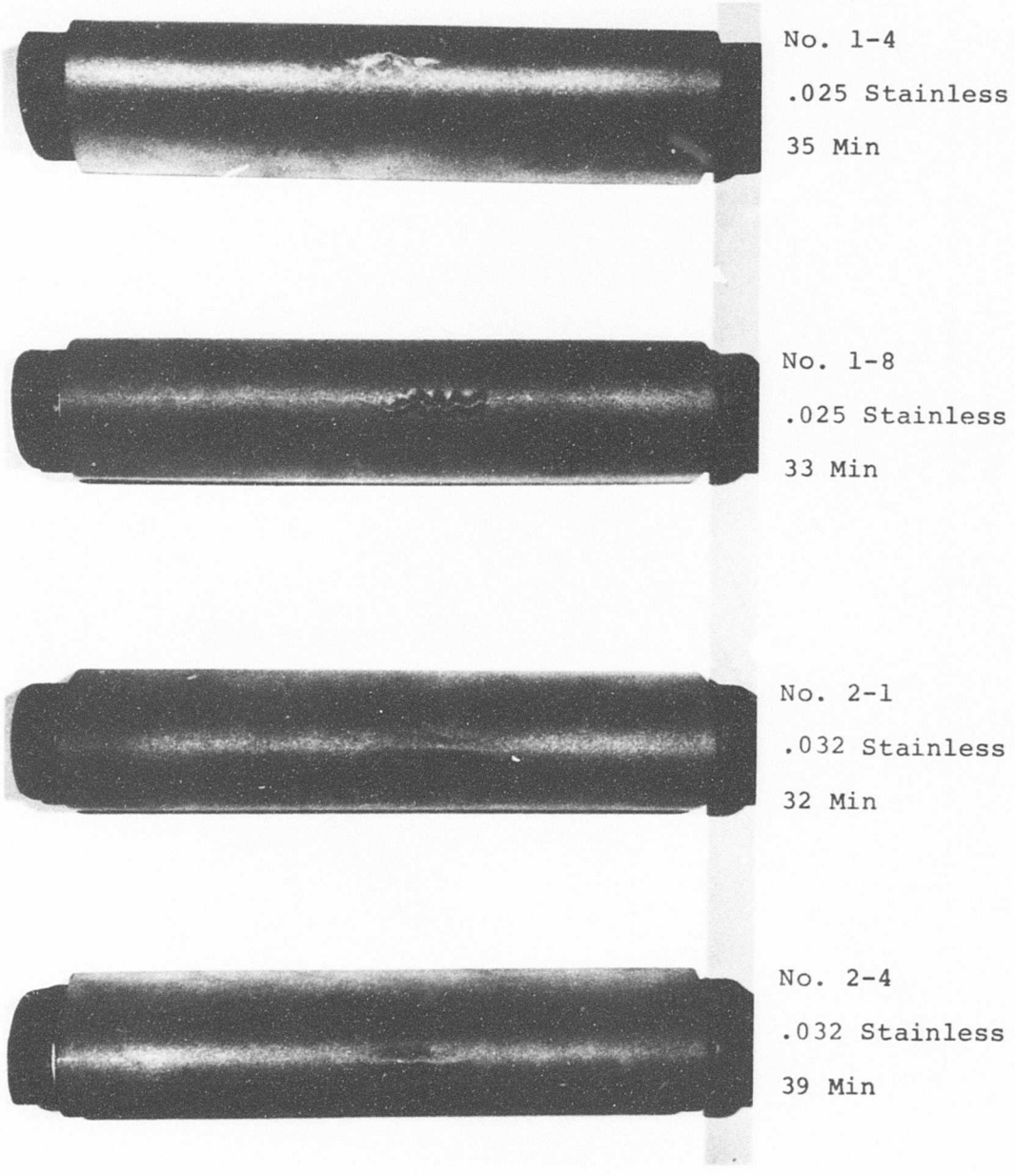

Figure 29. Stainless Steel Test Specimens After Sand Erosion.

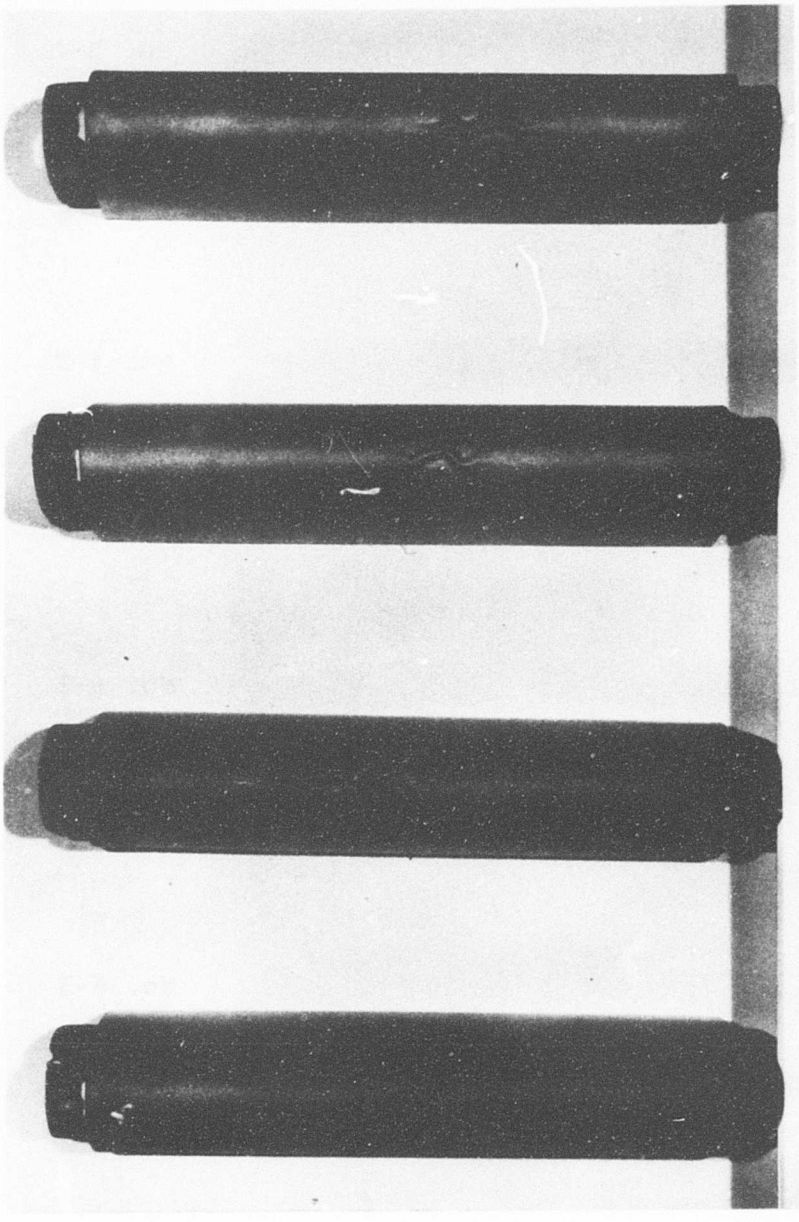

Figure 30. Stellite and Titanium Test Specimens After Sand Erosion.

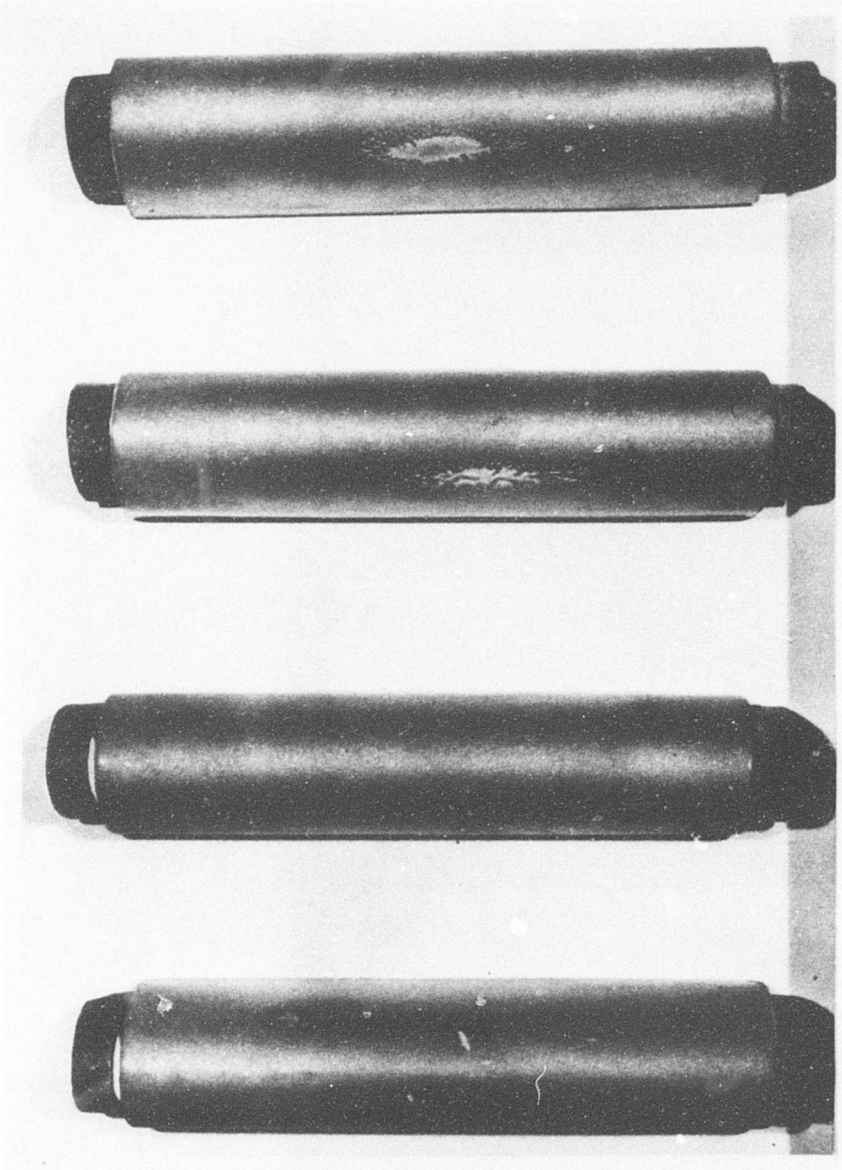

Figure 31. Electroformed Nickel Test Specimens After Sand Erosion.

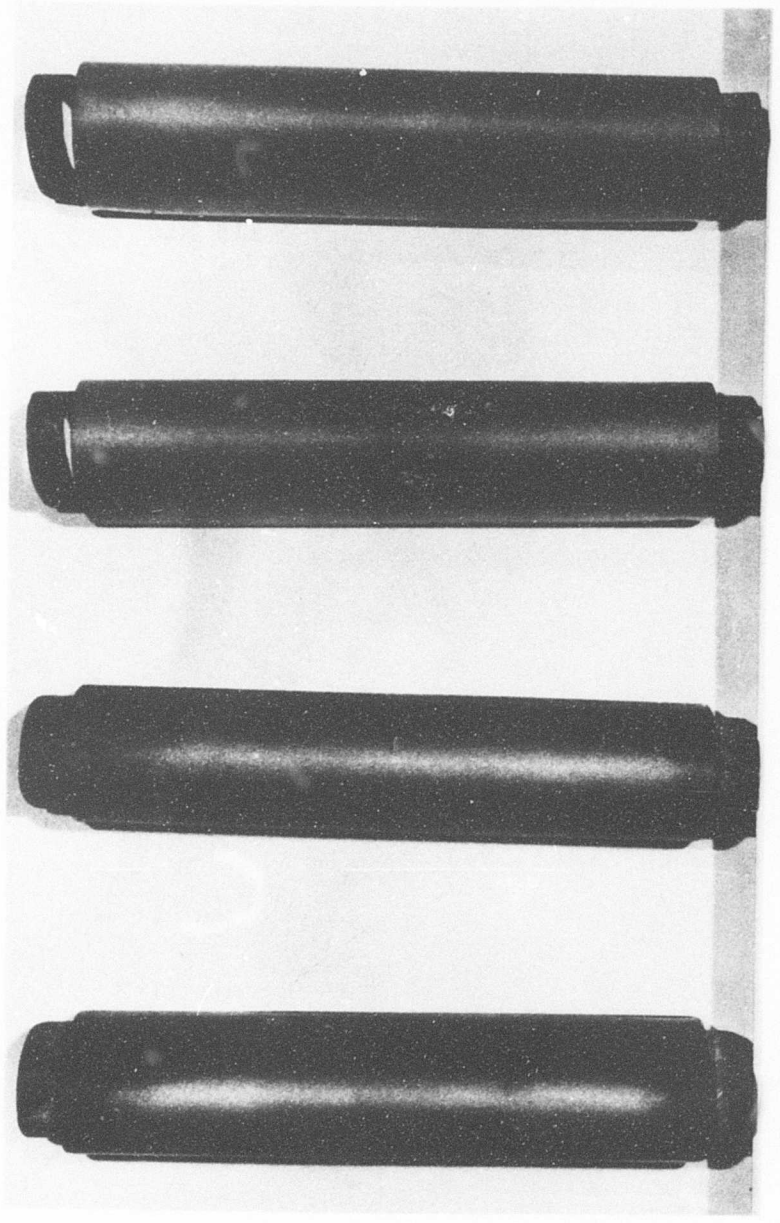

Figure 32. Electroformed and Manganese Chrome Oxide Ceramic-Coated Test Specimens After Sand Erosion.

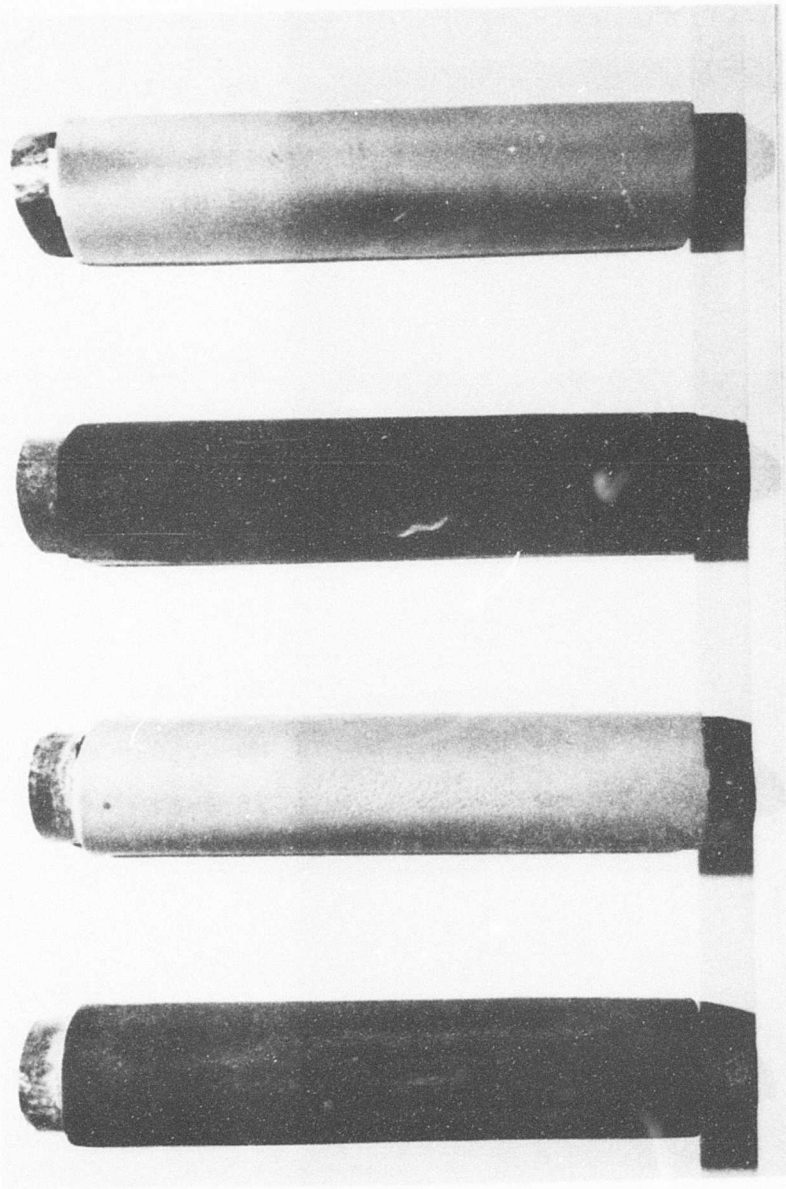

Figure 33. Urethane-Covered Test Specimens After Sand Erosion.

DISCUSSION

A tabulation of the wear rates, time to failure, and relative thickness wear in sand is shown for each configuration in Table VII. The wear rate reported is the average rate of all specimens in each category. The identical wear rate of .190 gram per minute for both stainless steel configurations indicated that the difference in the underlying substrate material did not influence their performance. The difference in wear rates shown for the .016-inch and .032-inch electroformed nickel of .133 gram per minute and .145 gram per minute, respectively, was very slight and for practical consideration essentially equivalent. Specimens of each metal configuration were sectioned and measured to determine remaining thickness at the nose after sand testing. These measurements reported in Table VII showed that buckling occurred at a final thickness of .004-.008 inch.

All of the materials showed a lower wear rate than the stainless steel base-line configuration except for Stellite 6B and manganese-chrome oxide coating. Titanium and electroformed nickel exhibited equivalent wear rates, approximately 25 percent lower than stainless steel. Assuming that the weight loss on each specimen was confined to a unit area and dividing this weight loss by the material density, the relative wear rate in inches of thickness can be calculated. On this basis, 1 mil of electroformed nickel was equivalent to 2 mils of stainless steel and to 2.5 mils of titanium. In other words, electroformed nickel provides twice the erosion protection as stainless steel, and stainless steel provides approximately 25 percent more erosion protection than titanium. On the same thickness basis, Stellite 6B affords more protection than titanium but not quite as much protection as stainless steel. The Stellite 6B material did not meet expectation as reported in Bell Helicopter Company Report No. 599-144-900, Analytical and Test Material Evaluation - Rotor Blade Leading Edge Erosion. Aluminum was not tested in this program, but data previously obtained on the Olin rig under identical test conditions was made available and included in Table VII. Aluminum exhibited a wear rate equivalent to electroformed nickel, but on a thickness basis eroded four times as fast as electroformed nickel.

The polyurethane elastomers, as a group, showed equivalent wear rates, approximately one order of magnitude below the metallic configurations.

TABLE VII. SAND EROSION TESTING ON OLIN RIG, 144 GRAMS/MIN AT 530 MPH (777 FPS)

Config	Description	Nose Thickness[1] at Failure (in.)	Wear Rate (gr/min)	Time to Failure (min)	Relative Wear Thickness[2]
1	.025 S.S. over .032 Aluminum over GRP	.005-.006	.190	33-35	2
2	.032 S.S. over GRP	.007-.008	.190	32-39	-
3	.031 Stellite (6B) over GRP	.004-.005	.269	27-29	2.25
4	.032 Titanium (6Al-4V) over GRP	.004	.143	30-36	2.5
5	.016 Electroformed Ni over .032 Aluminum over GRP	.008	.133	26-30	-
6	.032 Electroformed Ni over GRP	.015	.145	59-60	1
7	Manganese-Chrome Oxide over S.S. over GRP	-	-	0	-
8	.030 Polyurethane (PO 655) over GRP	-	.015	115[3]	-
9	.030 Polyurethane (Estane) over GRP	-	.022	52[3]	-
10	.060 Polyurethane (PO 655) over GRP	-	.016	120 Runout	-
11	.060 Polyurethane (Estane) over GRP	-	.018	120 Runout	-
	2024 Aluminum[4]	-	.138	-	4

(1) Minimum specimen thickness except for Configurations 5 and 6, which eroded to zero aft of nose.

(2) Compared to Electroformed Nickel as unity.

(3) Failed, 3/8 inch aft of nose on top surface. Note: Configuration 9 contained tapered thickness erosion coatings.

(4) Olin supplied data.

RAIN TESTING

All configurations underwent rain testing except Stellite 6B and manganese-chrome oxide ceramic, which showed the least sand resistance, and the .016-inch electroformed nickel because of its equivalent wear rate to the .032-inch electroformed nickel.

The designated configurations were first whirled at 530 mph (777 fps) in sand at a sand drop rate of 144 grams per minute. Time in this environment was set at one-half of each configuration's predetermined life in sand. The test rig was converted for rain testing, and these same specimens were whirled at 500 mph (733 fps) in a 1-inch-per-hour rainfall. Specimens were run to failure or the test was terminated after 2 hours running time in rain.

The data for this test appears in Table VIII. All metal specimens, which included the .025-inch stainless steel baseline configuration, .032-inch stainless steel, .032-inch titanium and .032-inch electroformed nickel, endured 2 hours of rain exposure without any visual change or discernible weight loss.

The .030-inch tapered estane boot started to break down at 21 minutes by both erosion and coating delamination.

The .030-inch PO 655 urethane boot failed after 20 minutes of test by the development of a small blister or bond-line delamination, 1/8 inch x 1/4 inch in size, which was immediately cut away by the rain. Visually no additional damage was evident.

The .060-inch tapered estane boot was removed from test after 17 minutes because of poor rain impingement. It was conjectured that the roughened surface developed by the previous sand test and a slight step between the aft end of the specimen and the whirling arm created a turbulence which disrupted the droplets.

The .060-inch PO 655 urethane underwent 87 minutes in the rain before exhibiting erosion pits on the nose and a bond delamination surrounding a pinpoint puncture through the coating.

The condition of the polyurethane specimens after rain testing is shown in Figure 34. Note that specimens 9-2 and 11-1 in Figure 34 were dusted with a talcum powder to reveal the surface texture on the photographic plate.

Weights on the elastomeric specimens were not reported either before or after the half-life testing in sand; consequently, a check of the wear rate on the elastomeric specimens was not possible. In addition, specimen 11-1, which was not subjected

TABLE VIII. WHIRLING ARM RAIN EROSION TEST DATA, 500 MPH (733 FPS) AT 1 INCH/HR RAINFALL

Specimen No.	Test Time in Sand (min)	Wt After Sand Test (gr)	Test Time in Rain (min)	Final Wt (gr)	Delta Wt* (gr)	Remarks
1-5	17	77.3177	120	77.2950	-.0227	Runout, no visual change.
1-6	17	76.6621	120	76.6610	-.0011	Runout, no visual change.
2-7	16	71.2072	120	71.1650	-.0422	Runout, no visual change.
2-8	16	69.6021	120	69.5574	-.0447	Runout, no visual change.
4-2	18	54.5648	120	54.5592	-.0056	Runout, no visual change.
4-8	18	58.0558	120	58.0622	+.0064	Runout, no visual change.
6-5	29	67.7503	120	67.7483	-.0020	Runout, no visual change.
6-7	29	71.9247	120	71.9295	+.0048	Runout, no visual change.
8-2	58	-	20	-	-	Small blister cut by rain.
9-2	26	-	21	-	-	Intercoat delaminations.
10-1	60	-	87	-	-	Erosion and pinhole to substrate and localized blistering.
11-1	60	-	17	-	-	Premature removal - poor rain impingement.

*No significant weight change due to rain testing.

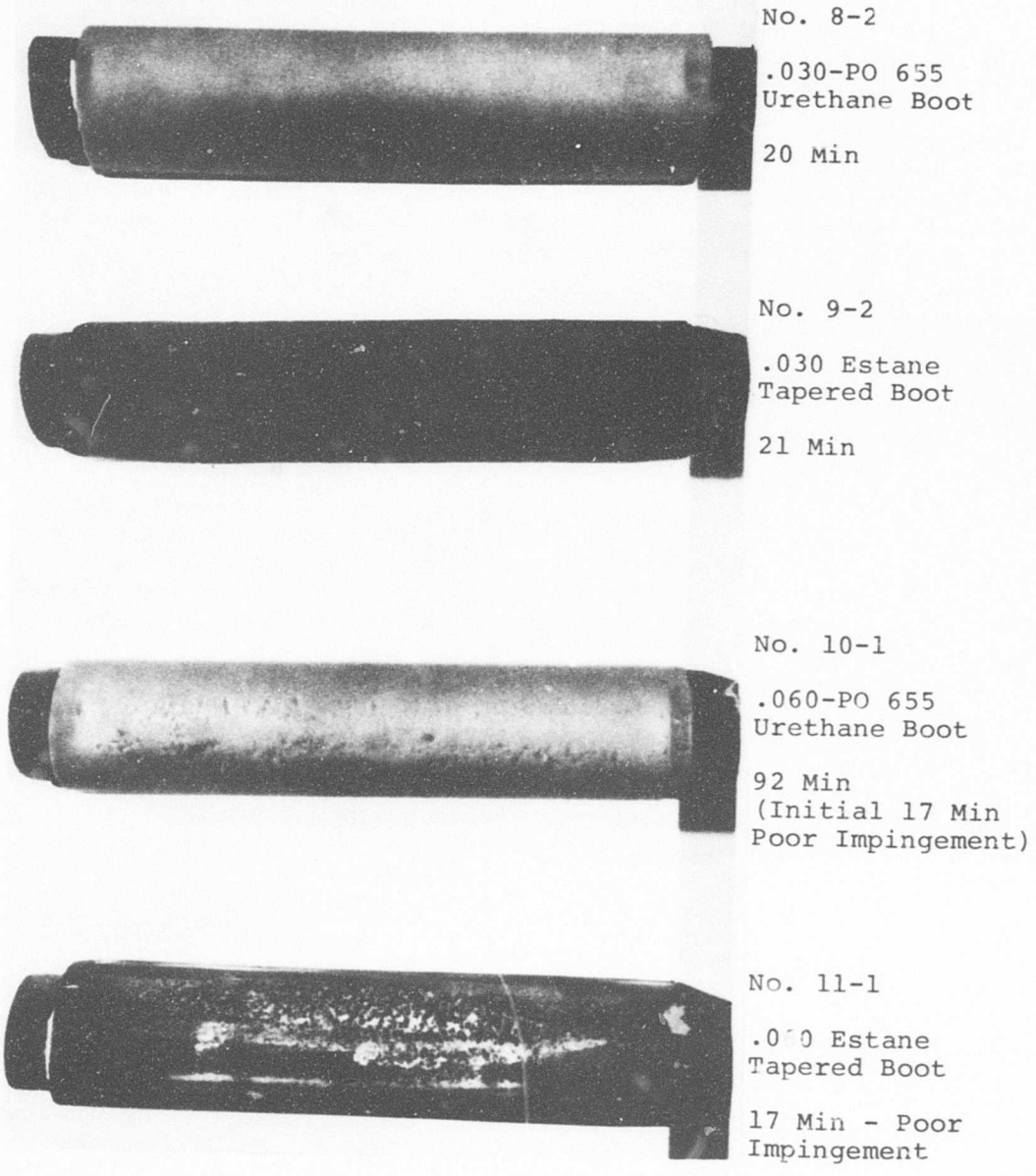

Figure 34. Urethane-Covered Test Specimens After Rain Erosion.

to any significant rain impingement, appeared to be more severely eroded after 60 minutes in sand compared to its counterpart, specimen 11-2, after 2 hours in sand. This difference in appearance can be seen in Figures 33 and 34. Another factor is the increase in the wear rate on specimen 10-2 during the last 70 minutes of testing. This portion of the testing was performed at a later date and during the same time frame as the half-life testing on the elastomers.

From these observations, it is possible that all the elastomeric specimens subjected to half-life erosion testing were eroded more severely than those previously used to establish sand wear rate, and that the results of rain testing on the specimens may be invalid or conservative.

COST EFFECTIVENESS

Reviewing the erosion test data of Table VII for time to failure for equivalent thickness material, the electroformed nickel shows a life improvement over stainless steel by a factor of approximately 2. Titanium exhibits a life almost equivalent to that of stainless steel, whereas Stellite indicates a life equivalent to approximately 80 percent that of stainless steel. This relationship is also evident on the basis of relative thickness wear. Ranking of materials on this data alone is not necessarily sufficient, since the weight differential between the materials could definitely influence the basic design.

The relative thickness wear numbers presented in Table VII hold the same relationship to volume of material eroded when the wear is considered to be confined to a unit surface area. Multiplying this factor by the material density and dividing by the density of electroformed nickel, a new factor of relative weight for equivalent protection is obtained as follows:

			Relative Weight
Electroformed Nickel	1 x 8.9/8.9	=	1
Aluminum	4 x 2.77/8.9	=	1.2
Titanium	2.5 x 4.54/8.90	=	1.3
Stainless Steel	2 x 7.93/8.90	=	1.78
Stellite	2.25 x 8.8/8.9	=	2.2

Electroformed nickel still represents the optimum choice of the metallic materials on the basis of weight. In addition, the electroforming process can generate a tapered-thickness leading edge without additional cost so that further weight improvements can be visualized. Aluminum and titanium are the next two choices and now rank higher than stainless steel. Stellite still shows the lowest ranking.

A cost estimate for procurement, fabrication and adhesive bonding of leading-edge erosion guards of the required thickness to provide equivalent life to .032-inch electroformed nickel calculates to the following ratio:

	Relative Cost
Aluminum	1
Stainless Steel	1.5
Stellite	2
Electroformed Nickel	3
Titanium	3.5

From the cost standpoint, aluminum leading edge .125 inch thick affords maximum cost effectiveness, but a weight penalty of 20% must be recognized compared to electroformed nickel. Stainless steel at .064 inch thick is second in the cost ranking, but the 80% weight penalty is excessive and could not be tolerated without significant design modification. Titanium and Stellite are last in the ranking on the basis of maximum cost and severest weight penalty. The position of electroformed nickel, which exhibits high cost but minimum weight, depends on significance assigned to the weight factor.

Reverting back to Table VII test data, the polyurethane erosion guard specimens underwent twice the test time as the electroformed nickel without failure with a weight factor (density 1.2 gm/cc) one-tenth that of electroformed nickel. On the same estimating basis as used for the metal guards, the urethane guard would cost the same as aluminum. This cost is equivalent to the cheapest metal erosion guard, but at substantial weight savings.

The polyurethane erosion guard is by far the best selection on the basis of sand erosion resistance. The one drawback to polyurethane material is the limited protection in rain. However, the .060-inch material indicates a significant life improvement over material thicknesses normally used in service. In addition, should the urethane erosion guard be damaged by extensive or severe rain exposure, field replacement is feasible at line level. On the other hand, wear-through of a bonded metal erosion guard would not be field replaceable and would most probably scrap the rotor.

CONCLUSIONS

1. Polyurethane erosion guard provides the greatest resistance to sand abrasion by a factor of 10 over the best metallic material tested at a sand fall rate of 144 grams per minute at 530 mph (777 fps).

2. Electroformed nickel and titanium leading edge exhibit the lowest wear rates of the metallic materials tested. Although the wear rate in grams per minute is equivalent, the relative wear for titanium is 2.5 times that for nickel.

3. Electroformed nickel leading edges exhibit a failure mode characterized as wear, whereas stainless steel, Stellite and titanium after some wear exhibit a buckling type of failure mode at a thickness range of .004-.008 inch.

4. Stainless steel, titanium, and electroformed nickel leading edges can endure whirl test in a combination of sand and rainfall without damage from rain at 1-inch-per-hour rainfall at 500 mph (733 fps).

5. Polyurethane material cannot survive in a combination sand and rain environment, but merit for the thicker erosion guard was demonstrated.

6. Polyurethane material provides maximum cost effectiveness on the basis of maximum sand abrasion resistance, lowest weight, field repairability and low cost.

DAMAGE RESISTANCE AND BALLISTIC TOLERANCE

BACKGROUND

The tail rotor whirl blade, after 52 hours 46 minutes of whirl testing, was made available for the subject task. The tapered-thickness polyurethane leading-edge boot was added to the rotor for the damage resistance test.

Visual examination of the rotor disclosed no damage or breakdown from the previous whirl testing. The blade leading edge was then wet sanded, washed and dried to facilitate bonding of the tapered-thickness polyurethane erosion guard. The leading-edge guard was bonded from Station 28 to the outboard tip and the blade reinstalled on the whirl rig. The full erosion guard from the inboard rib as specified by the drawing was not feasible because of the presence of strain gage instrumentation on the inboard section.

DOWEL TEST

Maple dowels of various diameters from 1/4 inch to 5/8 inch were injected into the path of the whirling rotor to simulate operational contact with brush and light tree branches. To accomplish this task, a fixture was erected to grip one or two dowels at a 2-foot span length centered with the whirling rotor as shown in Figure 35. After the blade was at the full rotor speed of 1650 rpm, the mechanism was released, swinging the dowels into the rotor. Dowels were marked with colored chalk to ascertain the blade and station taking the hit. After each hit, the rotor was shut down and examined for damage.

GRAVEL AND CRUSHED STONE TEST

Gravel and crushed stones were injected into the whirling rotor to assess susceptibility to damage from foreign objects. Material utilized for this test was sized through a 5/16-inch screen and retained on a 1/8-inch screen. The gravel consisted of a variety of materials including sandstone, feldspars and quartz and was characterized by fairly smooth or rounded edges as shown in Figure 36. The crushed stone consisted entirely of basalt and was characterized by very sharp and jagged edges as shown in Figure 37.

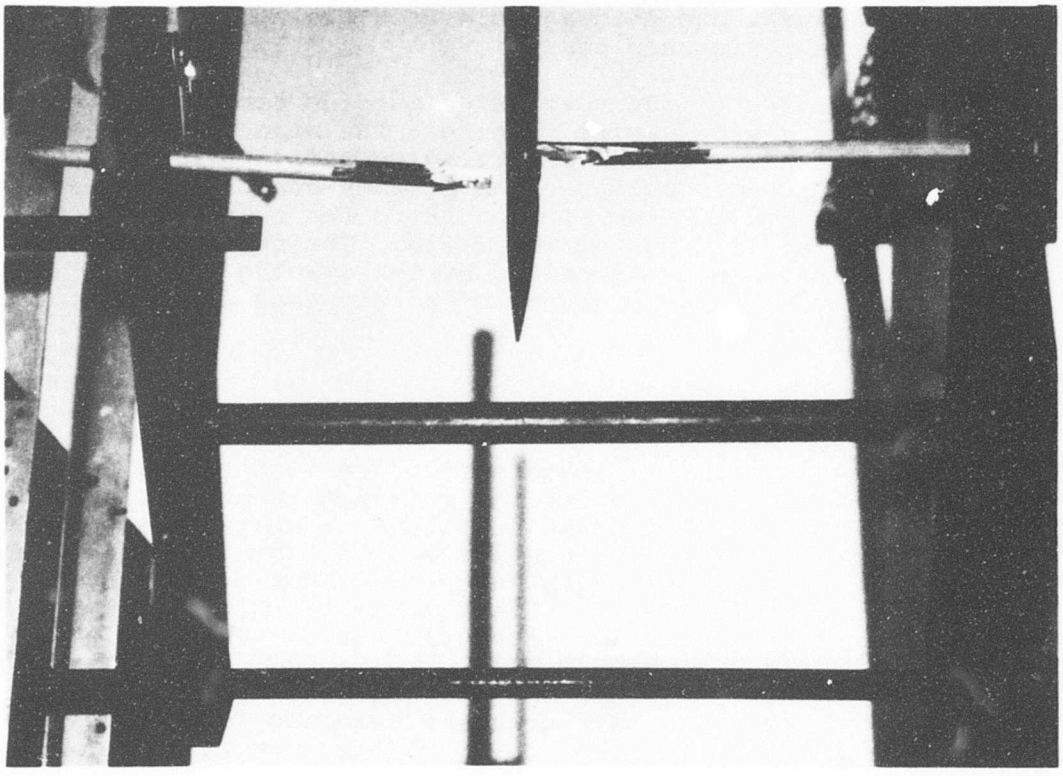

Figure 35. Installation for Dowel Test Fixture in Retracted Position With Severed Dowel.

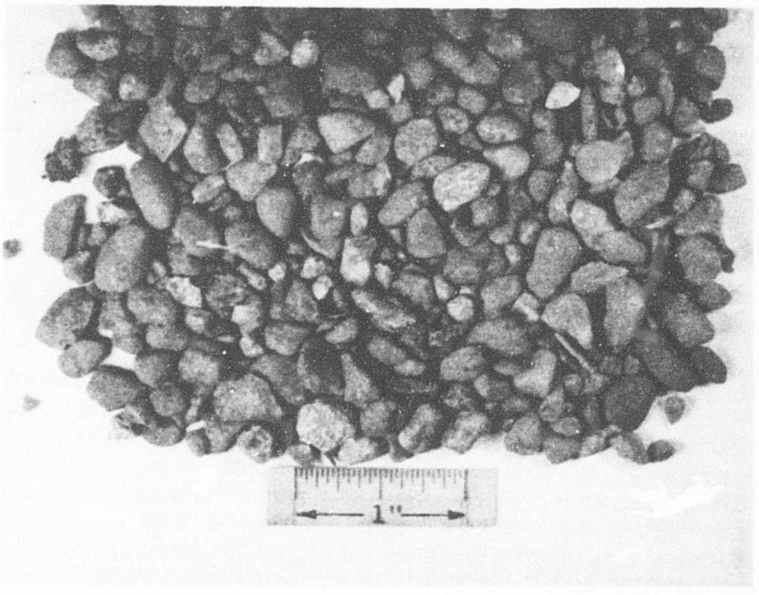

Figure 36. Typical Sample of Gravel Injected Into Whirling Rotor.

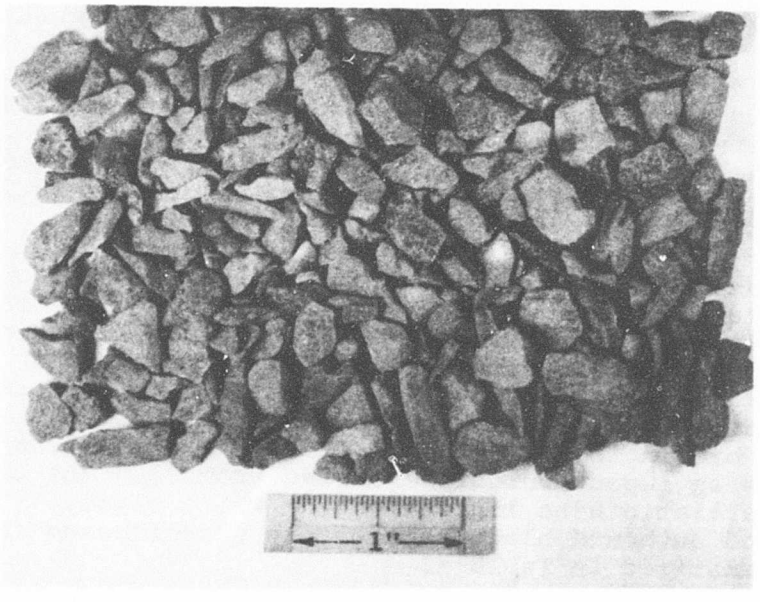

Figure 37. Typical Sample of Crushed Stone Injected Into Whirling Rotor.

The gravel was fed into the rotor by placing a weighed quantity of material in a hopper containing a hinged door with a regulated screw stop to control the opening as shown in Figure 38. To preclude an onrush of stone, it was necessary to keep the maximum opening quite small so as not to allow free flow, and to rely on the vibration level in the staging to facilitate a continuous trickle of stone.

BALLISTIC TEST

Ballistic damage tolerance was assessed by firing 7.62mm ball type ammunition into the blade from a distance of 15-20 feet. A total of 6 hits, 4 through fiberglass skin to core aft section, 1 through trailing-edge spline, and 1 through aluminum leading edge, were inflicted on the rotor. The rotor underwent subsequent whirl after these ballistic hits. On termination of whirl, additional hits with 7.62mm AP ammunition were inflicted on the outboard tip ballast weight region, and through the spar structure. Spar specimen 2A, after completion of fatigue test, and one blade section were sent to the Ballistic Research Laboratories, Aberdeen Proving Ground, Maryland for eight hits with 12.7mm AP ammunition. All firings were performed without load on the specimens.

TEST RESULTS

The sequence of the various damage resistance and ballistic tolerance tests is presented in Table IX. This table correlates the whirl run number, duration of the run, pertinent data related to the test, and a description of the damage inflicted. The duration reported for each run is the actual time at full rotor rpm.

The whirl test was concluded at the end of Run 12 after 6 hours 25 minutes of cumulative running time, since damage inflicted by subsequent ballistic firings rendered further whirl testing risky. Additional ballistic damage inflicted on the whirl rotor, spar assembly and outboard blade sections with 7.62 and 12.7mm AP ammunition is shown with comments in Figures 55 through 63. All ballistic firings with 12.7mm AP ammunition were conducted at an impact velocity ranging from 2800 fps to 2875 fps. All ballistic hits imposed on the whirl blade, spar component and outboard blade section are superimposed on Figure 64 and summarized in Table X.

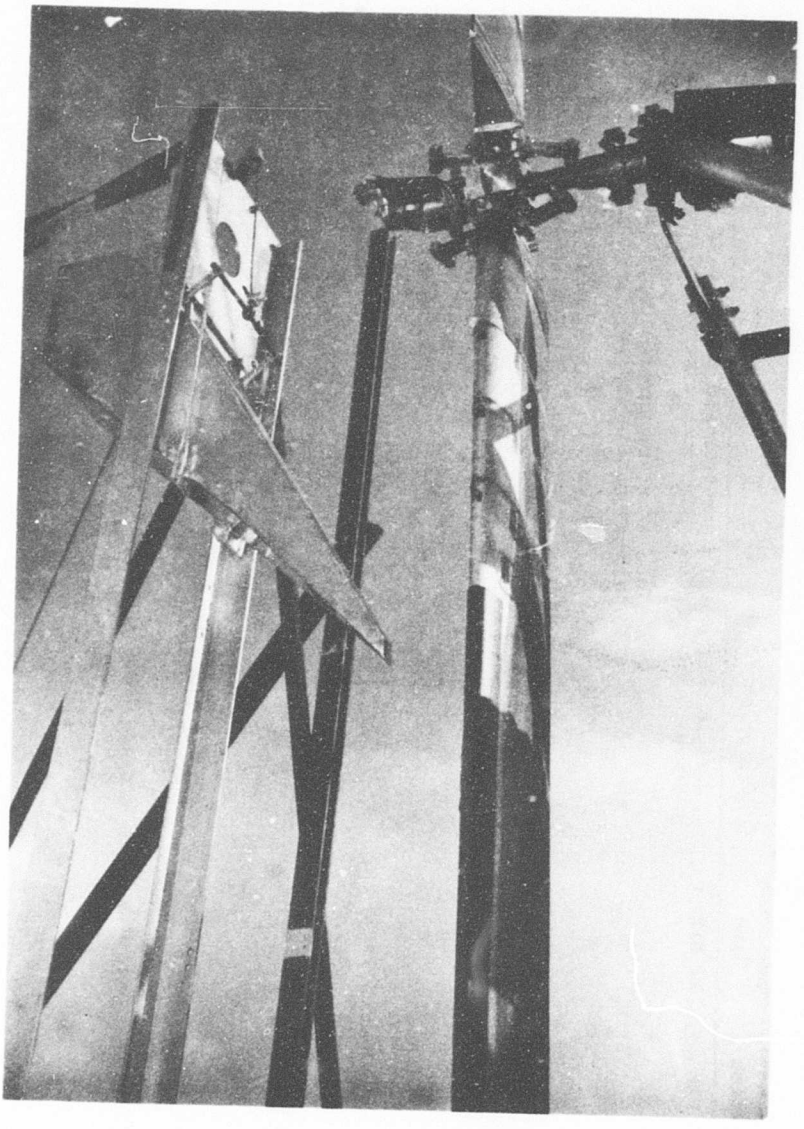

Figure 38. Rig Installation and Hopper Arrangement for Injecting Gravel and Stone.

TABLE IX. SEQUENCE OF FOREIGN OBJECT AND BALLISTIC DAMAGE IMPOSED DURING WHIRL PROGRAM

Whirl Run No.	Duration	Cumulative Time	Test Description	Notes
1	12 Min	12 Min	3.35 lb gravel	Gravel hits from Station 30.5 to Station 41 with predominant impacts between Stations 32.5 and 36.5. A-Blade exhibits numerous cuts and gouges in urethane erosion strips. B-Blade, same as A-Blade, plus 3 localized blisters approx 1/4-3/8 in. dia containing grit and sand.
2	8 Min	20 Min	2.75 lb gravel	Noise level changed; run aborted after 8 min. A-Blade - Boot damage more prevalent compared to Run 1 plus 3 localized blisters as shown in Figures 39 and 40. Boot repaired after completion of run. B-Blade - Boot torn open from Stations 32 to 37, revealing small impact indentations to .050 in. aluminum L.E. as shown in Figures 41 and 42. Figure 41 shows evidence of occasional hits along entire L.E. to the outboard tip, Station 51. Boot replaced after completion of run.
3	10 Min	30 Min	2 - 1/4 in. dowels	Both dowels hit B-Blade, one at Station 49, other at Station 50.5. No damage evident.
4	10 Min	40 Min	2 - 3/8 in. dowels	One dowel hit both blades; on A-Blade, contact made on outboard face of outboard rib apparent glancing blow; and on B-Blade at Station 50. Second dowel hit A-Blade at Station 50. No damage evident.
5	5 Min	45 Min	1 - 1/2 in. dowel	Hit B-Blade, Station 50. No damage evident.

TABLE IX - CONTINUED

Whirl Run No.	Duration	Cumulative Time	Test Description	Notes
6	1 Hr 20 Min	2 Hr 5 Min	Ballistic damage	Tail rotor removed from rig for two .30 cal shots through skin to core bonds. A-Blade hit at Station 30, clean hole, no delamination. B-Blade hit at Station 44.5, clean hole, no delamination. No propagation of damage after completion of Run 6.
7	5 Min	2 Hr 10 Min	1 - 1/2 in. dowel	Hit A-Blade, Station 49. No damage evident.
8	5 Min	2 Hr 15 Min	1 - 5/8 in. dowel	Hit A-Blade, Station 50.5. Approx 1/8 in. dent on L.E. and L.E. deformed to open .015 in. gap with ballast block on one side of airfoil. No other damage. See Figures 43 and 44.
9	3 Hr 40 Min	5 Hr 55 Min	Ballistic damage	Tail rotor removed from rig for four additional .30 cal shots. A-Blade hit through L.E. at Station 45, and through skin/core at Station 42. See Figures 45 and 46. B-Blade hit through spline at Station 48. Localized skin delamination on exit side approx 7/8 in. dia. T.E. delamination 5/8 in. long. See Figures 47 and 48. No propagation of damage after completion of Run 9.

TABLE IX - CONTINUED

Whirl Run No.	Duration	Cumulative Time	Test Description	Notes
10	8 Min	6 Hr 3 Min	Crushed Stone 300 gm injected	Numerous cuts in boot evident, 1/4 in. max length, exposing aluminum L.E. Several stones imbedded in boot removed. One stone trapped under the boot in B-Blade.
11	2 Min	6 Hr 5 Min	Crushed Stone 62 gm injected	Boots tore open on both A- and B-Blade. Loose edges of boot cut away for next run. Numerous dents and cuts in .050 in. aluminum L.E.
12	20 Min	6 Hr 25 Min	Gravel 130 gm injected	Hopper lowered 6 in. Gravel hits primarily between Station 37 to Station 43. Boot tore open on both blades at Stations 37 to 40. Blades ran for approx 20 min prior to discharge of gravel. Boot failure occurred within 1 min after discharge. Run immediately terminated. A-Blade disclosed additional boot delamination on L.E. to Station 43 with gravel trapped under boot at Station 43. Figures 49 through 54 show damage from Runs 10, 11 and 12.

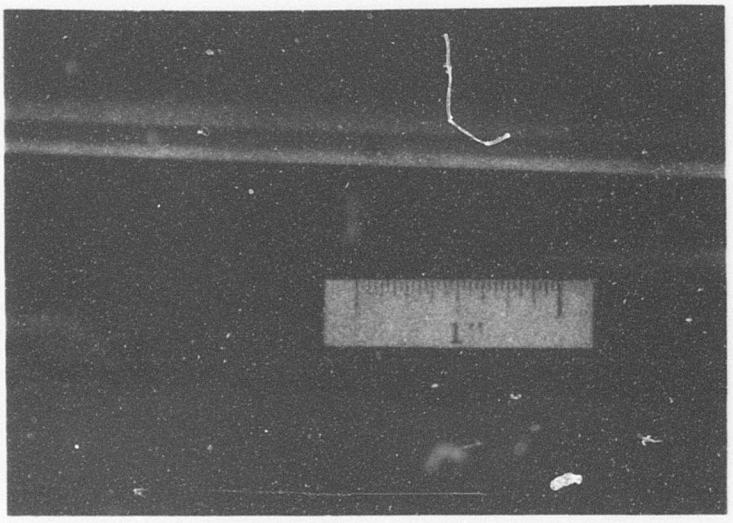

Figure 39. Condition of Erosion Guard on A-Blade From Gravel Impingement After Completion of Run 2.

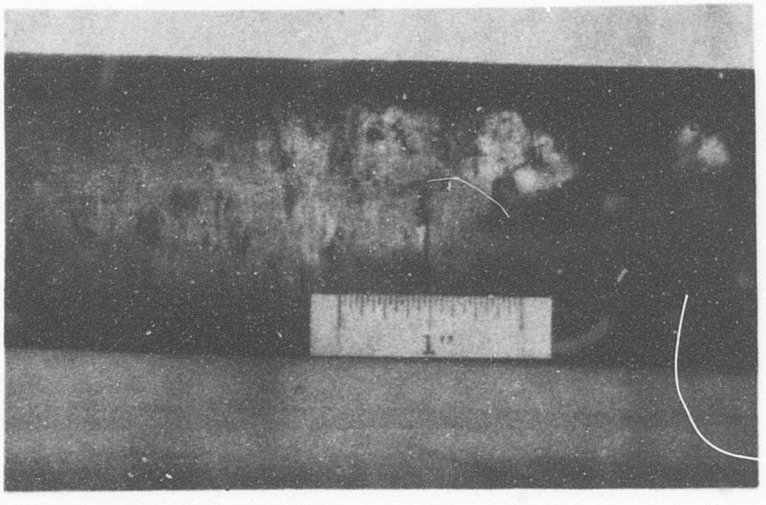

Figure 40. Side View of Erosion Guard on A-Blade, Showing Blisters Caused by Pulverizing of Gravel on Penetration Through the Erosion Guard.

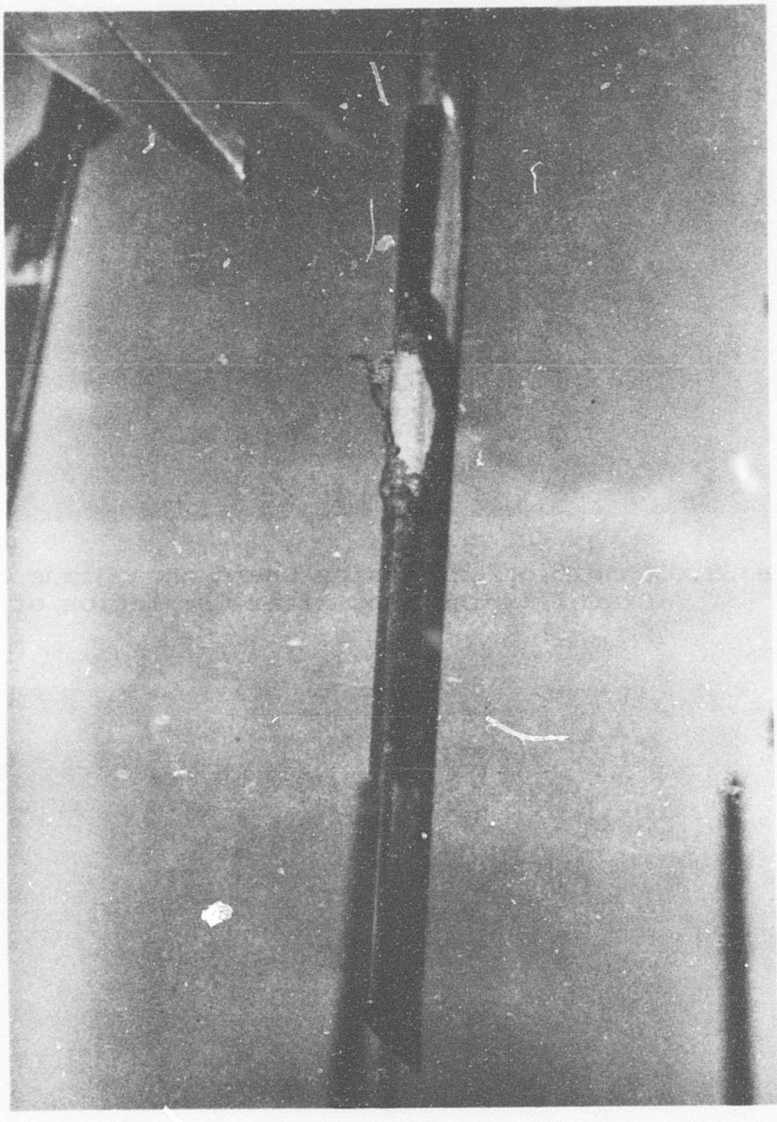

Figure 41. Condition of B-Blade From Gravel Impingement After Completion of Run 2.

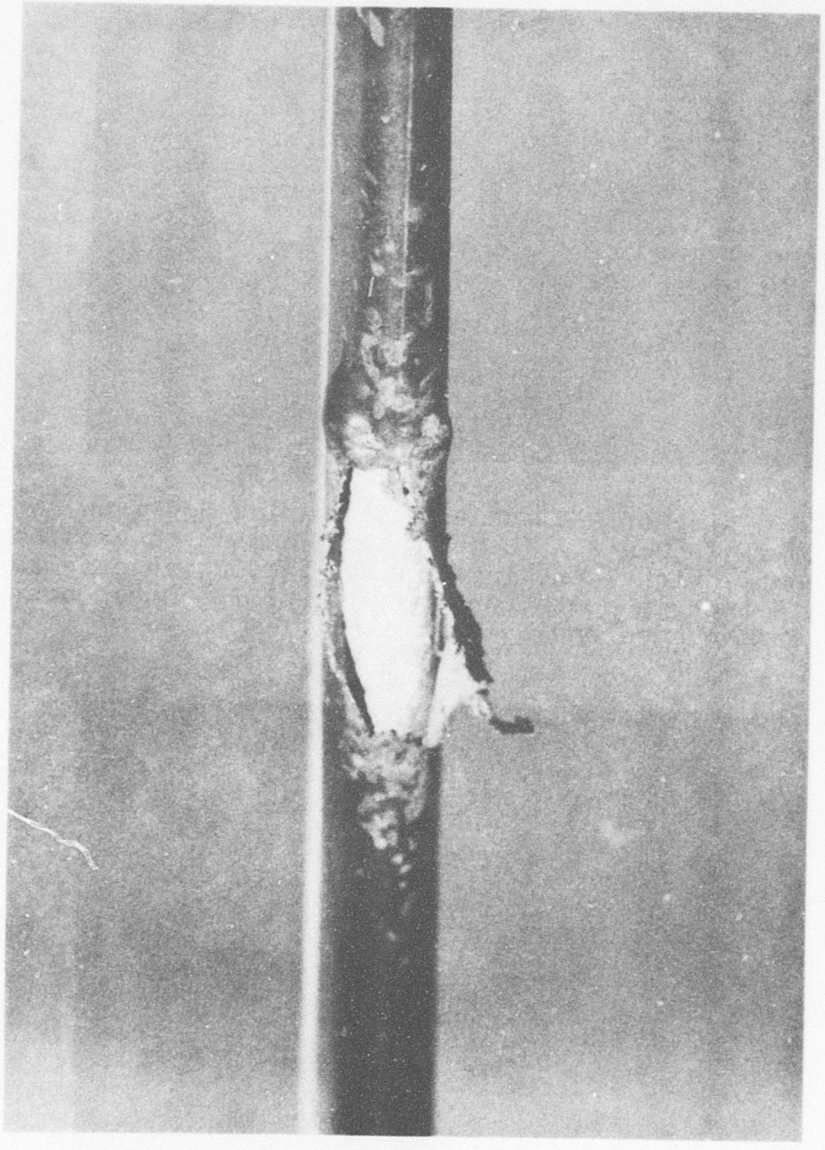

Figure 42. Close-Up View of Gravel Impingement Damage. (Same View as Figure 41.)

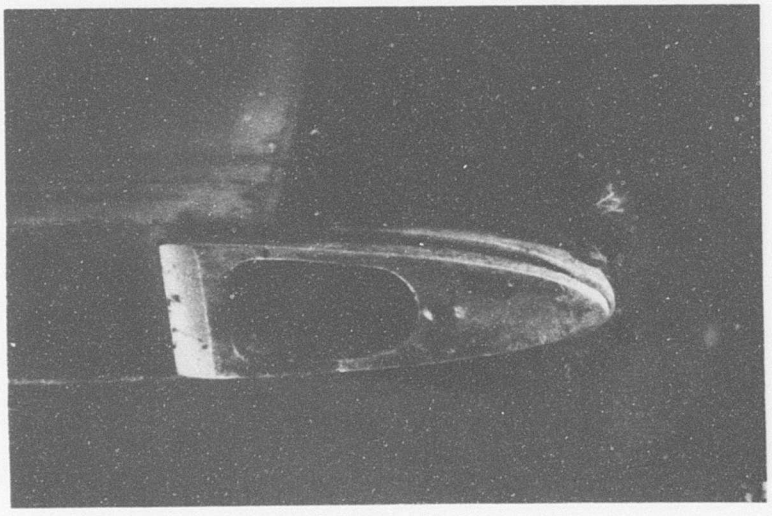

Figure 43. Condition of A-Blade After Severing 5/8-Inch Maple Dowel in Run 8. (Dowel caused damage to erosion boot, slight dent in aluminum leading edge approx 1/8 inch in depth, and opened .015-inch gap between leading edge and ballast block.)

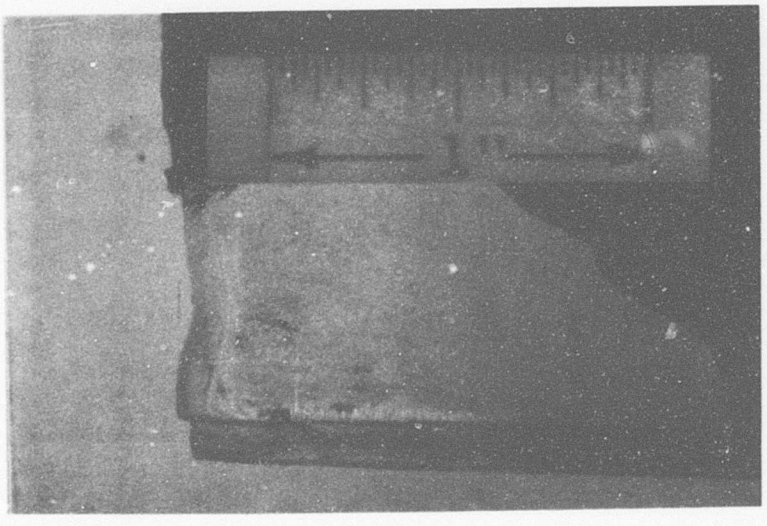

Figure 44. Side View of A-Blade After Severing 5/8-Inch Maple Dowel in Run 8.

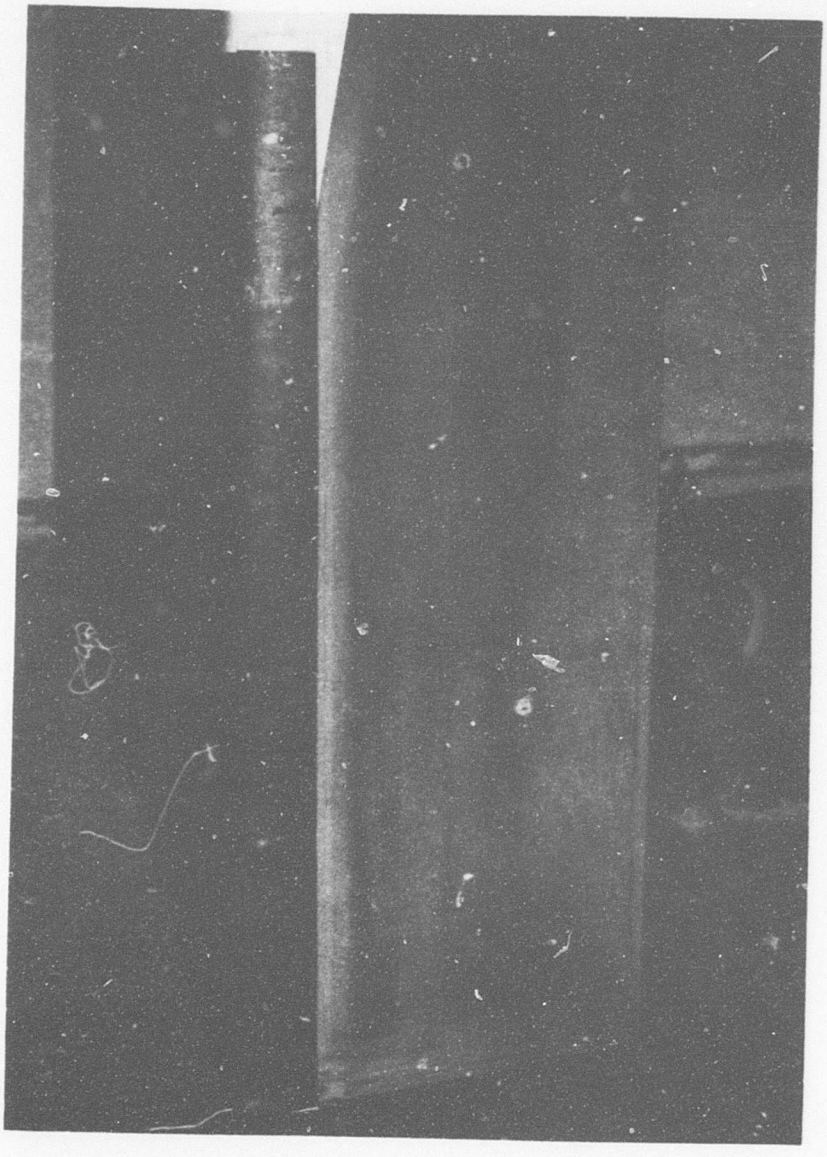

Figure 45. Ballistic Damage to A-Blade From 7.62mm Ball - Entry Side of Bullet. (Two outboard hits inflicted just prior to Run 9. Inboard hit made prior to Run 6. Shot through erosion guard and .050-inch aluminum leading edge caused localized boot unbonding. Shots through fiberglass skin to core created no damage other than hole.)

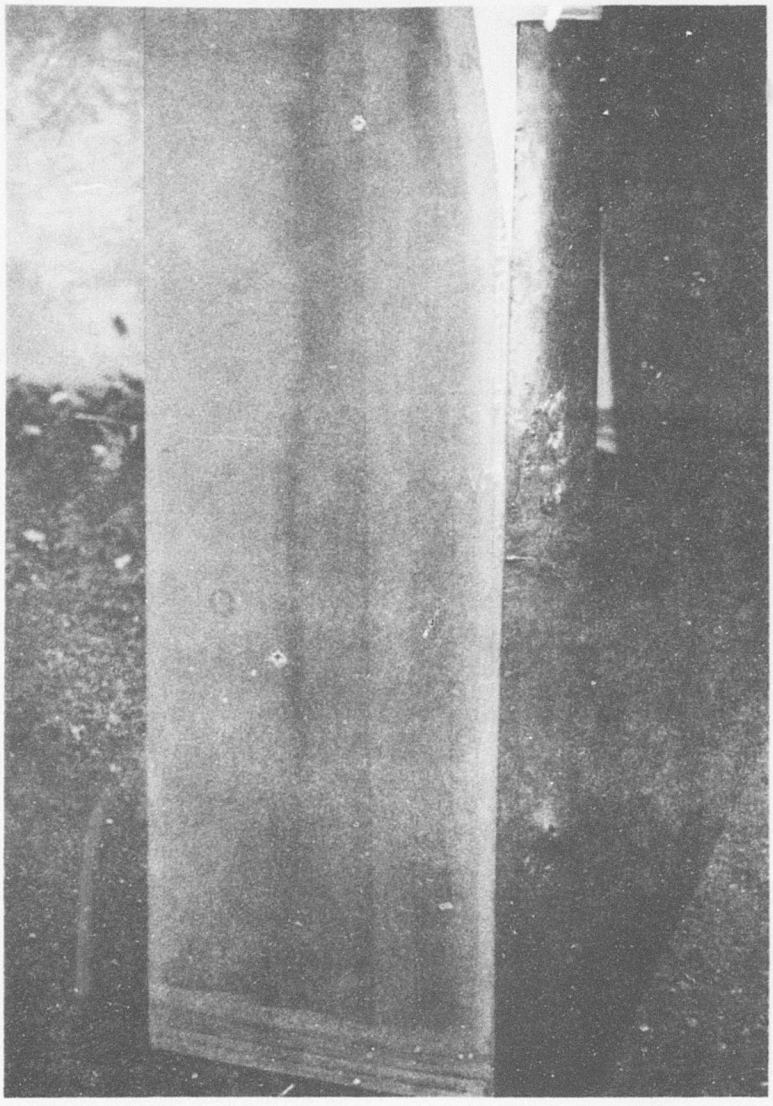

Figure 46. Ballistic Damage to A-Blade From 7.62mm Ball - Exit Side of Bullet. (Same hit as Figure 45. Bullet created a uniform cone-like projection hole on exit.)

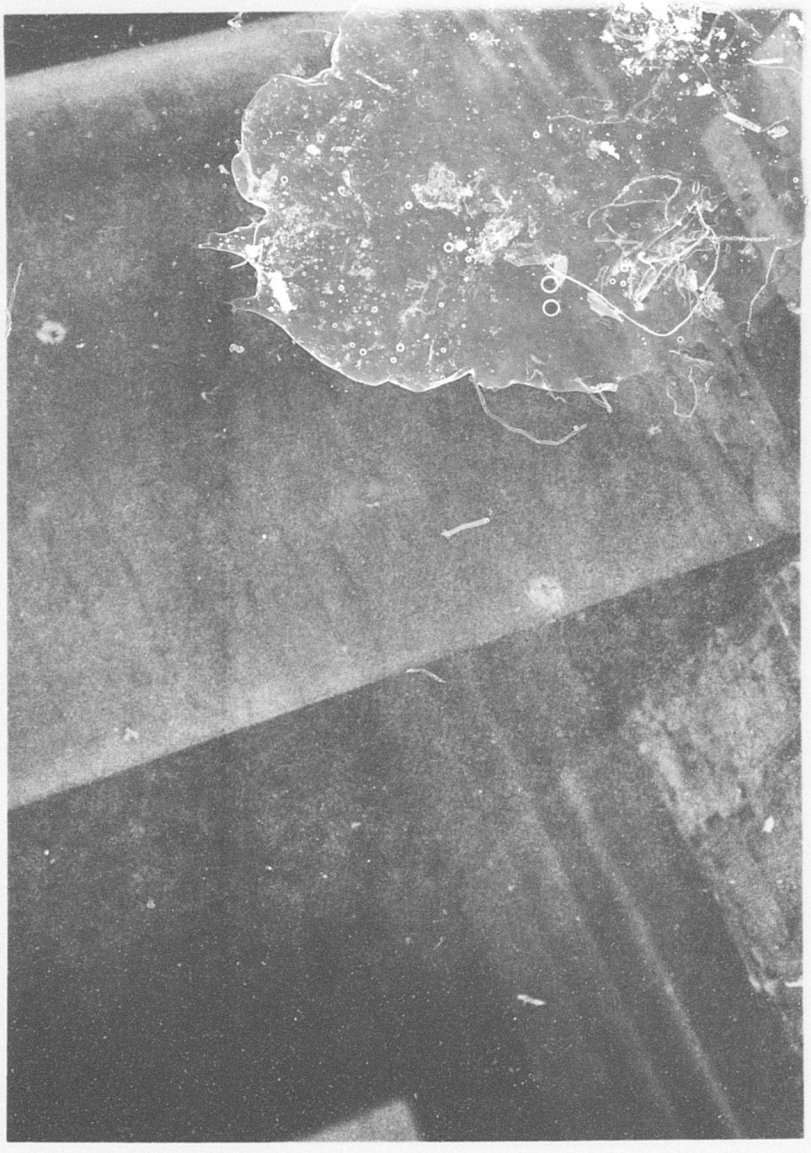

Figure 47. Ballistic Damage to B-Blade From 7.62mm Ball - Entry Side of Bullet. (Hit through fiberglass skin to core inflicted prior to Run 6. Shot through fiberglass skin to fiberglass spline occurred prior to Run 9.)

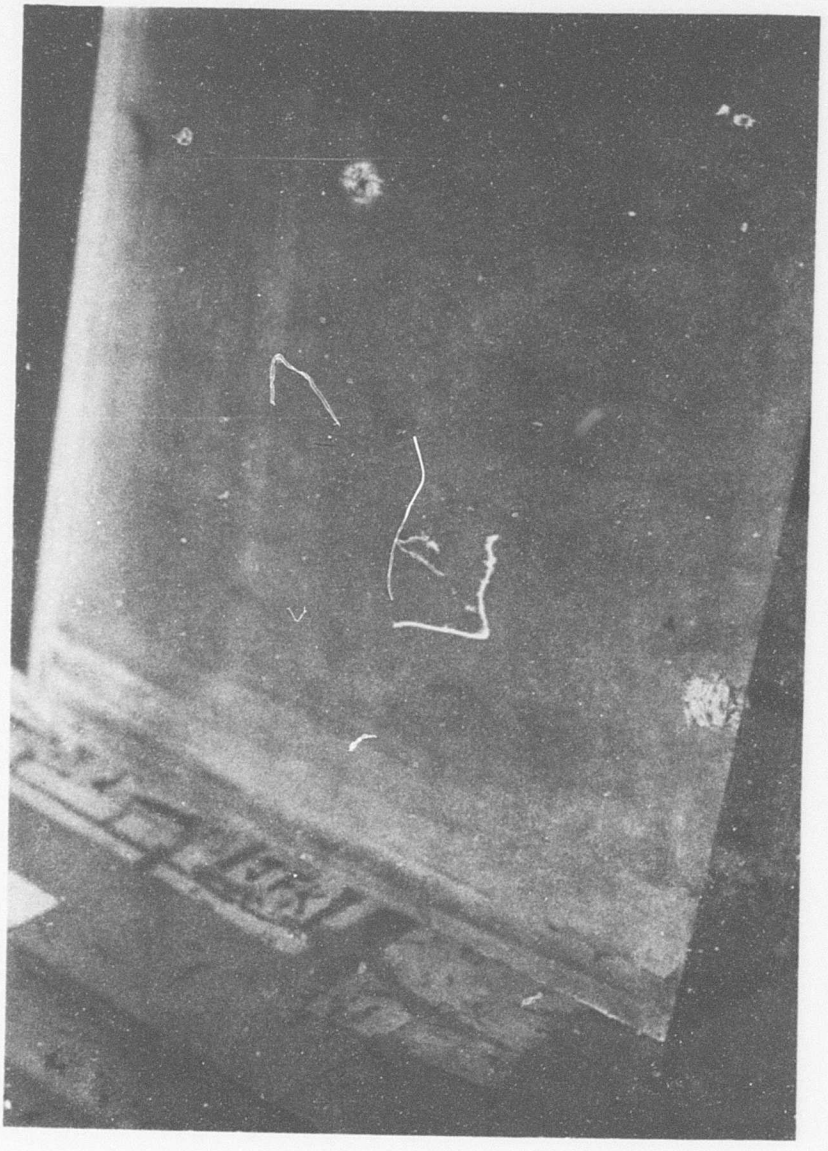

Figure 48. Ballistic Damage to B-Blade From 7.62mm Ball - Exit Side of Bullet. (Extent of damage other than hole was a 7/8-inch-diameter skin delamination around hole through spline as evident. Delamination opened to trailing edge for 5/8-inch length.)

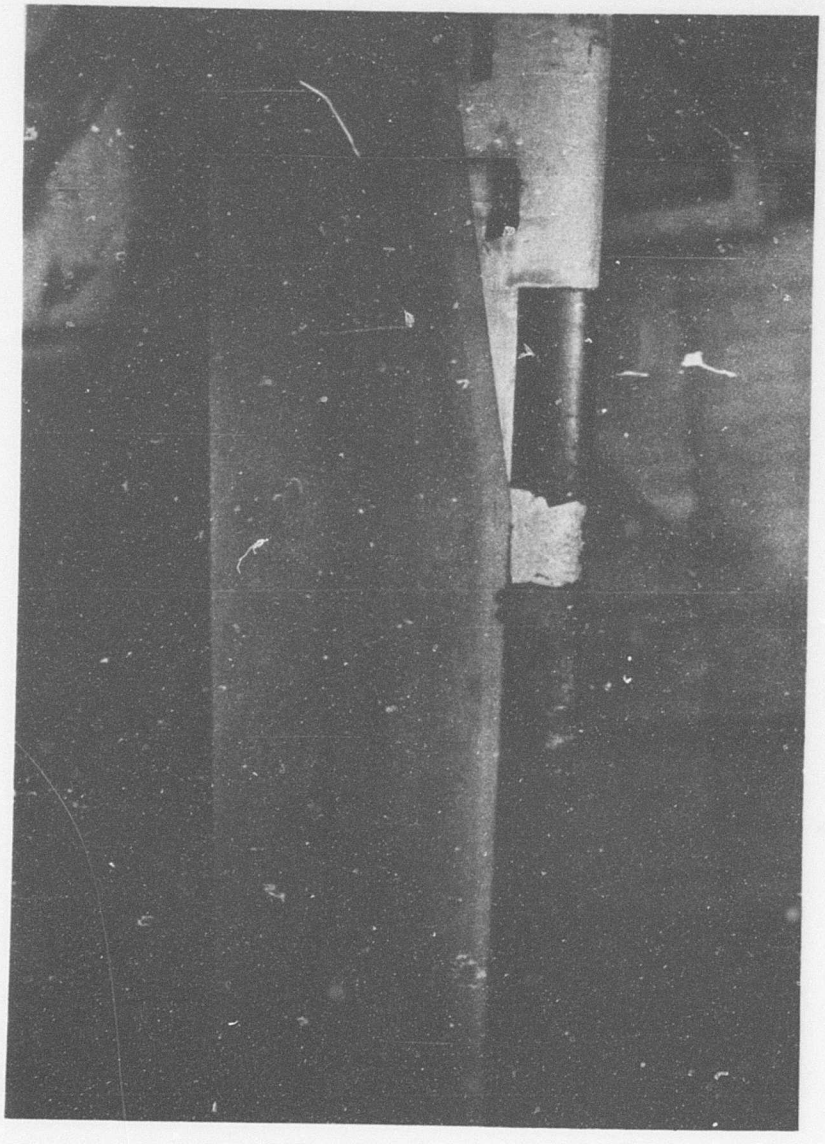

Figure 49. Condition of A-Blade From Crushed Stone Impingement After Termination of Run 11.

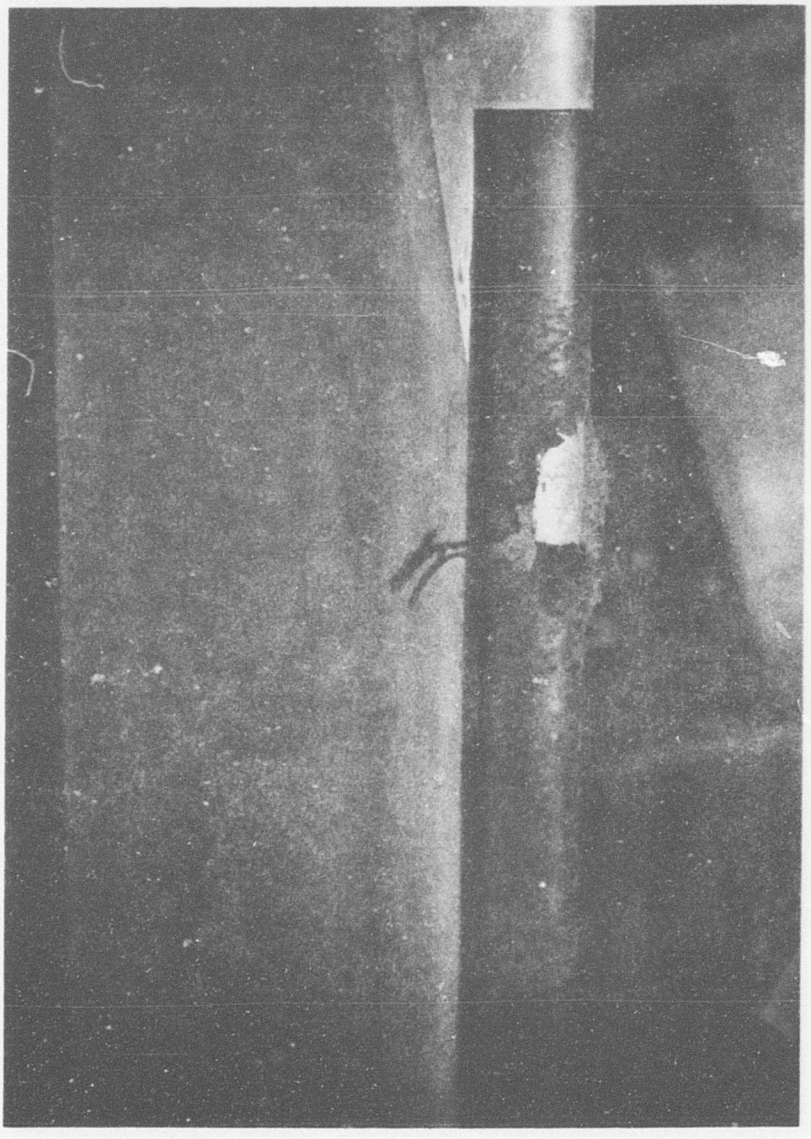

Figure 50. Condition of B-Blade From Crushed Stone Impingement After Termination of Run 11.

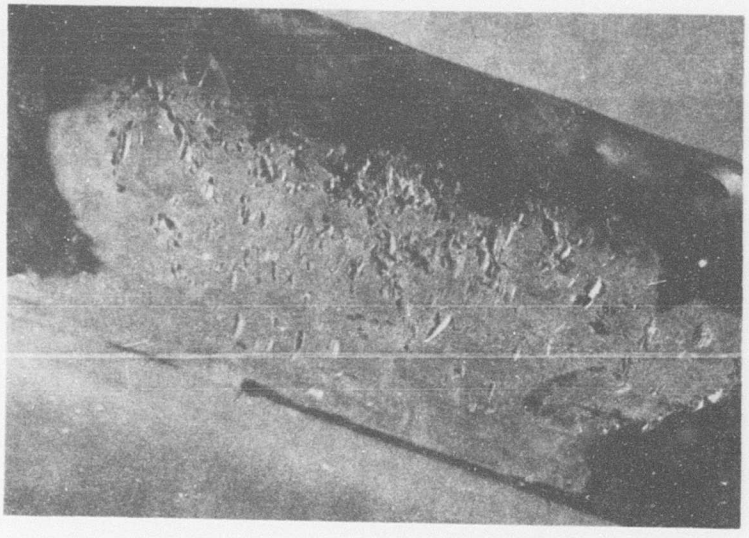

Figure 51. Damage to Aluminum Leading Edge of A-Blade Caused by Run 11.

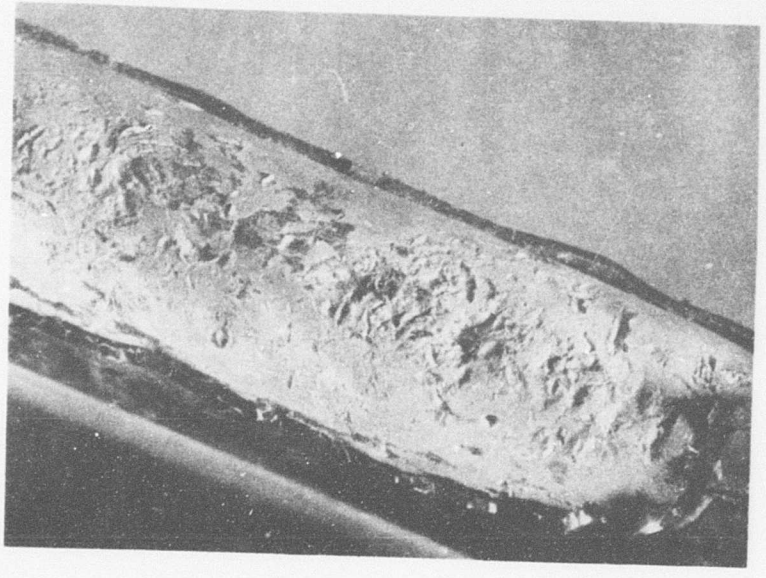

Figure 52. Damage to Aluminum Leading Edge of B-Blade After Run 11.

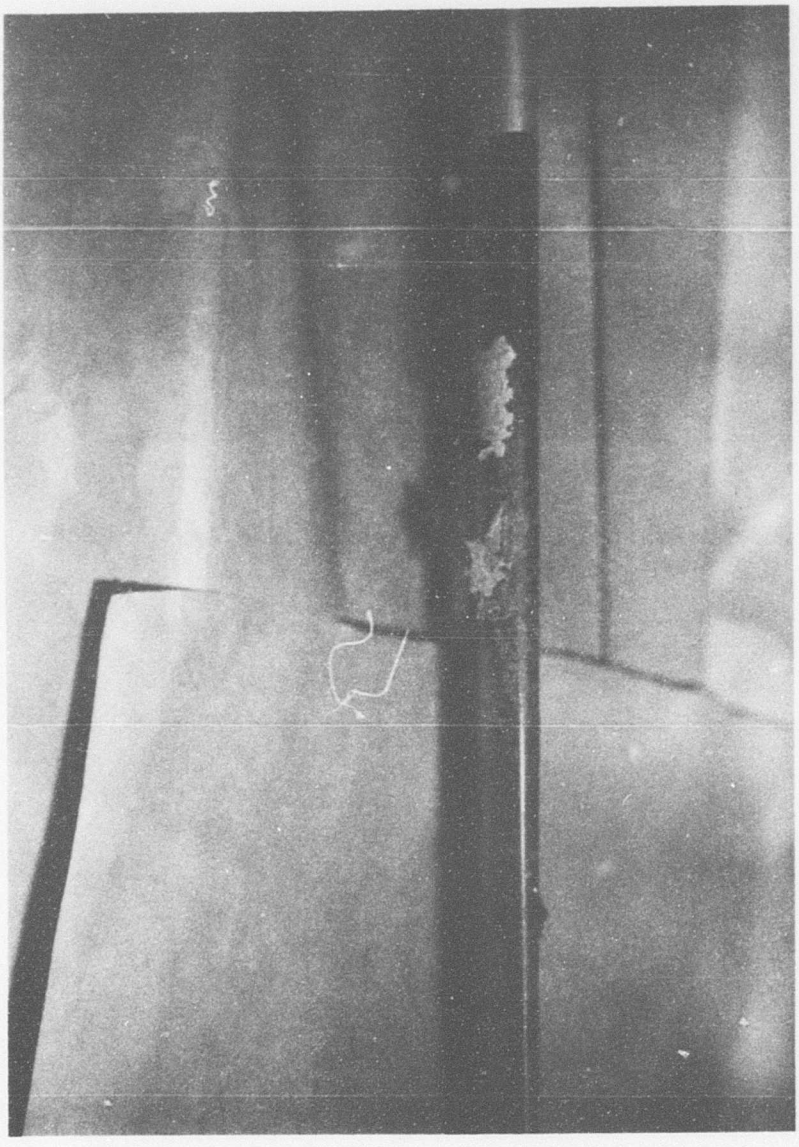

Figure 53. Condition of A-Blade From Gravel Impingement After Termination of Run 12. (Only lower break in erosion guard caused by Run 11 testing.)

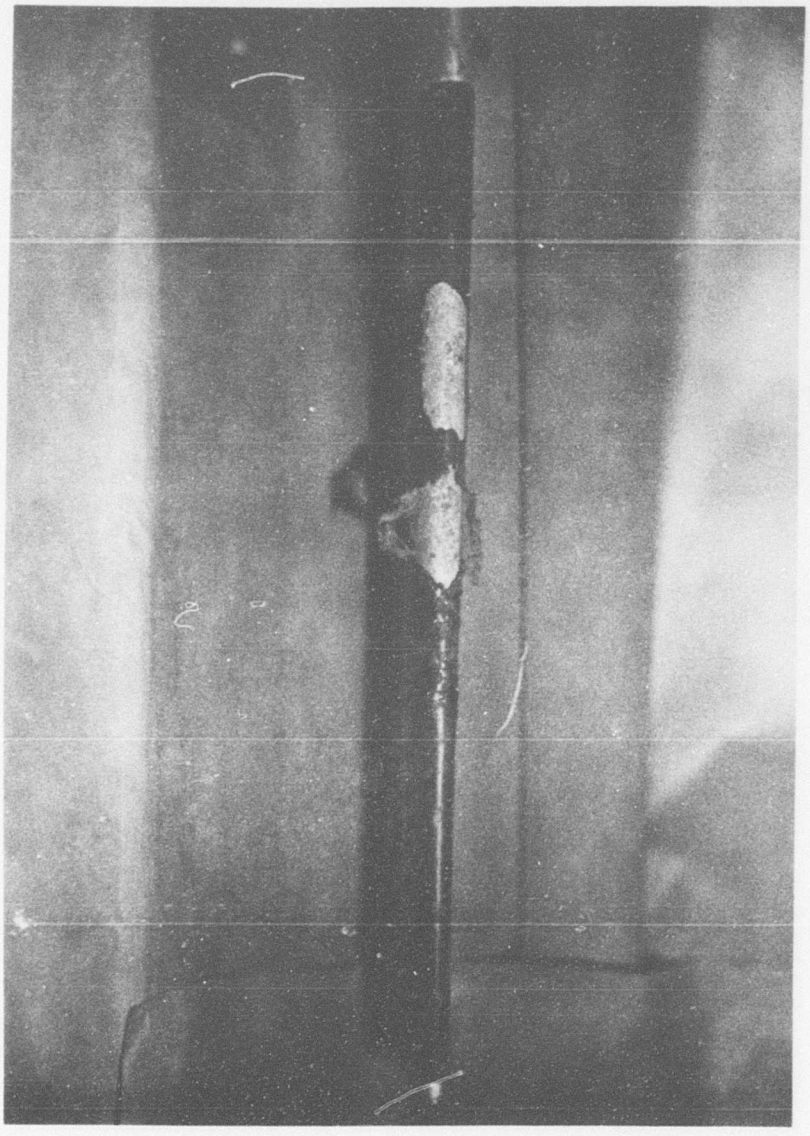

Figure 54. Condition of B-Blade From Gravel Impingement After Termination of Run 12. (Only lower break in erosion guard caused by Run 11 testing.)

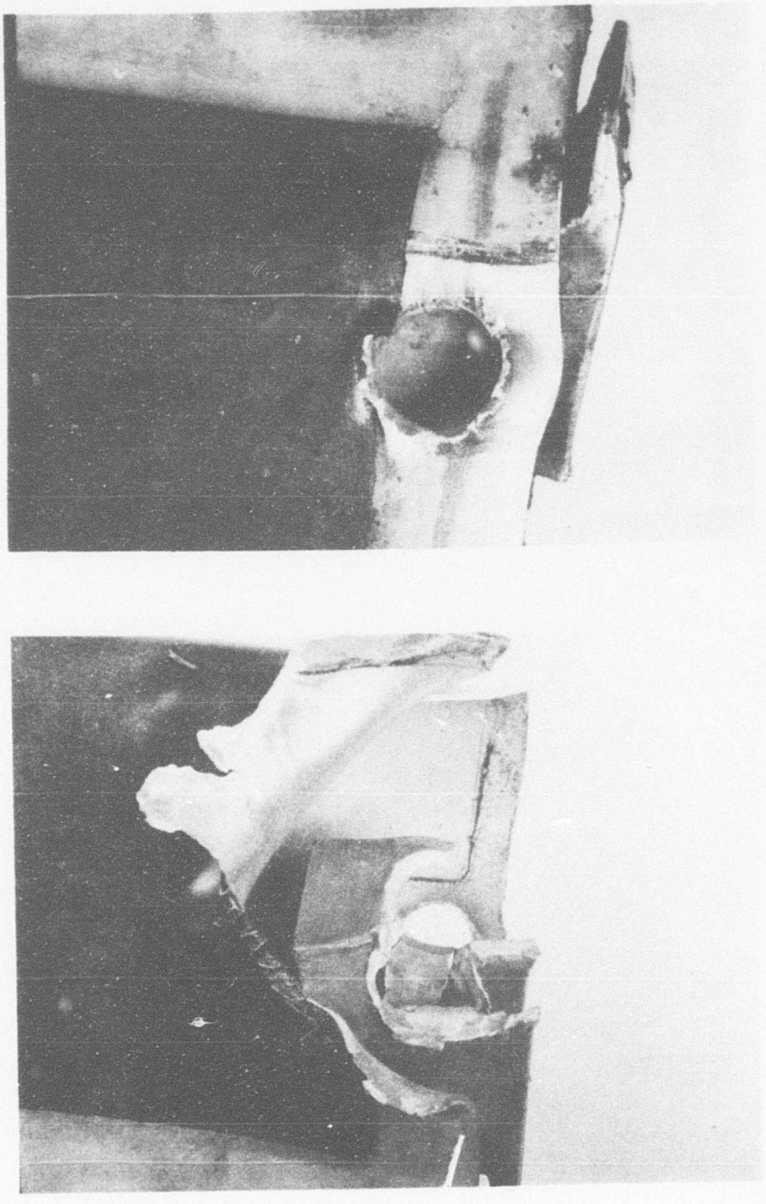

Figure 55. Ballistic Damage to B-Blade at Outboard Ballast Weight Region From 7.62mm AP Hit. (Entry side, top view. Exit side, lower view.) (Leading-edge section of aluminum ballast weight severed by the hit. No bond delamination experienced.)

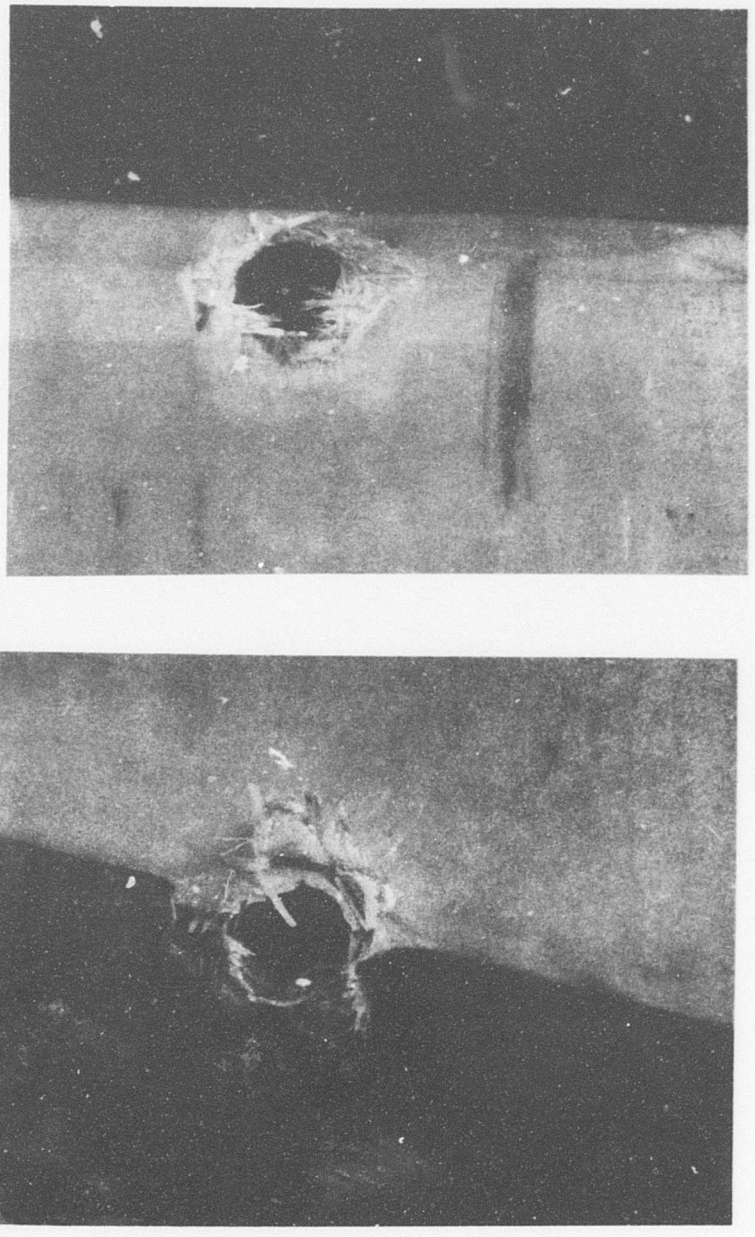

Figure 56. Ballistic Damage to B-Blade at Station 37.5 From 7.62mm AP Hit Through Forward Channel Section. (Bullet entered top surface as shown in upper view, penetrated through spar, and exited from bottom side as shown in lower view.)

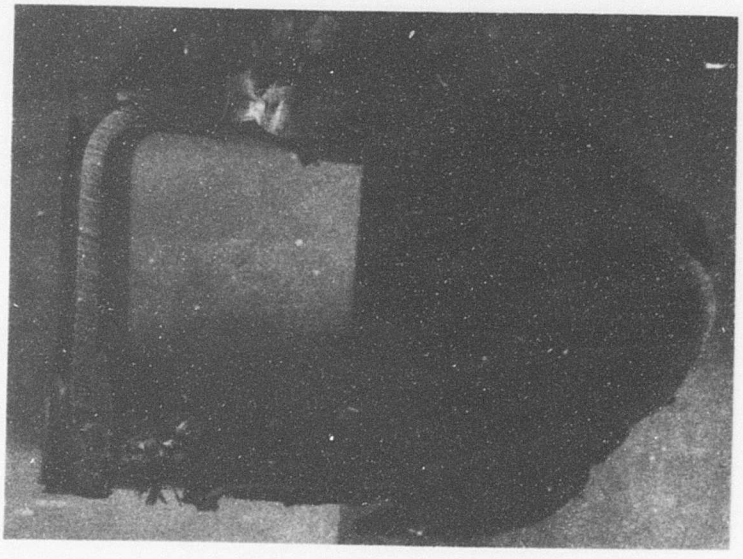

Figure 57. Sectioned View Through B-Blade at Station 37.5, Showing Forward Channel. (Same hit as shown in Figure 56. Bond delamination between channel to leading edge confined to immediate vicinity of hit. Delamination attributed to metal deformation rather than shock.)

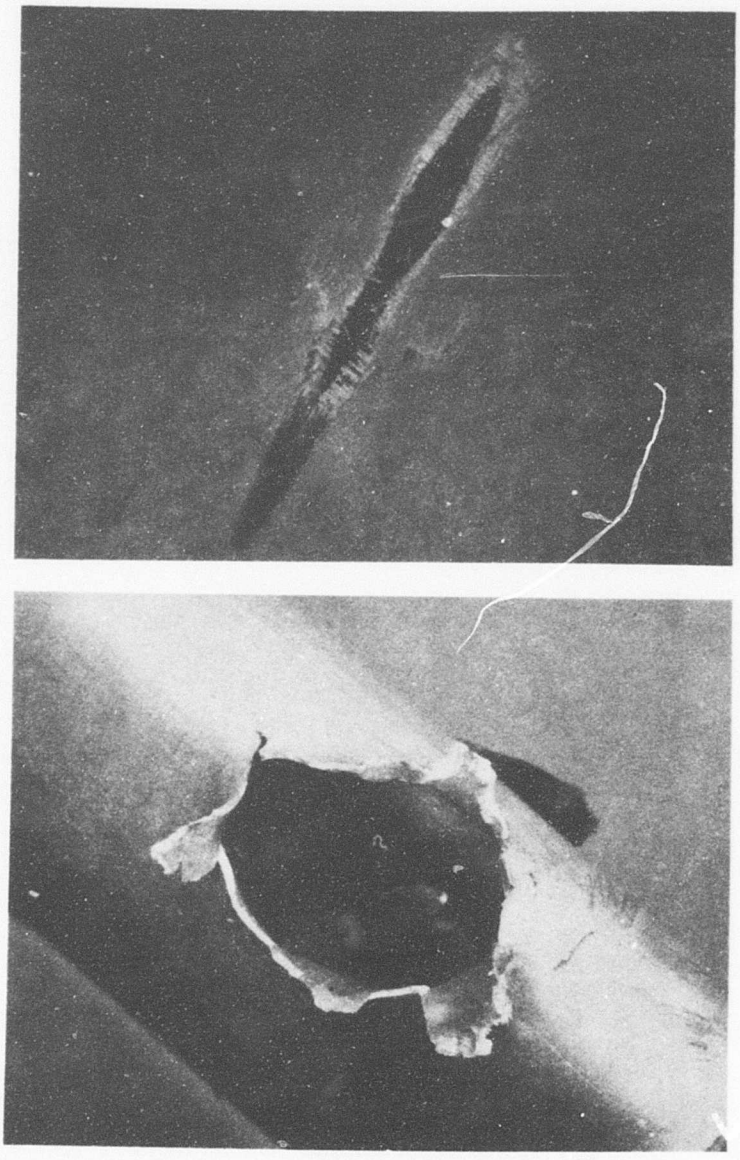

Figure 58. Ballistic Damage to B-Blade at Station 27 From 7.62mm AP Hit. (Bullet entered blade at pocket skin as shown in upper view, penetrated spar from aft face, and exited through aluminum leading edge as shown in lower view.)

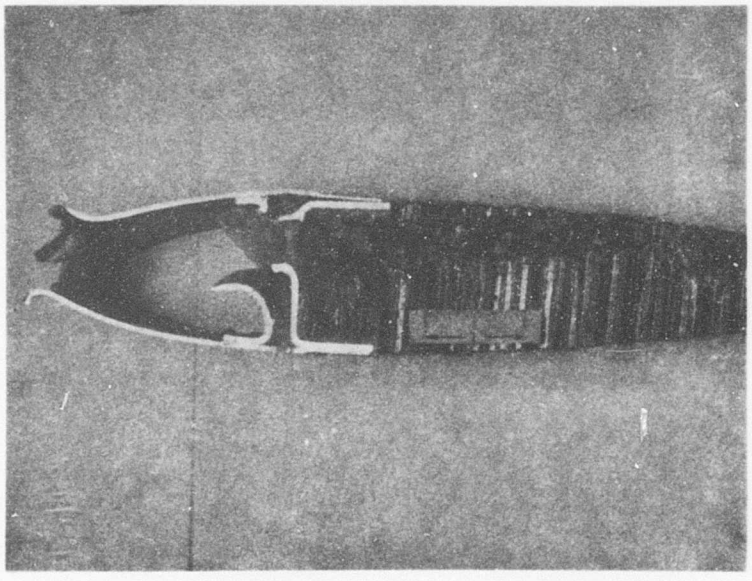

Figure 59. Sectioned View of Ballistic Damage to B-Blade at Station 27. (Same hit as shown in Figure 58. Station 27 is just inboard of the termination point for the GRP spar in the tapered section region. Delamination of bond is again localized to the damaged area and attributed to deformation rather than shock.)

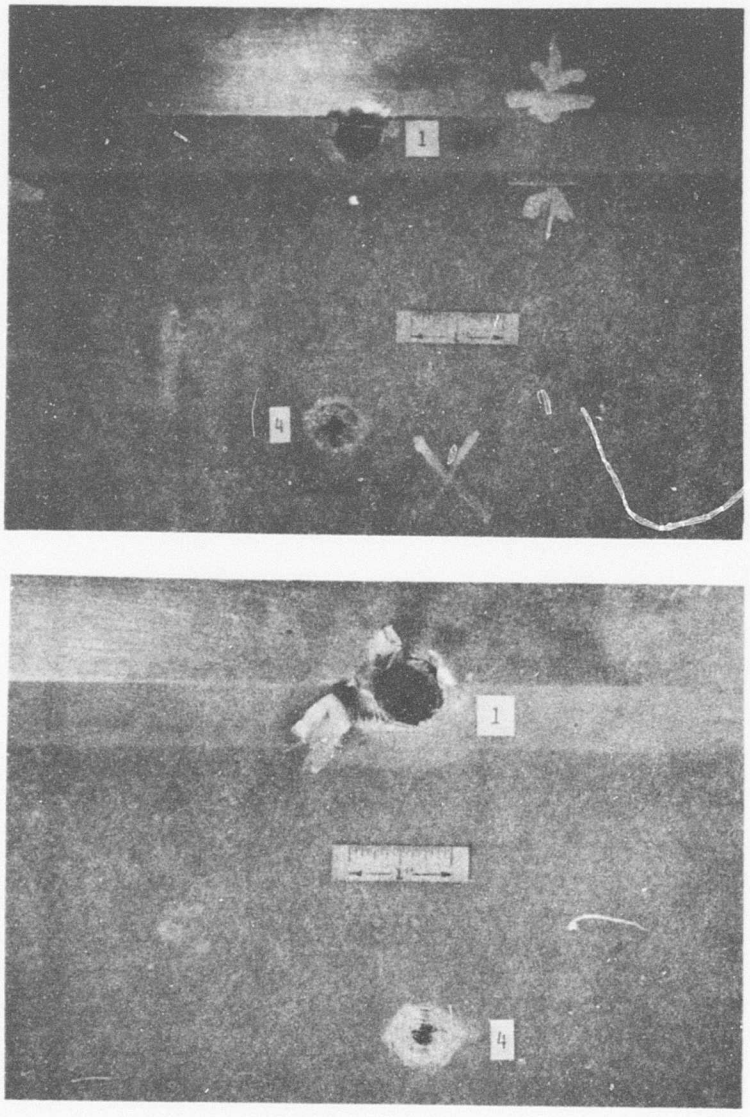

Figure 60. Ballistic Damage to Blade Section From 12.7mm AP Hits. Entry Side, Top View. Exit Side, Lower View. (Shot No. 1 is through forward channel - leading-edge section equivalent to Figure 56. Bond delamination confined to immediate vicinity of the hit and attributed to localized deformation rather than shock. Shot No. 4 through skin-core structure produced no significant damage.)

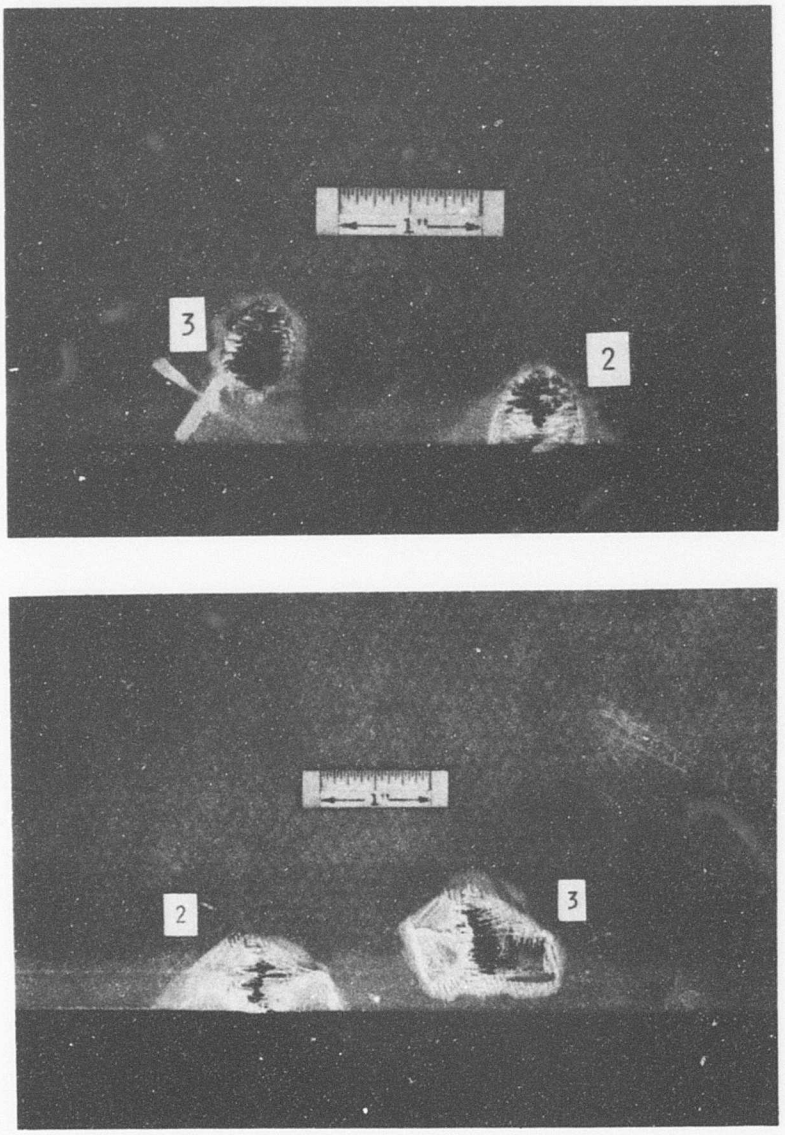

Figure 61. Ballistic Damage to Blade Trailing Edge From 12.7mm AP Hits. Entry Side, Top View. Exit Side, Lower View. (Shot No. 2 completely severed spline. Shot No. 3 just nicking the spline caused localized skin to spline delamination on entry side, but spline remained intact.)

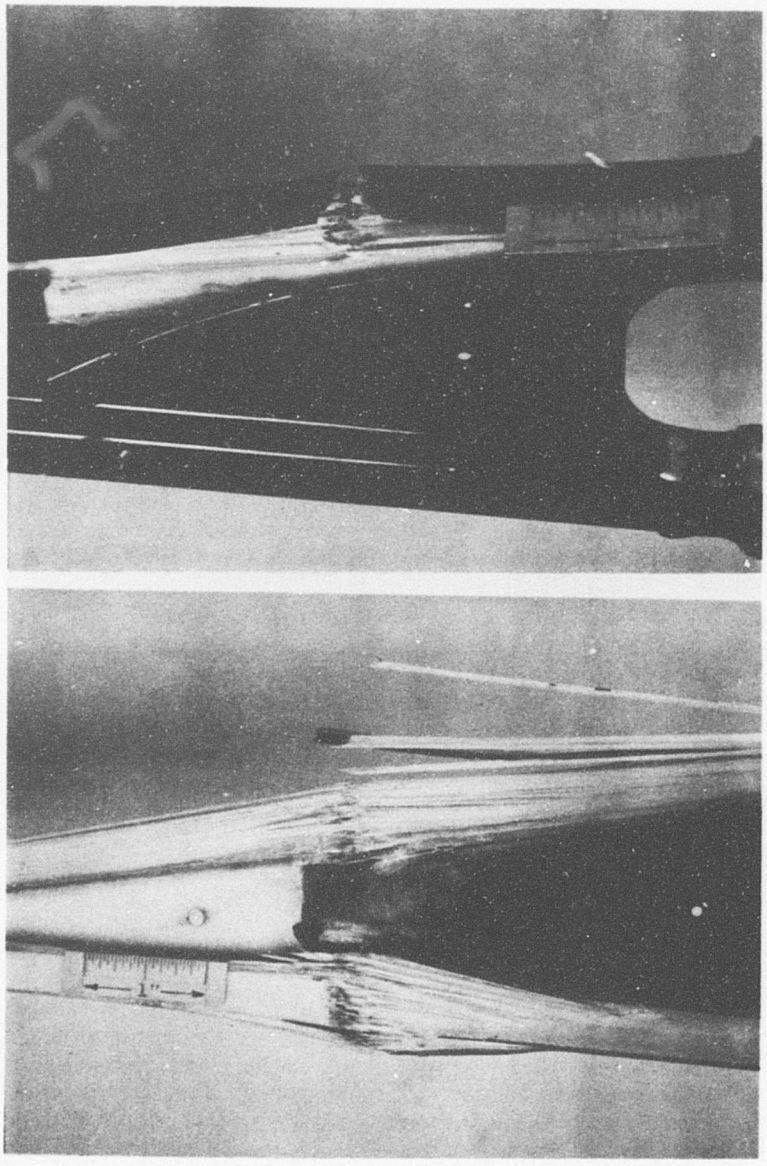

Figure 62. Ballistic Damage to Spar Component From 12.7mm AP Hits. (The upper view shows the damage to a single strap from Shot No. 5 normal to the edgewise plane severing the protective coating and fragmenting one-third of the section. The lower view shows damage to both straps from Shot No. 7 parallel to the flatwise plane fragmenting the outer layers of fibers.)

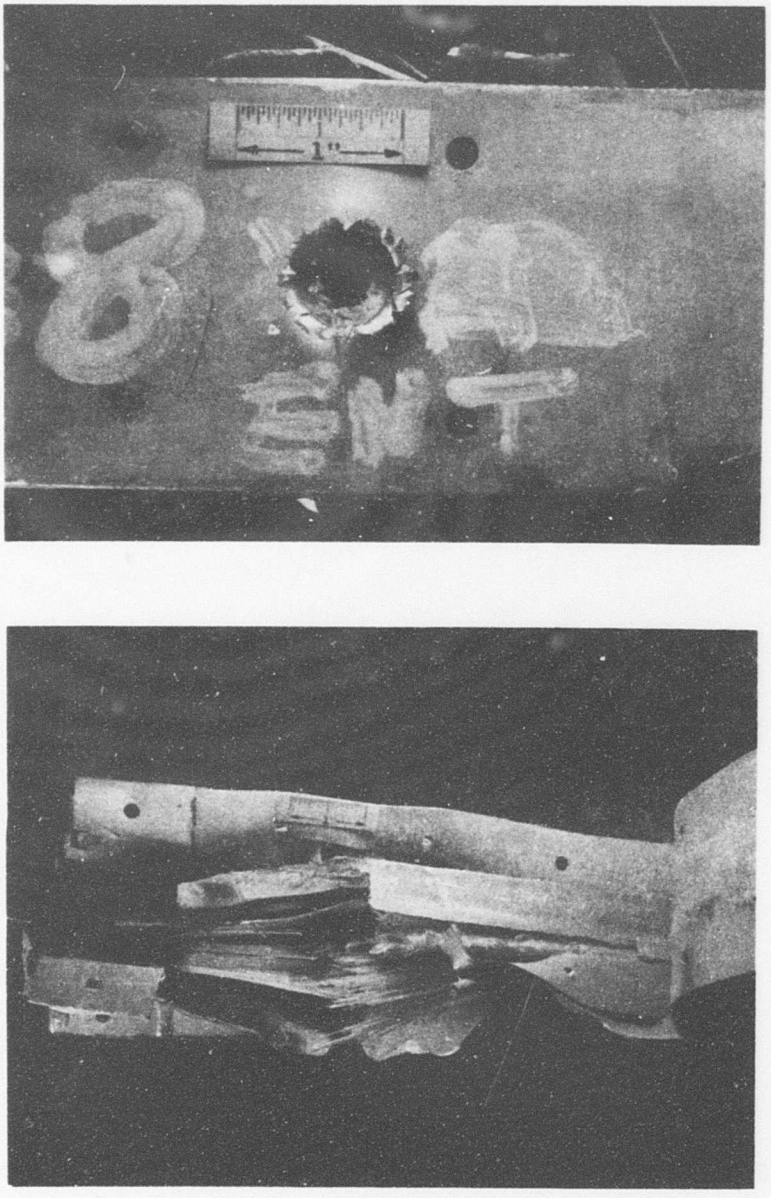

Figure 63. Ballistic Damage to Spar-Channel at Section From 12.7mm AP Hit. Entry Side, Top View. Exit Side, Lower View. (Hit directed at the bond interface between straps.)

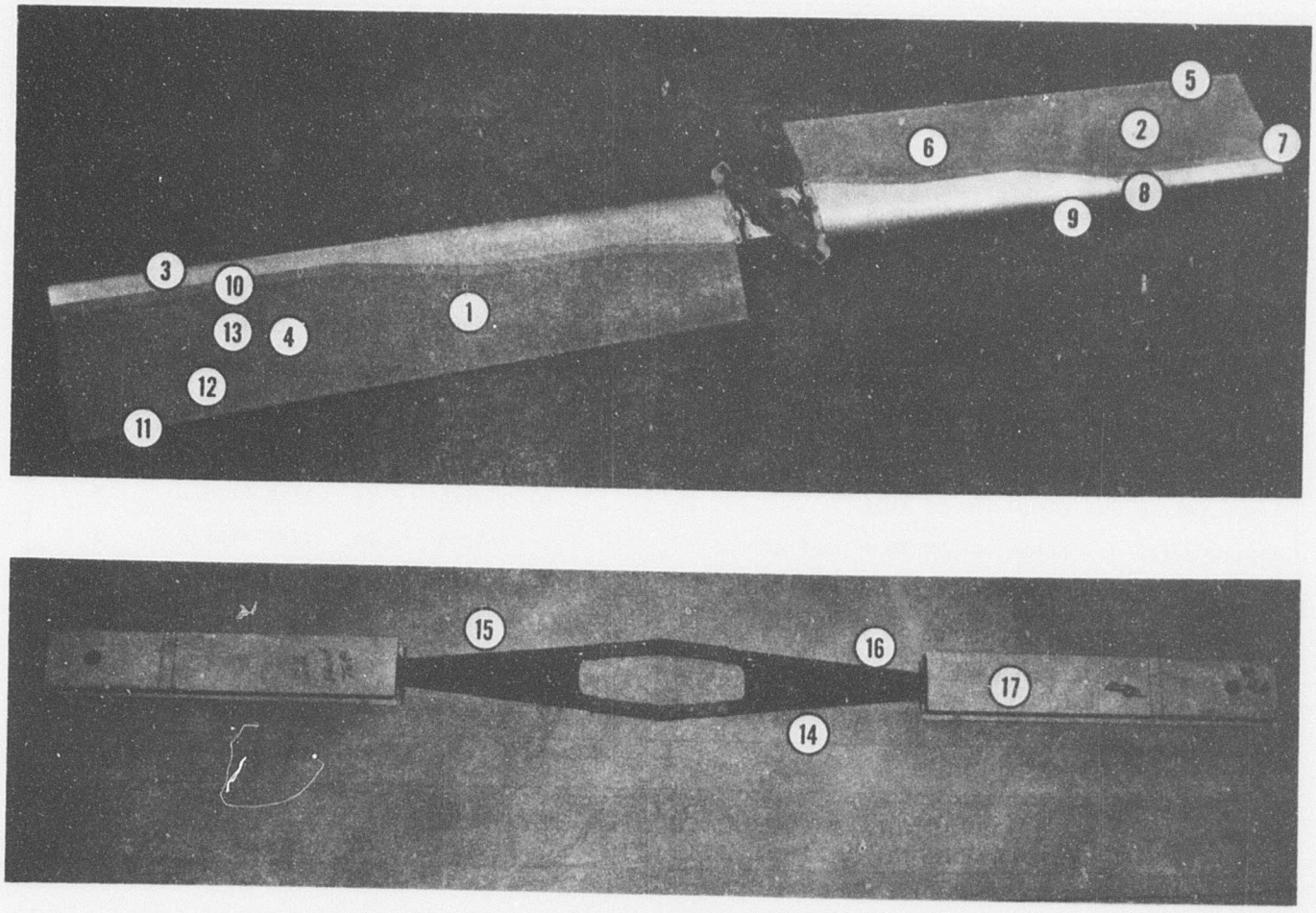

Figure 64. Sequences of Location of Ballistic Firing on Elastic Pitch Beam Tail Rotor Blade and Spar.

TABLE X. SUMMARY OF BALLISTIC TESTING ON ELASTIC PITCH BEAM TAIL ROTOR BLADE AND SPAR

Firing Sequence	Ammunition	Sta No.	Structure	Figure No.	Notes
1	7.62mm Ball	30	Skin/Core	45-46	5 hr 4 min whirl - no delamination
2	7.62mm Ball	45	Skin/Core	47-48	5 hr 4 min whirl - no delamination
3	7.62mm Ball	45	Leading Edge	45-46	4 hr 20 min whirl - no delamination
4	7.62mm Ball	42	Skin/Core	45-46	4 hr 20 min whirl - no delamination
5	7.62mm Ball	48	Spline	47-48	4 hr 20 min whirl - no delamination
6	7.62mm Ball	28	Skin/Core	-	4 hr 20 min whirl - no delamination
7	7.62mm AP	51	Ballast Retention Block	55	Damage precluded further whirl
8	7.62mm AP	37.5	Channel/Leading Edge	56-57	Damage precluded further whirl
9	7.62mm AP	27	Core/Spar/Leading Edge	58-59	Damage precluded further whirl
10	12.7mm AP	46	Channel/Leading Edge	60	Shot No. 1 Second Blade Sample
11	12.7mm AP	42	Spline	61	Shot No. 2 Second Blade Sample
12	12.7mm AP	44	Skin/Core	61	Shot No. 3 Second Blade Sample
13	12.7mm AP	46	Skin/Core	60	Shot No. 4 Second Blade Sample
14	12.7mm AP	5.5	Spar	62	Shot No. 5 Spar Component
15	12.7mm AP	7	Spar	-	Shot No. 6 Spar Component
16	12.7mm AP	9.5	Spar	62	Shot No. 7 Spar Component
17	12.7mm AP	15	Spar/Blade Attachment	68	Shot No. 8 Spar Component

DISCUSSION

During Whirl Runs 1 and 2, a total of 6.1 lb of gravel was injected into the rotor in a running time of 20 minutes. A barrage of pinging sounds was continuously heard as the battered stones struck various structures adjacent to the rig. Many stones in addition were observed to burst into a cloud of dust on impact with the rotor. High-speed filming of the gravel test also confirmed a very high incidence of stone hits by the rotor. The amount and size of the gravel injected into the rotor were considered to be far in excess of that which would be encountered in service and lend credence to the durability of the urethane erosion boot in this environment. The amount of damage sustained by the .050-inch aluminum leading edge appeared to be minor and did not preclude further whirl runs. In contrast, Runs 10 and 11 utilizing crushed stone of the same sieve size illustrated the severity of damage created by sharp foreign objects. Approximately 0.8 lb of this material severely damaged both erosion guards and dented the aluminum leading edge.

For Run 12, the chute was lowered 6 inches for stone impingement further outboard. Approximately 20 minutes of whirl time was accumulated in the run prior to discharging the gravel. Within 1 minute from the discharge of 130 grams of gravel, both erosion guards tore open. This early failure is attributed to erosion guard damage sustained from prior runs and not to the small quantity of gravel hitting the rotor at a station of increased velocity. During Runs 1 and 2, the blades had sustained many hits out to Station 51 without similar failure.

The breaking of dowels from 1/4-inch to 1/2-inch diameter had no effect on the rotor. Each blade hit disintegrated a 2- to 3-inch section from the mid span of each dowel into slivers. The 5/8-inch dowel did create minor deformation to the leading edge as shown in Figures 43 and 44, but not sufficient to inhibit further whirl. Seasoned maple represents one of the stronger hard woods with strength properties appreciably higher than green or live woods. It is therefore conceivable that the whirling rotor could contact live brush and tree limbs somewhat larger than 5/8-inch diameter without damage.

Gunfire shots of 7.62mm ball resulted in clean holes through the skin core structure without additional damage or damage propagation from subsequent whirl. The one shot through the trailing edge created a clean hole without severing the spline. However, a localized skin-to-spline delamination occurred on the exit surface. This delamination did not grow in size from subsequent whirling. The 7.62mm shot through the .050-inch-thick leading edge produced a clean hole with a cone-like

projection on the exit side. No bond delamination or damage from subsequent whirl resulted from this hit. The following hit with 7.62mm AP ammunition to the outboard ballast weight region, Figure 55, resulted in damage considered too risky to allow further running, so the whirl test was concluded. Two additional 7.62mm AP firings through the forward channel and inboard of the spar termination point resulted in the damage shown in Figures 56 through 59. It is conceivable that the damage resulting from the last three hits would not have been catastrophic, but would have resulted in vibration sufficient to abort the mission.

Damage inflicted to the structure by 12.7mm AP hits in the skin-honeycomb structure and aluminum leading edge did not appear significant to abort a mission. A hit severing the trailing-edge spline could lead to the formation of a chordwise crack in the aft section resulting in severe vibration and a possible loss of blade section. A direct hit on the spar structure would inflict catastrophic damage as evidenced by Figures 62 and 63.

CONCLUSIONS

1. The Elastic Pitch Beam Tail Rotor will sever seasoned maple dowels up to 5/8-inch diameter without significant damage to preclude continued flight. Since seasoned maple represents one of the stronger hard woods and is stronger than green maple, it is feasible to assume that live brush and tree branches somewhat larger than 5/8-inch diameter could be digested by the rotor without inflecting damage.

2. Polyurethane erosion guard provides protection against stone and gravel hits in excess of that normally encountered in service.

3. The Elastic Pitch Beam Tail Rotor will survive ballistic hits from 7.62mm and 12.7mm ammunition in both the leading edge and aft structure. A direct hit on the spar structure is likely to cause catastrophic damage.

REFERENCES

1. MATERIALS SELECTOR, Reinhold Publication, 1974.

2. HELICOPTER ROTOR BLADE EROSION PROTECTIVE MATERIALS, TCREC Technical Report 62-111, U.S. Army Transportation Research Command, Fort Eustis, Virginia, December 1962.

3. E. R. Givens, POLYURETHANE AS EROSION RESISTANT MATERIAL FOR HELICOPTER ROTOR BLADES, USAAML Technical Report 65-39, U.S. Army Aviation Materiel Laboratories, Fort Eustis, Virginia, May 1965.

4. M. H. Chopin, EVALUATION OF RAIN-EROSION-RESISTANT MATERIALS TO PROTECT THE HH43B/F HELICOPTER ROTOR, SEG-TR 65-53, Air Force Systems Command, Wright-Patterson Air Force Base, Ohio, August 1966.

5. J. F. Moraveck, RAIN AND SAND EROSION RESISTANT POLY-URETHANE PROTECTIVE COATINGS, AFML-TR 67-227, Part II, Air Force Systems Command, Wright-Patterson Air Force Base, Ohio, July 1969.

6. N. E. Wahl, INVESTIGATION OF THE PHENOMENA OF RAIN EROSION AT SUBSONIC AND SUPERSONIC SPEEDS, Technical Report AFML-TR 65-330, Air Force Systems Command, Wright-Patterson Air Force Base, Ohio, October 1965.

7. J. H. Weaver, ELECTRODEPOSITED NICKEL COATINGS FOR EROSION PROTECTION, Technical Report AFML-TR 70-111, Air Force Systems Command, Wright-Patterson Air Force Base, Ohio, July 1970.

APPENDIX

AIR FORCE WHIRL RIG AT OLIN MATHISEN CHEMICAL CORPORATION NEW HAVEN, CONNECTICUT

1. GENERAL DESCRIPTION

A testing apparatus was built to evaluate protective coatings under simulated conditions for rain and sand erosion resistance. It includes two areas: a test pit and control house (Figure 65). The no-pitch propeller ("whirling arm") in the pit turns horizontally, is centrally supported, and is driven by an electric motor positioned directly above on the pit roof. The rain-field apparatus is suspended from the ceiling and is located over the path described by the actual test specimens mounted on the blade (Figure 66). Sand can be distributed at four equidistant delivery points over the specimen path from sand hoppers on the pit roof (Figure 67).

Within the control house are located the electric motor starter and speed controls, a viewing periscope, a digital frequency counter to exactly measure blade revolutions, and the water tank and pump to supply the rain-field apparatus.

This unit is equipped with stroboscopic lighting so actual test progress and specimen performance can be viewed and closely followed. Temperature sensing is also provided so specimen temperature can be monitored under actual test conditions.

To run a typical evaluation, the following sequence of events was involved. All equipment was checked out as operational. Then the airfoil test specimens were attached to the blade, and, depending on erosive agent, rainfall or sand rate calibration was set. The pit was then closed, the blade was started and brought to operating speed (500 to 600 mph), and the rain or sand flow and timer were simultaneously started. Performance was constantly monitored through the periscope, and observations were recorded.

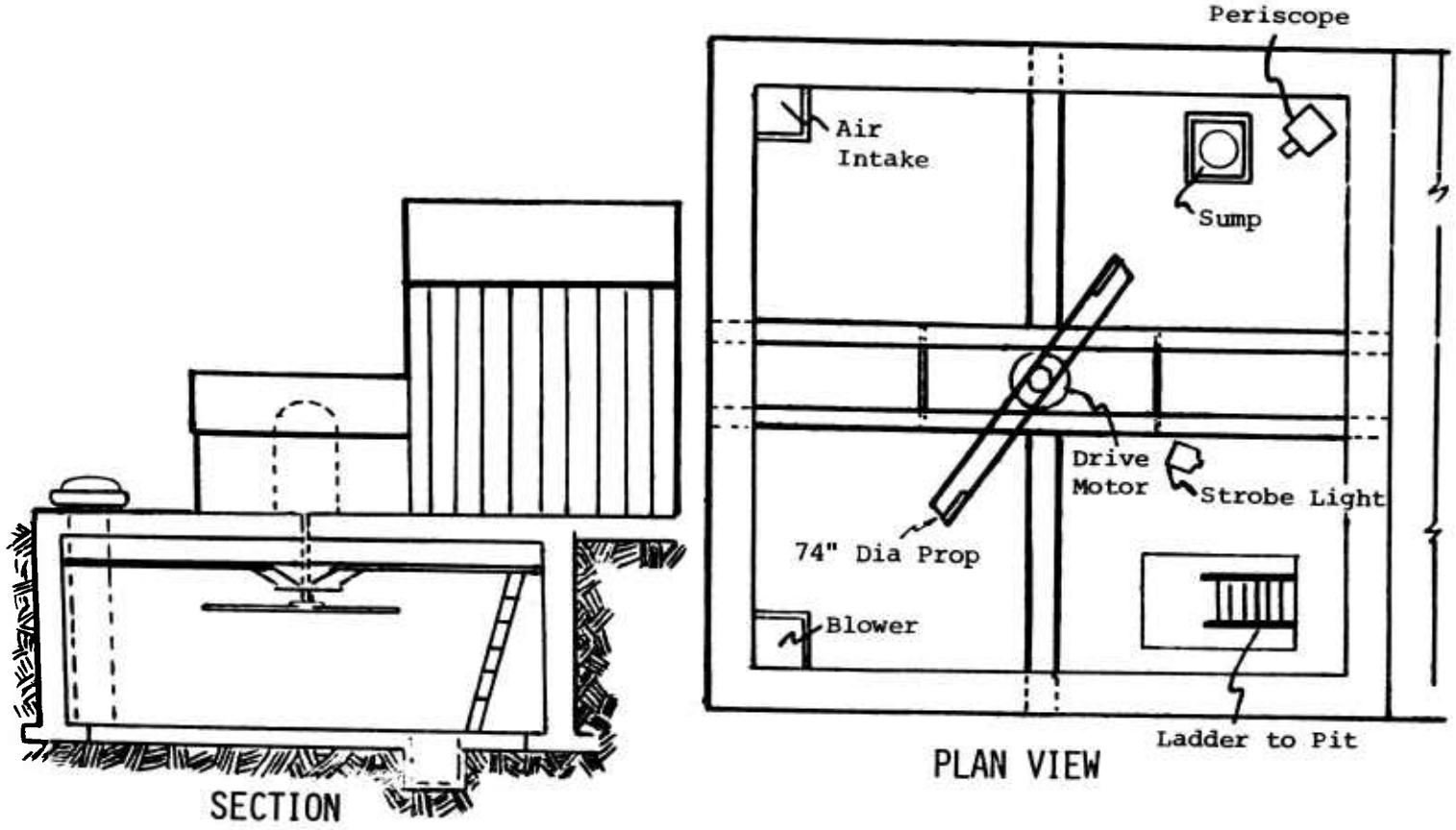

Figure 65. Erosion Apparatus.

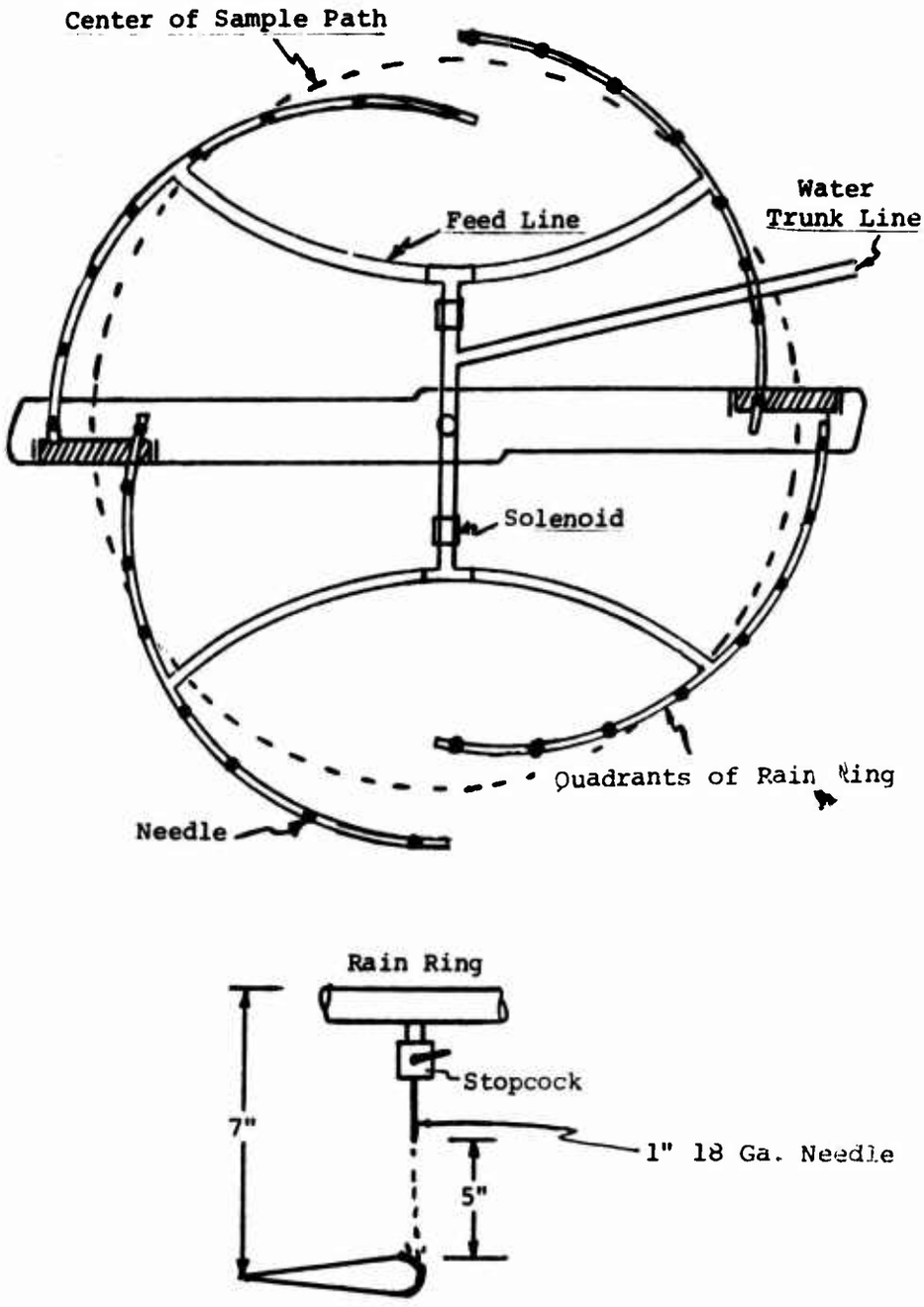

Figure 66. Rain Ring Simulator.

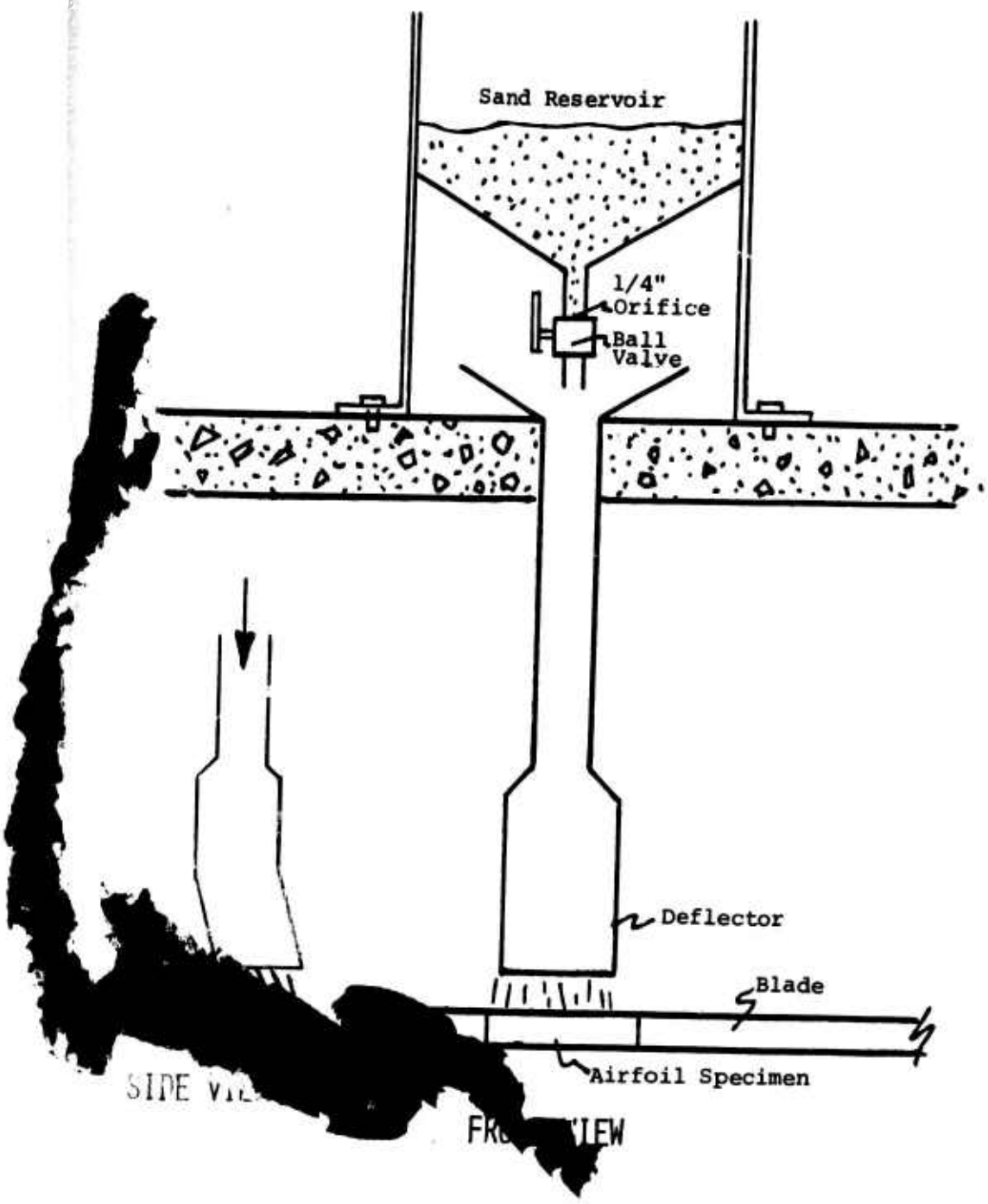

Figure 67. Sand Distribution Apparatus.

2. TESTING AREA

a. Pit

Dimensions are 14 ft x 14 ft x 6 ft.
Construction is concrete.

Floor and roof are 4 inches thick, poured and reinforced. Walls are block. An air intake duct and exhaust blower are roof mounted. A sump and pump are located in one corner. The periscope's objective end projects down through the roof from the control house. Four 1000-watt, 240-volt strip heaters and thermostats furnish winter temperature control (Figure 65).

The roof is supported by two parallel 12-inch x 6.5-inch 24-lb WF I-beams. At right angles at the center are connected two 12-inch x 4.75-inch 31.8-lb I-beam sections which provide cross bracing and strengthen the main support. This construction furnishes the base for supporting the motor and for holding the shaft.

Pit entry is gained through a trap door and by a ship's ladder from the control house.

b. Drive

A 40-hp Westinghouse, 230-volt, DC, Type SKH, 2500 to 3500 rpm, shunt wound, vertical shaft motor drives the blade. It is mounted on a 1-inch steel base plate and is positioned directly over the center of the supporting I-beam structure. The shaft passes down through the base plate and is connected to the blade drive shaft by a special flexible coupling.

The drive shaft is retained by two normal thrust bearings. Both are rigidly mounted, and the lower one is carefully braced (12-inch channel beams) to minimize vibration. The assembly is protected with a vibration cutoff switch.

c. Blade

The blade is mounted to rotate horizontally to better simulate wing or helicopter rotor leading edges knifing through rainfall or sand dust. It is firmly bolted to the shaft.

This "no pitch" propeller is 74 inches long, is made of AISI 4340 high-strength alloy steel, and conforms to a NACA .0025 configuration with a 4-inch chord.

The leading edges of each end are indented to permit mounting two test specimens. This indentation is 4 inches long and 1 inch from the blade tips, so the outboard end of the test specimen is 36 inches from the center of the blade; inboard end, 32 inches; and specimen center, 34 inches. The machining was done so that the metal specimen's surface would exactly match the blade's surface.

d. Stroboscopic Lighting

The test specimens can be synchronously illuminated for viewing through the periscope during dynamic testing with the use of a General Radio type 1539-A Stroboslave, Type 1536-A Photoelectric Pick-off and Type 1531-P2 Flash Delay.

e. Periscope

The objective end of the periscope projects down into the test pit and is permanently positioned to view part of the path the specimen describes. The stroboscope lighting arrangement affords excellent performance monitoring.

f. Rain Ring

A 6-ft-diameter ring made of 1/2-inch copper tubing is the basic configuration. This ring is divided into separate and equal quadrants, each being suspended and supplied with water independently. Each quadrant carries eight Becton-Dickinson hypodermic stopcocks and needles mounted equidistantly along the arc. Each quadrant is positioned with respect to the circular specimen path so water delivered will cover its entire width. One end is directly over the inside edge of the sample path, and the other end is over the outside edge (Figure 66).

With the 32 needles appropriately regulated, the standard rainfall for the 880-square-inch annular specimen path can be achieved. For example, a 2-inch-per-hour rainfall would require 1760 cu in. water (2x880) or 480.1 ml/min and would be achieved by adjusting each of the 32 needles to deliver 15 ml/min. Similarly, a 1-inch-per-hour rainfall would equate to 7-1/2 ml/min/needle. To achieve uniform 2mm raindrop size, 18-ga. beveled needles 1 inch long are used for the 2-inch-per hour rainfall and 3/4-inch beveled 20-ga. needles for the 1-inch-per-hour rate.

Water is supplied to each quadrant at constant rate and pressure. The water storage and delivery equipment is in the control area.

g. Sand Apparatus

Sand is stored in and delivered from four 20-gallon hoppers mounted on the reinforced concrete roof. These hoppers are equidistantly located over the specimen path. Sand delivery is regulated by orifice, and on-off control is provided by ball valves. The sand drops into a funnel and tubing, passes through the roof, and is then dispersed over the entire width of the test specimen path by inclined deflector plates 1/2 inch above the blade.

The deflector plates are angled in the same direction that the blade rotates (Figure 67).

The ball valves must be manually operated and are the only operations which cannot be carried out from the control room.

No. 4 Silica, AGSCO Corporation, Patterson, New Jersey, is the sand used for testing.

To protect the sand delivery apparatus against weather, a 6-ft x 8-ft gabled roof was used. Incidentally, it also protects the motor.

3. CONTROL AREA

a. Housing

The control room is housed in an 8-ft x 16-ft Priggin insulated metal building which covers part of the test pit and also extends onto the adjacent ground. The building is heated with two Quartzone tube radiant heaters suspended from the ceiling.

Access to the test pit is through a trap door and down a ship's ladder. The trap door is 2 inches thick, constructed from wood, protected with 1/4-inch boiler plate, and counterweighted for easy operation. There is a safety switch on the door to prevent operation of the blade while the door is open.

b. Periscope

The viewing end of the periscope projects up into the control room. It is equipped with 7 x 35 wide-angle binoculars for

sharp, accurate monitoring of test specimen performance. As noted, strcboscopic lighting is provided for sample illumination and stop-action viewing.

c. Digital Frequency Counter

For precisely adjusting and measuring speed, a General Radio Digital Frequency Meter 1150 B is used. It operates off its own photoelectric pick-off head mounted on the shaft and provides an accurate rpm reading. This has proven vital to successful operations.

d. Motor Control and Main Rheostat

The 40-hp Westinghouse motor is equipped with a nonreversing magnetic starter. Starter relays are under current sensing control. Speed is adjusted in increments with a rheostat. Power requirement is monitored with a 250-ampere ammeter.

e. Water Storage and Delivery

Filtered city water is stored in a 40-gallon tank in the control room. A variable-speed pump and two solenoid-operated valves are used to control and actuate the delivery of water at constant rate and low pressure to the rain ring in the test pit.